NTNU – Trondheim
Norwegian University of
Science and Technology

Numerical Analysis of Wave Transmission behind Floating Breakwaters

Sutrisno Sutrisno

Coastal and Marine Civil Engineering
Submission date: June 2013
Supervisor: Raed Khalil Lubbad, BAT
Co-supervisor: Øivind Asgeir Arntsen, BAT
Basile Bonnemaire, Multiconsult

Norwegian University of Science and Technology
Department of Civil and Transport Engineering

ERASMUS MUNDUS MSC PROGRAMME

COASTAL AND MARINE ENGINEERING AND MANAGEMENT
COMEM

NUMERICAL ANALYSIS OF WAVE TRANSMISSION BEHIND FLOATING BREAKWATERS

Norwegian University of Science and Technology, Trondheim, Norway
26th June 2013

Sutrisno
4192192

The Erasmus Mundus MSc Coastal and Marine Engineering and Management is an integrated programme organized by five European partner institutions, coordinated by Delft University of Technology (TU Delft).
The joint study programme of 120 ECTS credits (two years full-time) has been obtained at three of the five CoMEM partner institutions:

- Norges Teknisk- Naturvitenskapelige Universitet (NTNU) Trondheim, Norway
- Technische Universiteit (TU) Delft, The Netherlands
- City University London, Great Britain
- Universitat Politècnica de Catalunya (UPC), Barcelona, Spain
- University of Southampton, Southampton, Great Britain

The first year consists of the first and second semesters of 30 ECTS each, spent at NTNU, Trondheim and Delft University of Technology respectively.
The second year allows for specialization in three subjects and during the third semester courses are taken with a focus on advanced topics in the selected area of specialization:

- Engineering
- Management
- Environment

In the fourth and final semester an MSc project and thesis have to be completed.
The two year CoMEM programme leads to three officially recognized MSc diploma certificates. These will be issued by the three universities which have been attended by the student. The transcripts issued with the MSc Diploma Certificate of each university include grades/marks for each subject. A complete overview of subjects and ECTS credits is included in the Diploma Supplement, as received from the CoMEM coordinating university, Delft University of Technology (TU Delft).

Information regarding the CoMEM programme can be obtained from the programme coordinator and director

Prof. Dr. Ir. Marcel J.F. Stive
Delft University of Technology
Faculty of Civil Engineering and geosciences
P.O. Box 5048
2600 GA Delft
The Netherlands

NORWEGIAN UNIVERSITY OF SCIENCE AND TECHNOLOGY
DEPARTMENT OF CIVIL AND TRANSPORT ENGINEERING

Report Title: **NUMERICAL ANALYSIS OF WAVE TRANSMISSION BEHIND FLOATING BREAKWATERS**	Date: **22-06-2013**			
	Number of pages (incl. appendices): **126**			
	Master Thesis	●	Project Work	
Name: **Sutrisno**				
Professor in charge/supervisor: **Raed Lubbad**				
Other external professional contacts/supervisors: **Øivind Asgeir Arntsen, Basile Bonnemarie**				

Abstract:

Floating breakwaters (FBs) have been widely used as an alternative solution to protect coastal sites especially small harbors and certain areas which are not suitable for rubble mound breakwaters. Floating breakwater cannot completely stop the incident wave action. Instead, it attenuates the wave action by partially transmitting, partially reflecting, and partially dissipating the incident wave. The efficiency of the FBs profiles and configurations can be quantified by its transmission coefficient which is the ratio of the significant wave height at the lee side of the FBs over the significant wave height at the front side. The aim of this master thesis was to perform a numerical analysis of FBs structures by means of WAMIT and MultiSurf. The study was focused on the wave transmission behind the FBs and the response motions of the structure. Twelve cases based on laboratory experiments were numerically analyzed and some of the results were compared to available measurement data. Some results were satisfactorily confirmed to the experiment result while other results were still far from perfect. Some improvement methods were recommended to be carried out in the future work i.e. trying out more structure geometry representation, simulating more cases which are comparable to the experiments, and more detail study of how the experiments were carried out and how the final outputs were calculated.

Keywords:

1. Floating breakwaters
2. WAMIT
3. MultiSurf
4. Transmission coefficient

_____

NTNU
Det skapende universitet

MASTERKONTRAKT
- uttak av masteroppgave

1. Studentens personalia

Etternavn, fornavn **Sutrisno, Sutrisno**	Fødselsdato **11. feb 1984**
E-post **sutrisno2879@yahoo.com**	Telefon **45170880**

2. Studieopplysninger

Fakultet **Fakultet for Ingeniørvitenskap og teknologi**	
Institutt **Institutt for bygg, anlegg og transport**	
Studieprogram **Coastal and Marine Civil Engineering**	Studieretning **Coastal Engineering**

3. Masteroppgave

Oppstartsdato **04. feb 2013**	Innleveringsfrist **01. jul 2013**
Oppgavens (foreløpige) tittel **Numerical Analysis of Wave Transmission behind Floating Breakwaters**	
Oppgavetekst/Problembeskrivelse Wave transmission behind floating breakwaters has been studied in the specialization project last semester. The SWAN was used and the results were validated against measurement from physical model conducted in wave flume of UPC Barcelona. Continuing the specialization project topic, numerical analysis of wave transmission through and reflection against floating breakwaters will be carried out. The floating breakwaters and wave propagation will be modeled and simulated by means of WAMIT software. Output result will be compared to available measurements from model tests of the simulated breakwater. The finding from this analysis shall be used together with SWAN model should time permit.	
Hovedveileder ved institutt **Førsteamanuensis Raed Khalil Lubbad**	Medveileder(e) ved institutt **Øivind Asgeir Arntsen**
Ekstern bedrift/institusjon **Multiconsult**	Ekstern veileder ved bedrift/instutisjon **Basile Bonnemaire**
Merknader **1 uke ekstra p.g.a påske.**	

4. Underskrift

Student: Jeg erklærer herved at jeg har satt meg inn i gjeldende bestemmelser for mastergradsstudiet og at jeg oppfyller kravene for adgang til å påbegynne oppgaven, herunder eventuelle praksiskrav.

Partene er gjort kjent med avtalens vilkår, samt kapitlene i studiehåndboken om generelle regler og aktuell studieplan for masterstudiet.

Trondheim, 08.02.2013
Sted og dato

Student

Raed Lubbad
Hovedveileder

Originalen lagres i NTNUs elektroniske arkiv. Kopi av avtalen sendes til instituttet og studenten.

MASTER THESIS

(TBA4920 marine Civil Engineering, master thesis)

Spring 2013
for
Sutrisno

Numerical Analysis of Wave Transmission behind Floating Breakwaters

BACKGROUND

Floating breakwaters (FBs) have been widely used as an alternative solution to protect coastal sites especially small harbours and certain areas which are not suitable for rubble mound breakwaters. FBs characteristics and configurations alleviate some of limitations that oppose the construction of rubble mound breakwater i.e. poor foundations capability, high construction cost in deep waters, and strict requirement of water circulation in certain areas (Ruol, 2008). FBs are also preferable over rubble mound breakwater for wave energy attenuation when involving short wave periods (Ozeren, et al., 2011). The uses of FBs are considered to be economical for wave periods of less than approximately 3-5 seconds (Tørum, 2011).

Floating breakwater cannot completely stop the incident wave action (Koutandos, et al., 2005). Instead, it attenuates the wave action by partially transmitting, partially reflecting, and partially dissipating the incident wave. Energy dissipation are due to damping, friction, and eddies generation. The structure motion also generates radiated waves which are propagated in offshore and onshore directions. These cause an extremely complex hydrodynamic problem on FBs.

The efficiency of the FBs profiles and configurations can be quantified by its transmission coefficient. The transmission coefficient is defined as ratio of the significant wave height at the lee side of the FBs over the significant wave height at the front side.

Many experiments and models have been performed to study the FBs efficiency. One of them is an experiment in large-scale facility which was performed by Koutandos et al. (2005) to study the hydrodynamic interaction of regular and irregular waves with FBs in shallow and intermediate water. Several test cases with different FBs configurations and wave parameters were examined. The results showed the dependency of FBs efficiency on breakwater width to wavelength ratio and also on the breakwater draught to water depth ratio. Koutandos et al. (2005) suggested a most efficient FBs configuration without considering the cost-effectiveness.

Another experiment of FBs efficiency was conducted by Stansberg et al. (1990) as mentioned by Tørum (2011). An FB structure with specific configuration was tested in the Ocean Basin at Marintek. Resulted from this experiment, the FBs profile has to be relatively wide in relation to the wave length in order to give adequate wave attenuation and it will be uneconomical for incident wave with large periods (approximately 10-15 seconds).

The FBs efficiency experiments was also performed by Zidan et al. (2012) by examining the hydrodynamic interaction of regular waves with FBs for in intermediate and deep waters. The general finding from this experiment was the influence of FBs relative draft and width to the FBs efficiency.

From these experiments results, it can be inferred that the FBs efficiency is closely related to the incident wave length and periods. The FBs profile and configuration therefore must be designed for the specific site to take into account the longer wave that may propagate toward the site.

The aim of this master thesis is to generate a numerical model of FBs structures by means of WAMIT. The study will be focused on the wave transmission behind the FBs and the transmission coefficient resulted from the output data analysis. The structure motions as response to the incoming wave will also be studied. Furthermore, the model is expected to be a supporting tool, at a relatively lower cost compared to physical model, in designing the efficient FBs profile and configuration.

TASK DESCRIPTION

A literature survey was performed by Syltern (2004) to compare the performance of different FBs cross sections. Among other comparison methods, variation of transmission coefficients (Ct) against relative width to wavelength (W/L) of each FB was compared. An experimental study of FBs was also performed by Syltern (2005) as his master thesis work. These study reports and data will be the main reference of numerical model generation in this master thesis study.

The works that will be carried out during this study is as following;
1. Generating a numerical model of wave transmission behind FBs and FBs motion response motions by using WAMIT.
2. Validating result of generated model with available measurement data.
3. Using the result in combination with SWAN model should time permits.
4. Performing sensitivity analysis by applying varied wave period, wave direction, and FBs degree of freedom.

REFERENCES

Koutandos, E., Prinos, P. & Gironella, X., 2005. Floating breakwaters under regular and irregular wave forcing: reflection and transmission characteristics. *Journal of Hydraulic Research,* Vol. 43(Iss. 2), pp. 174-188.

Ozeren, Y. et al., 2011. Experimental Investigation of Cylindrical Floating Breakwater Performance with Various Mooring Configurations. *Journal of Waterway, Port, Coastal, and Ocean Engineering,* 137(6), pp. 300-309.

Ruol, P., 2008. *Vlaams Instituut voor de Zee*. [Online]
Available at: http://www.vliz.be/wiki/Floating_breakwaters
[Accessed 19 February 2013].

Syltern, J. A., 2004. Floating Breakwaters – A literature Survey. Trondheim.

Tørum, A., 2011. Coastal Structures: Lecture Notes. Trondheim.

Zidan, A. R., Rageh, O. S., Sarhan, T. E. & El-Sharabasy, M. M., 2012. *Wave Interaction with Single and Twin Pontoon*. Istanbul, Turkey, IWTC 16.

General about content, work and presentation

The text for the master thesis is meant as a framework for the work of the candidate. Adjustments might be done as the work progresses. Tentative changes must be done in cooperation and agreement with the professor in charge at the Department.

The reporting of the work should be academic anchored and well described with respect to the theoretical and scientific basis so that the work could be implemented in the field of international research.

In the evaluation thoroughness in the work will be emphasized, as will be documentation of independence in assessments and conclusions. Furthermore the presentation (report) should be well organized and edited; providing clear, precise and orderly descriptions without being unnecessary voluminous.

The report shall include:

- Standard report front page (from DAIM, http://daim.idi.ntnu.no/)
- Title page with abstract and keywords.(template on: http://www.ntnu.no/bat/skjemabank)
- Preface
- Summary and acknowledgement. The summary shall include the objectives of the work, explain how the work has been conducted, present the main results achieved and give the main conclusions of the work.
- Table of content including list of figures, tables, enclosures and appendices.
- If useful and applicable a list explaining important terms and abbreviations should be included.
- The main text.
- Clear and complete references to material used, both in text and figures/tables. This also applies for personal and/or oral communication and information.
- Text of the Thesis (these pages) signed by professor in charge as Attachment 1..
- The report musts have a complete page numbering.

Advice and guidelines for writing of the report is given in: "Writing Reports" by Øivind Arntsen. Additional information on report writing is found in "Råd og retningslinjer for rapportskriving ved prosjekt og masteroppgave ved Institutt for bygg, anlegg og transport" (In Norwegian). Both are posted on http://www.ntnu.no/bat/skjemabank

Submission procedure

Procedures relating to the submission of the thesis are described in DAIM (http://daim.idi.ntnu.no/). Printing of the thesis is ordered through DAIM directly to Skipnes Printing delivering the printed paper to the department office 2-4 days later. The department will pay for 3 copies, of which the institute retains two copies. Additional copies must be paid for by the candidate.

On submission of the thesis the candidate shall submit a CD with the paper in digital form in pdf and Word version, the underlying material (such as data collection) in digital form. Students must submit the submission form (from DAIM) where both the Ark-Bibl in SBI and Public Services (Building Safety) of SB II has signed the form. The submission form including the appropriate signatures must be signed by the department office before the form is delivered Faculty Office.

Documentation collected during the work, with support from the Department, shall be handed in to the Department together with the report.

According to the current laws and regulations at NTNU, the report is the property of NTNU. The report and associated results can only be used following approval from NTNU (and external cooperation

partner if applicable). The Department has the right to make use of the results from the work as if conducted by a Department employee, as long as other arrangements are not agreed upon beforehand.

Tentative agreement on external supervision, work outside NTNU, economic support etc.
Separate description to be developed, if and when applicable. See http://www.ntnu.no/bat/skjemabank for agreement forms.

Health, environment and safety (HSE) http://www.ntnu.edu/hse
NTNU emphasizes the safety for the individual employee and student. The individual safety shall be in the forefront and no one shall take unnecessary chances in carrying out the work. In particular, if the student is to participate in field work, visits, field courses, excursions etc. during the Master Thesis work, he/she shall make himself/herself familiar with " Fieldwork HSE Guidelines". The document is found on the NTNU HMS-pages at http://www.ntnu.no/hms/retningslinjer/HMSR07E.pdf

The students do not have a full insurance coverage as a student at NTNU. If you as a student want the same insurance coverage as the employees at the university, you must take out individual travel and personal injury insurance.

Start and submission deadlines
The work on the Master Thesis starts on (date) 04 February 2013

The thesis report as described above shall be submitted digitally in DAIM at the latest (date) 01 July 2013 at 3pm.

Professor in charge: Raed Khalil Lubbad

Other supervisors: Øivind Asgeir Arntsen, Basile Bonnemaire

Trondheim, 05.03.2013.

_____
Professor in charge (sign)

I dedicate this thesis to Mama Frida and Mas Banyu for their endless love and to my family for their priceless support

Trondheim, 22-06-2013

PREFACE

This report is to present the study result of numerical analysis of floating breakwaters during the master thesis. Two software, which were new to author, were used to perform the study. Lots of times were spent at the beginning of the study to learn, have experiences, and gain some confidence in operating the software.

Total of three models of floating breakwaters with twelve different configurations were numerically analyzed. These cases were based on two laboratory experiments performed by Koutandos et al. (2005) and Syltern (2005). Initially, more cases were considered to be analyzed including the combination of parabolic beach, increasing width and draft of the breakwaters, and changing the incident wave direction. However, due to a very limited time, some of the cases were cancelled and considered to be done in future work.

The study was focused on the transmitted wave behind the breakwater and response motions of the structure. The breakwaters were assumed to be subjected to regular waves. It is sufficient since the results in irregular seas are possible to be obtained by linearly superposing results from regular wave components. The transmission coefficients as a definition parameter of floating breakwater efficiency were calculated and compared to the available experiment data.

The report consists of brief introduction to the topic and basic theories that related to the study. Cases detail and analysis procedures were presented as well as the output plot, calculated transmission coefficient, and the breakwater response amplitude operators. The conclusion of study was presented on the last chapter following the result analysis and discussions.

ACKNOWLEDGEMENTS

I would like to express my sincere gratitude to the CoMEM committee for letting me fulfill my dream of being a student here. To my thesis supervisor, Raed Lubbad, I am fully indebted for his guidance, patience, understanding, encouragement and for his enthusiasm during this study. To my thesis co-supervisors Øivind Asgeir Arntsen and Basile Bonnemarie, I am extremely grateful for their assistance and priceless suggestions throughout my thesis. To the staff of Department of Civil and Transport Engineering, thank you. To all my family, CoMEM students year 2011-2013, and all friends for motivating and helping me survive all the stress from this years and supporting me endlessly. Thank you.

TABLE OF CONTENTS

LIST OF SYMBOLS

General

Subscripts *i* generally denotes direction in generalized force direction *i*. Here *i* = 1, 2, 3 denotes x-, y-, and z-direction respectively and *i* = 4, 5, 6 denotes the moment components about the same axes. These *i* directions (or degrees of freedom) are denoted; 1 = surge, 2 = sway, 3 = heave, 4 = roll, 5 = pitch, 6 = yaw.

Roman symbols

A	Incoming wave amplitude
A_{ii}	Added mass coefficient
B_{ii}	Damping coefficient
C_{ii}	Hydrostatic and gravity restoring coefficient
Cr	Reflection coefficient
Ct	Transmission coefficient
g	Gravitational acceleration
H_i	Incident wave height
H_r	Reflected wave height
H_t	Transmitted wave height
h	Wave pool depth
I_{xx}	Mass moment of inertia about the x-axis
I_{yy}	Mass moment of inertia about the y-axis
I_{zz}	Mass moment of inertia about the z-axis
K	Mooring stiffness matrix
k_H	Vertical component of mooring stiffness coefficient
k_Z	Horizontal component of mooring stiffness coefficient
k_{mm}	Stiffness coefficient of each mooring line in a spread system mooring
L_c	Characteristic length use in WAMIT
l	Total length of mooring line
ls	Length of mooring line from ground touch point to mooring line connection on FBs
M_{ii}	Mass coefficient
r_x, r_y, r_z	Radii of gyration about the x-, y-, and z-axis, respectively
T	Incoming wave period
T_{ni}	Natural periods
T_Z	Vertical component of mooring line tension
T_H	Horizontal component of mooring line tension
T_M	Mooring line tension
X	Horizontal distance between the anchor and mooring line connection on FBs
x	Horizontal distance between ground touch point of mooring line and mooring line connection on FBs

x_m, y_m	Coordinates of mooring line connection on FBs in respect to its coordinate system
W	FBs width
w	Mooring line unit weight

Greek symbols

$\bar{\eta}$	Non-dimensional free surface elevation
η	Dimensional free surface elevation
ρ	Water density
ξ_1, ξ_2, ξ_3	Surge, sway, and heave motion
ξ_4, ξ_5, ξ_6	Roll, pitch, and yaw motion
$\bar{\xi}_i$	Non-dimensional translational motion
ξ_i	Dimensional translational motion
ψ_m	Angle between the mooring line and the x-axis
ω_{ni}	Natural frequencies
ω	Incoming wave frequency

Abbreviations

2D	Two Dimensions
ASCII	American Standard Code for Information Interchange
CoG	Center of Gravity
FBs	Floating Breakwaters
FRC	Force Control File
GDF	Geometric Data File
POT	Potential Control File
RAOs	Response Amplitude Operators
WG	Wave Gauge

LIST OF TABLES

LIST OF FIGURES

1. INTRODUCTION

1.1 Background

Floating breakwaters (FBs) have been widely used as an alternative solution to protect coastal sites especially small harbors and certain areas which are not suitable for rubble mound breakwaters. FBs characteristics and configurations alleviate some of limitations that oppose the construction of rubble mound breakwater i.e. poor foundations capability, high construction cost in deep waters, and strict requirement of water circulation in certain areas (Ruol, 2008). FBs are also preferable over rubble mound breakwater for wave energy attenuation when involving short wave periods (Ozeren, et al., 2011). The uses of FBs are considered to be economical for wave periods of less than approximately 3-5 seconds (Tørum, 2011).

Floating breakwater cannot completely stop the incident wave action (Koutandos, et al., 2005). Instead, it attenuates the wave action by partially transmitting, partially reflecting, and partially dissipating the incident wave. Energy dissipation are due to damping, friction, and eddies generation. The structure motion also generates radiated waves which are propagated in offshore and onshore directions. These cause an extremely complex hydrodynamic problem on FBs.

The efficiency of the FBs profiles and configurations can be quantified by its transmission coefficient. The transmission coefficient is defined as ratio of the significant wave height at the lee side of the FBs over the significant wave height at the front side.

Many experiments and models have been performed to study the FBs efficiency. One of them is an experiment in large-scale facility which was performed by Koutandos et al. (2005) to study the hydrodynamic interaction of regular and irregular waves with FBs in shallow and intermediate water. Several test cases with different FBs configurations and wave parameters were examined. The results showed the dependency of FBs efficiency on breakwater width to wavelength ratio and also on the breakwater draught to water depth ratio. Koutandos et al. (2005) suggested a most efficient FBs configuration without considering the cost-effectiveness.

Another experiment of FBs efficiency was conducted by Stansberg et al. (1990) as mentioned by Tørum (2011). An FB structure with specific configuration was tested in the Ocean Basin at Marintek. Resulted from this experiment, the FBs profile has to be relatively wide in relation to the wave length in order to give adequate wave attenuation and it will be uneconomical for incident wave with large periods (approximately 10-15 seconds).

The FBs efficiency experiments was also performed by Zidan et al. (2012) by examining the hydrodynamic interaction of regular waves with FBs for in intermediate and deep waters. The general finding from this experiment was the influence of FBs relative draft and width to the FBs efficiency.

From these experiments results, it can be inferred that the FBs efficiency is closely related to the incident wave length and periods. The FBs profile and configuration therefore must be designed properly to take into account the longer wave that may propagate toward the site.

1.2 Objective

The aim of this master thesis is to perform a numerical analysis of FBs efficiency by means of WAMIT and MultiSurf. The study is focused on the wave transmission behind the FBs and the transmission coefficient resulted from the output data analysis. The structure motions as response to the incoming wave is also studied. Furthermore, the model is expected to be a supporting tool, at a relatively lower cost compared to physical model, in designing the efficient FBs profile and configuration.

The analysis is generally carried out in three steps; WAMIT input files preparation, WAMIT computation, and WAMIT output processing. The input files preparation is involving hand calculations of model center of gravity, radii of gyration, and mooring stiffness matrices, and development of the model body geometry by MultiSurf. The WAMIT computation is done by using Windows command prompt to execute all the input files. The output processing is done to calculate the wave height and model motion from non-dimensional output given by WAMIT in Excel spreadsheets and Matlab environment.

1.3 Scope of works

Experimental studies of FBs were performed by Syltern (2005) and Koutandos et al. (2005) to compare the performance of different FBs configurations. Among other comparison methods, variation of transmission coefficients (*Ct*) against relative width to wavelength (*W/L*) of each FB was compared. These study reports and data are the main reference of numerical model generation in this master thesis study.

The works that is carried out during this study consist of generating a numerical model of wave transmission behind FBs and FBs motion response motions by using WAMIT and MultiSurf, and validating the result with available measurement data.

1.4 Report structure

The thesis background, objective, and scope of works are explained in Chapter 1. Basic theory is presented in Chapter 2. The cases, software, and method used in the analysis are given in Chapter 3. The output plot and calculated transmission coefficient and response amplitude operators are presented in Chapter 4. Conclusion and recommendation for future work are given in Chapter 5.

2. BASIC THEORY

2.1 Floating breakwaters response in regular waves

Analyzing the interaction between floating breakwater and an incident regular wave is very useful since the response of the breakwater to irregular seas is possible to be obtained by linearly superposing results from regular wave components (Faltinsen, 1990). The hydrodynamic analysis of floating breakwaters in incident regular waves is usually conducted in the frequency domain and quite often is based on linear wave theory. In this linear analysis, the floating breakwater is subjected to small amplitude motions which oscillate in all six degrees of freedom corresponding to surge, sway, heave, roll, pitch, and yaw, respectively.

The origin of the global coordinate system is usually placed on the free surface. While the body fixed coordinate system can be defined as a right-handed Cartesian coordinate system (x, y, z) stationary with respect to the global coordinate system and the floating breakwater. For the simplicity, the body origin is located on the center of gravity of the breakwater with positive z vertically upwards. The breakwater is symmetrical to the x-z plane.

The translational displacements in the x-, y-, and z-directions with respect to the origin are defined as ξ_1, ξ_2, and ξ_3 corresponding to surge, sway, and heave displacement, respectively. While the rotational motions about the x-, y-, and z-axis are defined as ξ_4, ξ_5, and ξ_6 corresponding to roll, pitch, and yaw angle, respectively. The coordinate system and the translational and rotational motions are shown for the case of a moored box pontoon floating breakwater in Figure 2.1 below.

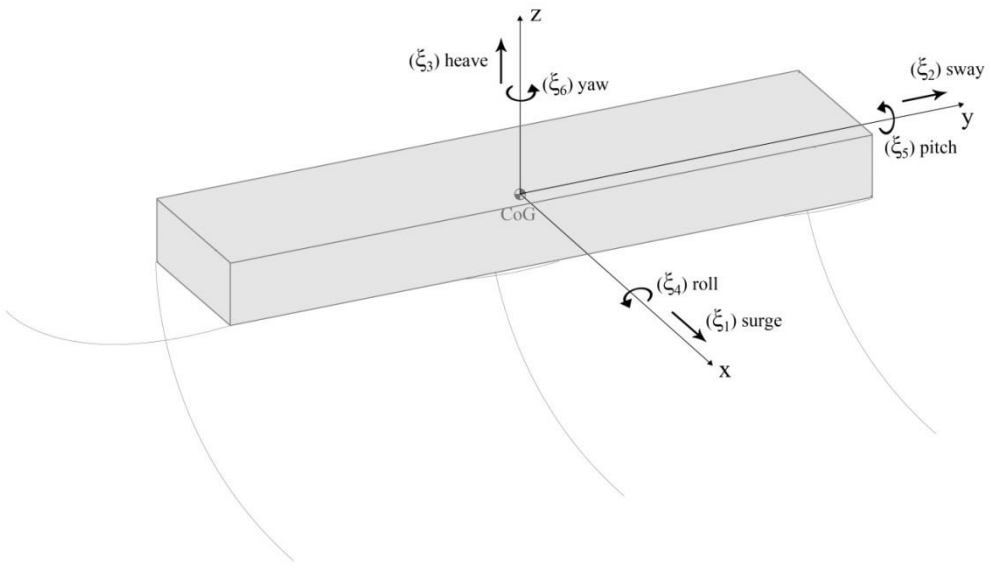

Figure 2.1 Coordinate system and motions of pontoon floating breakwater

The response amplitudes of floating breakwater motions ξ_j are obtained from the solution of below Equation 2.1.

$$\sum_{j=1}^{6}\left[-\omega^2\left(M_{ij}+M_{ij}^{E}+A_{ij}\right)+i\omega\left(B_{ij}+B_{ij}^{E}\right)+\left(C_{ij}+K_{ij}^{E}\right)\right]\xi_j = X_i \qquad \textbf{(2.1)}$$

where ω is the incident wave frequency, M_{ij} are the coefficients of the mass matrix of the body, A_{ij} and B_{ij} are the coefficients of the added mass matrix and damping matrix, and C_{ij} are the coefficients of hydrostatic and gravitational matrix. B_{ij}^{E} are the coefficients of the damping matrix caused by an external force (i.e. drag damping of the mooring lines and viscous damping) and K_{ij} are the coefficients of the external stiffness matrix caused by the mooring lines.

As an illustration of the concept of the added mass, considering in a forced harmonic heave emotion of a structure, the heave motion causes the surrounding fluid to oscillate which means there is a pressure field in the fluid. The whole fluid will oscillate with different fluid particle amplitudes throughout the fluid. For simplicity, this can be modeled as some volume of the fluid moving with the body and the amplitudes of the fluid at some degrees are negligible.

Added mass and damping coefficients consist of 36 coefficients each, half of which are zero for a structure where the submerged part has one vertical symmetry plane (Faltinsen, 1990). These coefficients are a function of body form, frequency of oscillation and forward speed. These are also influenced by other factors like finite water depth and restricted water area.

The response of the floating breakwater in each degree of freedom is expressed in terms of the response amplitude operator shown by below Equation 2.2.

$$RAO_j = \frac{\xi_j}{A} \qquad \textbf{(2.2)}$$

where A is the amplitude of the incident wave and $j = 1, \ldots, 6$.

2.2 Mooring line stiffness

The effect of the mooring line on the response of the floating breakwater is incorporated to the response motion by adding the stiffness coefficients of the mooring lines into the motion equation. The complete 6 X 6 stiffness coefficient matrix of the mooring lines is derived in six degrees of freedom based on the differential changes of mooring lines tensions caused by the static motions of floating breakwater. The stiffness is calculated in breakwater static average position, under the action of steady drift force.

In a mooring system, numbers of cables are attached to the floating breakwater at different points connecting the structure to the anchors at sea bed. The mooring system normally used to hold the breakwater in the desired location is a spread mooring system where several pre-tensioned anchor lines are arrayed around the breakwater. The anchors are usually can be easily moved implies that the anchor is restricted to a small vertical forces (Faltinsen, 1990). A significant part of the anchor lines should lie on the sea bed to ensure that the anchors are kept in position. Example of spread mooring system is shown in Figure 2.2.

The mooring lines can be made up of chain, rope, or combination of both. Segmented mooring lines are normally used to get a heavy line at the bottom and a light line close to the water surface. Comparing to the use of chain or rope alone, this mooring lines give greater stiffness and lighter mooring lines.

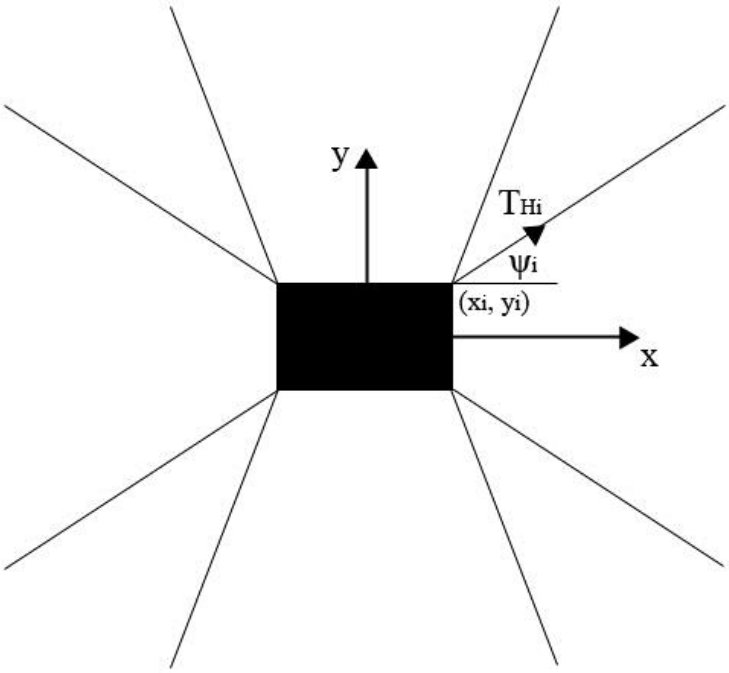

Figure 2.2 Spread mooring system (Faltinsen, 1990)

According to Faltinsen (1990), the mooring line analysis can be performed statically by assuming a horizontal sea bed and neglecting the bending stiffness and dynamic effects of the mooring lines. The line tension then can be calculated by following Equation 2.3.

$$T_M = T_H + wh + (w + \rho g A)z \quad \textbf{(2.3)}$$

where T_M the mooring line tension, T_H horizontal component of mooring line tension, w is the mooring line unit weight, h is the water depth, ρ is the water density, g is the gravitational acceleration, A the amplitude of incident wave, and z is the location of the observed point in z-axis.

The use of Equation 2.4 which expresses the relation between X and T_H resulting horizontal forces from the mooring line on the floating breakwater as a function of the horizontal distance X between the anchor and the point where the anchor line is connected to the breakwater. The illustration of the mooring lines and its tension components and parameters is shown in Figure 2.3 below.

$$X = l - h\left(1 + 2\frac{a}{h}\right)^{1/2} + a\cosh^{-1}\left(1 + \frac{h}{a}\right) \tag{2.4}$$

where $a = T_H/w$.

In a spread mooring system, the relationship between mean external loads on the vessel and its position is calculated by considering the contributions from each cable line separately. To find the linear restoring effects due to the mooring lines stiffness, following equations can be utilized.

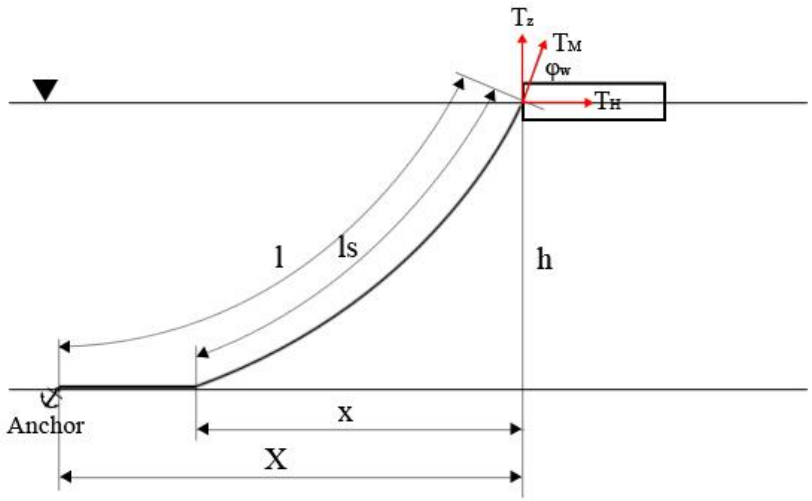

Figure 2.3 Mooring line configuration (Faltinsen, 1990)

$$K_{11} = \sum_{i=a}^{f} k_{Hi}\cos^2\psi_i \tag{2.5}$$

$$K_{22} = \sum_{i=a}^{f} k_{Hi} \sin^2 \psi_i \tag{2.6}$$

$$\mathbf{K_{33}} = \sum_{\mathbf{i=a}}^{\mathbf{f}} \mathbf{k_{Zi}} \tag{2.7}$$

$$K_{66} = \sum_{i=a}^{f} k_{Hi} \left(x_i \sin \psi_i - y_i \cos \psi_i\right)^2 \tag{2.8}$$

$$K_{26} = C_{62} = \sum_{i=a}^{f} k_{Hi} \left(x_i \sin \psi_i - y_i \cos \psi_i\right) \sin \psi_i \tag{2.9}$$

The coupling coefficients K_{16}, K_{61}, K_{12}, and K_{21} are zero since the mooring arrangement is symmetric about the *x*-*z* plane. Values of k_H and k_Z are given by following Equation 2.10.

$$k = w \left[\frac{-2}{\left(1 + 2\frac{a}{h}\right)^{1/2}} + \cosh^{-1}\left(1 + \frac{h}{a}\right) \right]^{-1} \tag{2.10}$$

2.3 Natural frequencies

The natural frequencies are one of the important parameter in assessing the response amplitude operator of the floating breakwater. If the floating breakwaters are subjected to incident wave with oscillation periods or frequencies that close to the natural frequencies, relatively large motions are likely to occur (Faltinsen, 1990).

The natural frequencies of floating breakwater in each degree of freedom are determined by the weight distribution of the breakwater (Fossen, 2011). The natural frequencies are independent of the origin if they are computed in a linear system using the six degrees of freedom coupled equations of motion. As opposed to this, the decoupled natural frequencies computation can be erroneous since the eigenvalues of the decoupled equations depend on the coordinate origin. However, according to Fossen (2011), the values of natural frequencies computed by coupled and decoupled equations are close to each other. Therefore the decoupled natural frequencies are considered as a representative parameter in assessing the response motions in this analysis.

The natural frequencies of heave, roll, and pitch are given by Equation 2.11 to Equation 2.13 as following.

$$\omega_{n3} = \sqrt{\frac{C_{33}}{m + A_{33}(\omega_{heave})}} \quad \textbf{(2.11)}$$

$$\omega_{n4} = \sqrt{\frac{C_{44}}{I_x + A_{44}(\omega_{roll})}} \quad \textbf{(2.12)}$$

$$\omega_{n5} = \sqrt{\frac{C_{55}}{I_y + A_{55}(\omega_{pitch})}} \quad \textbf{(2.13)}$$

where the ω_{n3}, ω_{n4}, and ω_{n5} are the natural frequencies of heave, roll, and pitch motions, respectively. A_{ii} and C_{ii} are the added mass and restoring coefficient for each degree of motion. I_x and I_y are the mass moment of inertia about the x- and y-axis and m is the mass coefficient.

2.4 Efficiency of floating breakwaters

Floating breakwaters attenuate the incident wave height by partially transmitting, partially reflecting and partially dissipating the incident wave. Energy dissipation are due to damping, friction, and eddies generation. The structure motion also generates radiated waves which are propagated in offshore and onshore directions. The efficiency of the floating breakwater is given by transmission coefficient (*Ct*). *Ct* is defined as a ratio between the incoming wave height and the transmitted wave height.

In addition, reflection coefficient (*Cr*) of the breakwater can also be used in assessing the floating breakwater efficiency. This coefficient is defined as a ratio between the reflected wave height with incoming wave height. *Ct* and *Cr* are calculated by following equations.

$$C_t = \frac{H_t}{H_i} \quad \textbf{(2.14)}$$

$$C_r = \frac{H_r}{H_i} \quad \textbf{(2.15)}$$

where H_t is the height of the transmitted wave, H_r is the height of the reflected wave, and H_i is the height of incident wave height.

3. CASES AND PROCEDURES

3.1 Cases

The starting point for the floating breakwater models analyzed in this thesis is two laboratory experiments conducted by Koutandos, et al. (2005) and Syltern (2005). The experiment by Koutandos, et al. (2005) was performed to study the hydrodynamic interaction of regular and irregular wave with floating breakwaters in shallow and intermediate waters. Several test cases with different configurations and generated waves parameters were examined.

The experiment by Syltern (2005) was performed to find the best floating breakwater profile and configurations to sell and distribute in Norway and international market. The basic configurations were provided by a marina manufacturer and supplier company in Norway. It was then expanded into various configuration with increasing width, draft, and combination with parabolic beach structures.

Some of the cases from both experiments were referred in this thesis and explained in Section 3.1.1 to Section 3.1.3. The cases summary is presented in Table 3.1 below. Case 13 was cancelled due to limited time and considered to be carried out on further work.

Table 3.1 Cases summary

Cases No.	Configuration	Incident Wave Height	Wave Periods
1	2D model - fixed (draft = 0.4 m)	0.2 m	2.04 s - 9.17 s
2	2D model - fixed (draft = 0.5 m)	0.2 m	2.04 s - 9.17 s
3	2D model - fixed (draft = 0.65 m)	0.2 m	2.04 s - 9.17 s
4	Molo model - free floating	0.6 m	1.00 s - 20.00 s
5	Molo model - vertical restrained	0.6 m	1.00 s - 20.00 s
6	Molo model - fixed	0.6 m	1.00 s - 20.00 s
7	Molo model – heave only	0.6 m	1.00 s - 20.00 s
8	Molo model - moored	0.6 m	1.00 s - 20.00 s
9	Maere model - free floating	0.6 m	1.00 s - 20.00 s
10	Maere model - vertical restrained	0.6 m	1.00 s - 20.00 s
11	Maere model - fixed	0.6 m	1.00 s - 20.00 s
12	Maere model – heave only	0.6 m	1.00 s - 20.00 s
13	Maere model – moored (*CANCELLED*)	0.6 m	1.00 s - 20.00 s

In addition to these cases, in order to have an experience operating software used in the floating breakwater analysis, some exercise cases were carried out. The cases standard outputs were given by WAMIT developer for model calibration. The exercises were done by rebuilding the geometry structure in MultiSurf from scratch, executing the computation by WAMIT, and comparing the results with the standard outputs. Some times were spent at the beginning of the study to obtain the correct results.

3.1.1 2D model

The experiment by Koutandos, et al. (2005) was performed in large-scale facility and wave flume with dimensions of 100 m length, 5 m depth, and 3 m width. The floating breakwaters were box shaped with 2 m width, 1.5 m height, and 2.8 m length.

The breakwater was fixed to the wall of flume hence no motions were allowed during the experiment. Three different drafts were used 0.4 m, 0.5 m, and 0.65 m. A regular wave with wave height of 0.2 m was used. The shortest wave period was 2.04 s and the longest was 9.17 s. The floating breakwater model is shown in Figure 3.1.

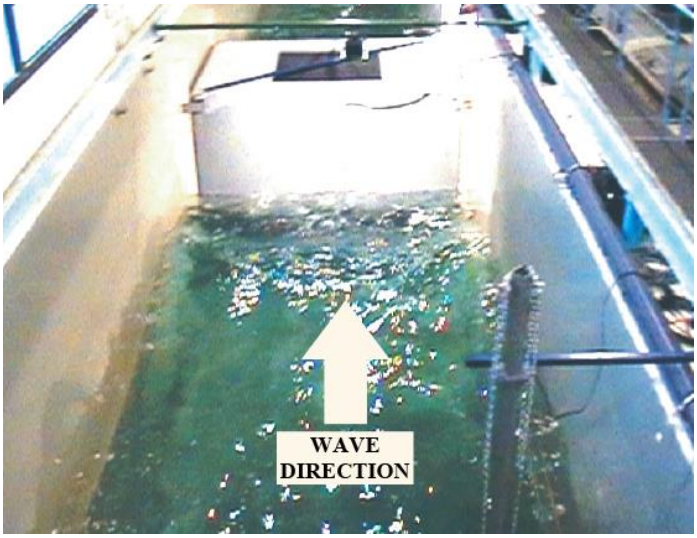

Figure 3.1 2D model in the wave flume (Koutandos, et al., 2005)

3.1.2 Molo model

The experiment by Syltern (2005) was performed with model scale of 1:10 in a wave pool with depth of 0.6 m. Two type of models were tested; Molo and Maere model. Molo model was constructed from 2 units of pontoons with total dimensions of 4 m length, 0.4 m width, and 0.2 m height. It was constructed as bottomless boxes of steel plate with thickness of 3 mm and polystyrene as the floating element. Two internal plates were installed on each pontoon dividing the pontoon into three equal spaces.

After being submerged for a long time, pontoons weight on air is approximately each 50 kg, indicating the polystyrene saturated with water. Several sea conditions with irregular waves were used in the experiment. However, a regular wave with wave height of 0.6 m and normal direction was selected and considered representative for the numerical models. The shortest wave period was 1.00 s and the longest was 20.00 s, with total of twenty wave frequencies were examined. The model is shown in Figure 3.2.

Five different model configurations of were used in the analysis; free floating, vertical restrained (heave, pitch, and roll are restrained), fixed, heave only, and anchored.

3.1.3 Maere model

Maere model is constructed from 7 units of pontoons with configuration of longitudinal and transversal pontoons. The pontoon dimension is 1.5 m length, 0.24 m width, and 0.16 m height. It is constructed as bottomless boxes of steel plate with thickness of 3 mm and polystyrene as the floating element. Two internal plates were installed on each pontoon dividing the pontoon into three equal spaces.

Total weight of each pontoon is approximately 25.8 kg. Similar to Molo model, several sea conditions with irregular waves were used in the experiment but only regular wave with wave height of 0.6 m and normal direction was selected for the numerical models. The shortest wave period was 1.00 s and the longest was 20.00 s, with total of twenty wave frequencies were examined. The model is shown in Figure 3.2.

Similar to Molo model, five different model configurations were used in the analysis; free floating, vertical restrained (heave, pitch, and roll are restrained), fixed, heave, and anchored.

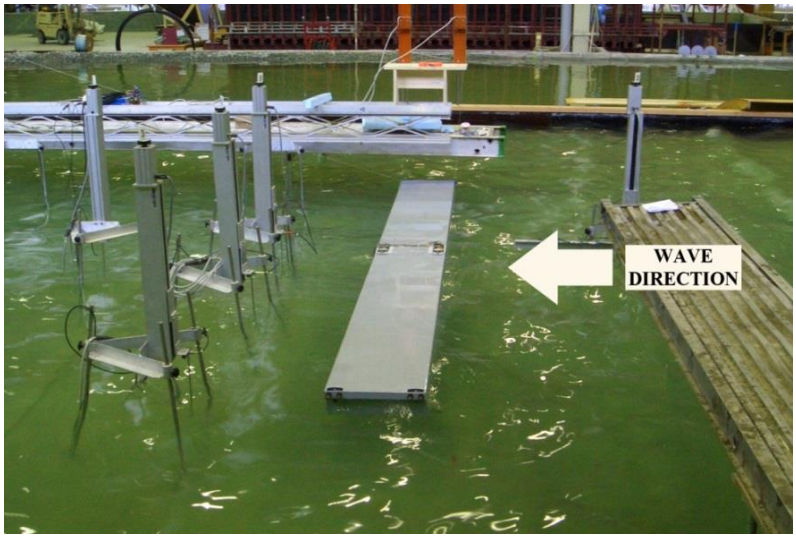

Figure 3.2 Molo model in the wave pool (Syltern, 2005)

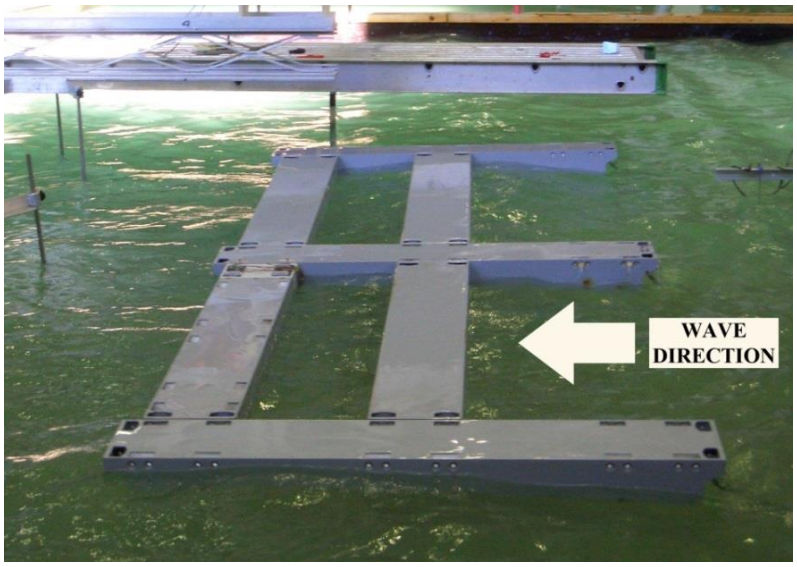

Figure 3.3 Molo model in the wave pool (Syltern, 2005)

3.2 Software

3.2.1 WAMIT V6.4

WAMIT version 6.4 was used on this master thesis to compute the wave height transmission and the response motion of the floating breakwaters. It is a radiation and diffraction panel program developed for the linear analysis of the interaction of waves with submerged or floating structures. A variety of options permit the dynamic analysis of bodies which are freely floating, restrained, or fixed in position. The radiation and diffraction velocity potentials on the body wetted surface are determined from the solution of an integral equation obtained by using Green's theorem with the free-surface source-potential as the Green function (WAMIT, 1998-2006).

There are two computation method available in WAMIT; low-order and high-order method. The high-order method was selected since it provides a more accurate solution, with smaller number of unknowns, compared to the low-order method. Specifically for case analysis in this thesis, it represents the floating breakwaters by geometry models developed in MultiSurf.

The different use of the word *order* here should be noted to avoid confusion. Following the usual conventions of marine hydrodynamics, first-order and second-order are always used to refer to linearization of the boundary conditions and solution, whereas low-order and high-order are used to refer to the method for representation of the body surface and solution.

WAMIT consists of two principal subprograms which normally are run sequentially; POTEN and FORCE. POTEN solves the velocity potential on the body surface and FORCE evaluates physical parameter including the force and motion coefficients, and field data including the fluid pressure, velocity, and free-surface elevation. Detail input files for both subprograms are explained in Section 3.3.4.

3.2.2 MultiSurf V8.2

By using WAMIT version V6.4, there is an option to link WAMIT with MultiSurf by Relational Geometry Kernel (RGKernel). In this option, a wide variety of body geometries are represented by MultiSurf and it can be input directly in the high-order method of WAMIT computation. Main advantages of this option are (a) the geometry representation is developed using the CAD environment of MultiSurf and (b) this representation can be input directly to WAMIT without significant effort or approximation (WAMIT, 1998-2006).

MultiSurf version 8.2 was used on this master thesis. A special procedure is available to create geometry input files for WAMIT. Basically, two output files from MultiSurf are required for WAMIT. Detail explanation of these files is given in Section 3.3.3.

3.3 Procedures

In general, the analysis was carried out in three steps; WAMIT input files preparation, WAMIT computation, and WAMIT output processing. The input files preparation involved hand calculations of model center of gravity, radii of gyration, and mooring stiffness matrices, and development of the model body geometry. The WAMIT computation was done by using Windows command prompt to execute all the input files. The output processing consisted of calculation of wave height and model motion from non-dimensional output given by WAMIT in Excel spreadsheets and Matlab environment.

3.3.1 Calculation of center of gravity (CoG) and radii of gyration

Calculation of center of gravity (CoG) and radii of gyration of Molo and Maere models are detailed in Appendix A. Two approaches of body representation are used in Molo model calculation to check its effect on the analysis results. In the first approach (Figure 3.4) the model is considered as one rigid composite body consists of steel plate, polystyrene, and amount of water filled the open compartment on the bottom model which moves along with the model. Whereas in the second approach (Figure 3.5) the amount of water filled the bottom open compartment is no longer considered.

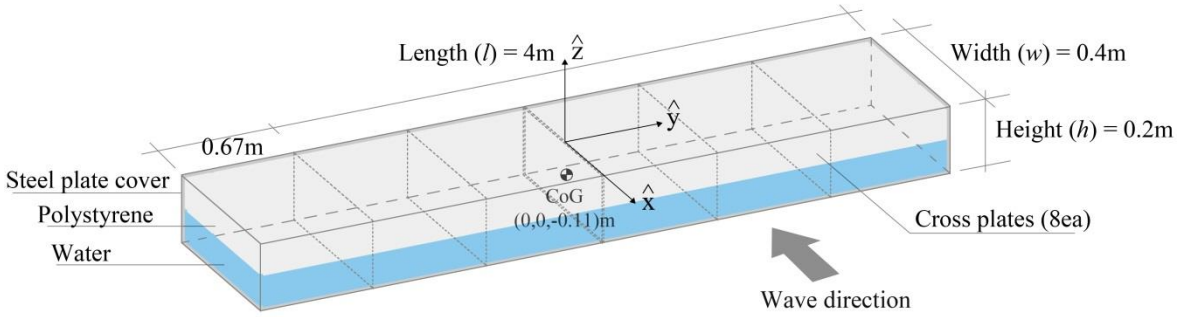

Figure 3.4 Molo model perspective (approach 1)

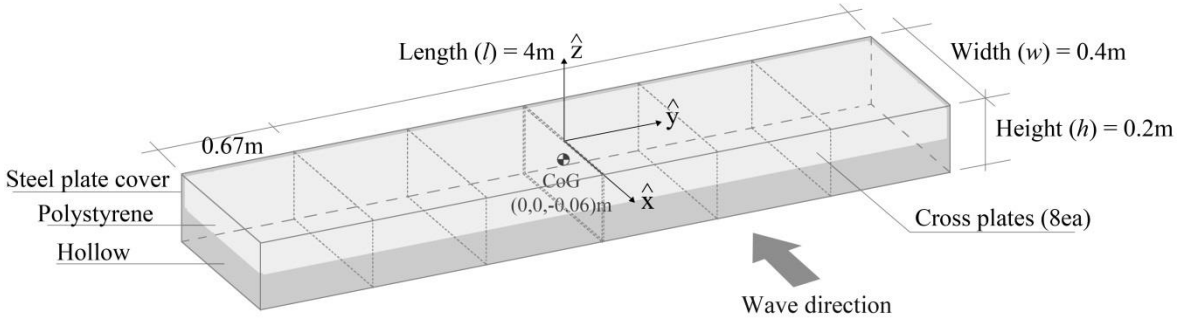

Figure 3.5 Molo model perspective (approach 2)

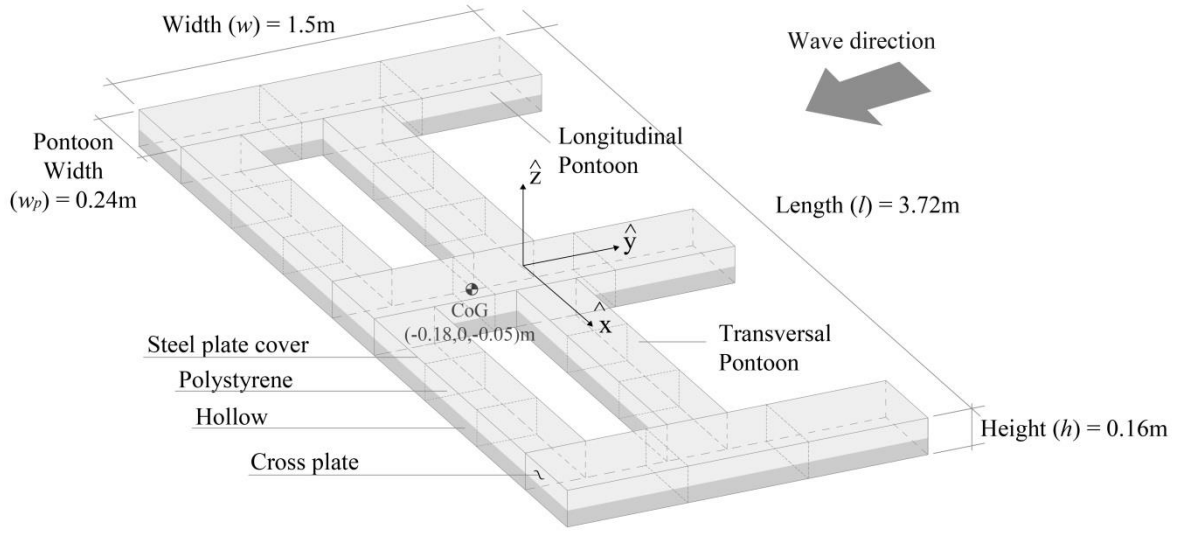

Figure 3.6 Maere model perspective

Comparing the analysis results using both approaches, it found that the results are qualitatively comparable in terms of wave diffraction, wave attenuation, and wave riding breakwater occurrence on certain incident wave conditions. Consequently, the second approach is used in further modeling and Maere model calculation (Figure 3.6) since it is representing the model more accurately. Summary of calculated radii of gyration is given in Table 3.2.

Table 3.2 Summary of calculated radii of gyration

Model	Radii of gyration relative to CoG		
	r_x (m)	r_y (m)	r_z (m)
Molo model (approach 1)	1.16	0.14	0.23
Molo model (approach 2)	1.83	0.17	0.25
Maere model	1.19	0.42	0.012

3.3.2 Calculation of mooring stiffness matrix

In order to have a comparable numerical model result with experiment by Syltern (2005), a moored Molo model configuration is analyzed.

Figure 3.7 and Figure 3.8 show the mooring configuration and spread mooring system of the breakwater Molo model. The mooring lines consisted of chain and rope with different total length for each middle and end mooring lines. The chain was galvanized and its weight was 235 grams per meter. Other parameters for the mooring lines are provided in Appendix B.

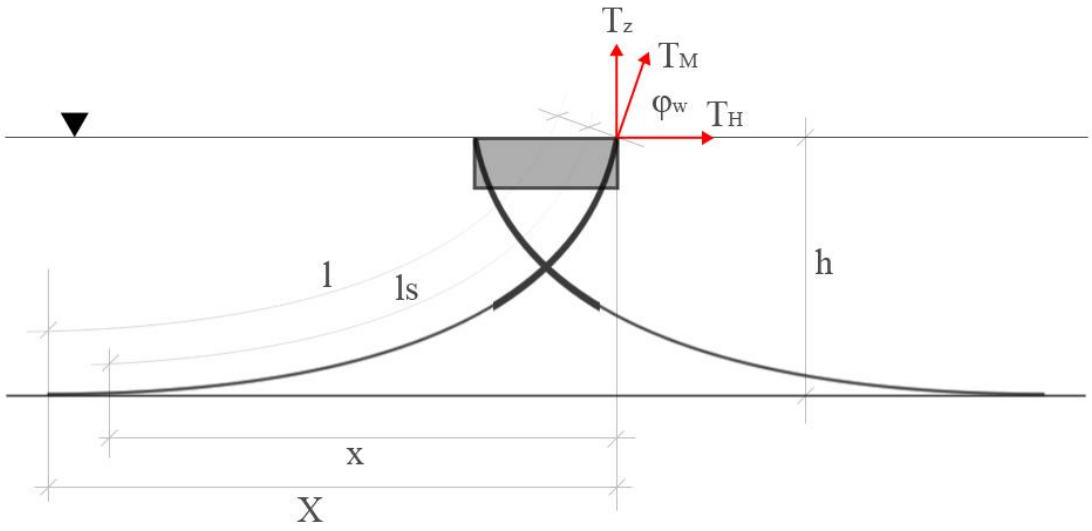

Figure 3.7 Molo model mooring configuration (side view)

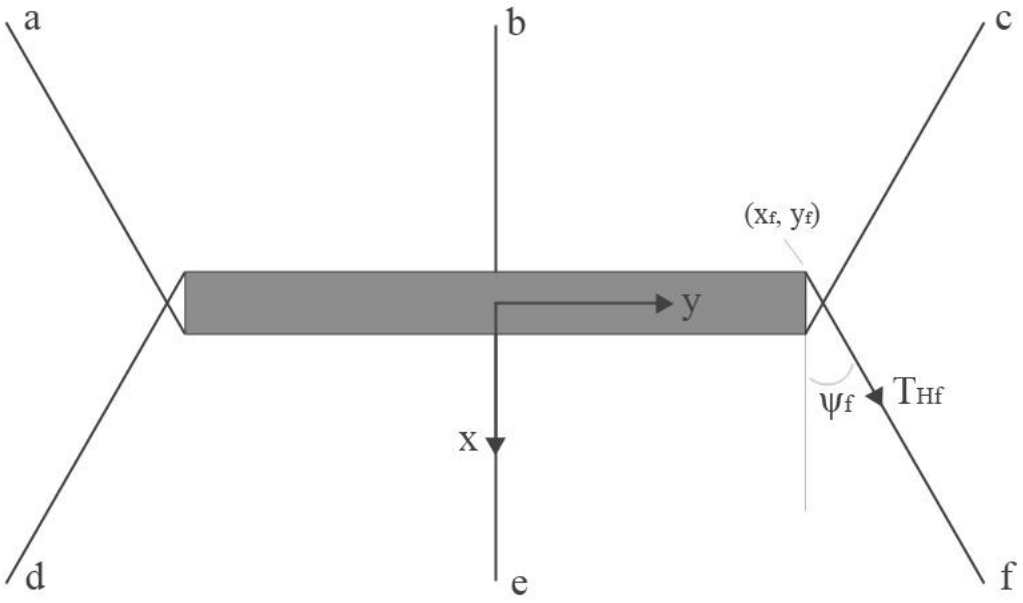

Figure 3.8 Molo model spread mooring system (top view)

Calculation of mooring stiffness matrix for Molo model is detailed in Appendix B. To simplify the analysis, solutions of the inelastic mooring line (catenary) equations are used (Faltinsen, 1990). The mooring lines are assumed to have constant weight per unit length.

Calculated linear restoring coefficients of the mooring lines in a spread mooring system are presented in Table 3.3.

Table 3.3 Mooring restoring coefficients

Mooring Line	x_m	y_m	ψ_m (deg)	k_H (N/m)	k_Z (N/m)	K_{11} (N/m)	K_{22} (N/m)	K_{33} (N/m)	K_{66} (N/m)	K_{26} (N/m)	K_{62} (N/m)
a	-0.1	-1	206.57	0.13	0.081	0.104	0.026	0.081	0.094	0.049	0.049
b	-0.1	0	180.00	0.25	0.085	0.250	0.000	0.085	0.000	0.000	0.000
c	-0.1	1	153.43	0.13	0.081	0.104	0.026	0.081	0.094	0.049	0.049
d	0.1	-1	333.43	0.13	0.081	0.104	0.026	0.081	0.093	-0.050	-0.050
e	0.1	0	0.00	0.25	0.085	0.250	0.000	0.085	0.000	0.000	0.000
f	0.1	1	26.57	0.13	0.081	0.104	0.026	0.081	0.094	-0.049	-0.049
					Σ	**0.916**	**0.104**	**0.494**	**0.375**	**0.000**	**0.000**

Complete 6 X 6 mooring stiffness matrix which is used for WAMIT input file is given below.

$$K = \begin{pmatrix} 0.916 & 0 & 0 & 0 & 0 & 0 \\ 0 & 0.104 & 0 & 0 & 0 & 0 \\ 0 & 0 & 0.494 & 0 & 0 & 0 \\ 0 & 0 & 0 & 0 & 0 & 0 \\ 0 & 0 & 0 & 0 & 0 & 0 \\ 0 & 0 & 0 & 0 & 0 & 0.375 \end{pmatrix}$$

3.3.3 Geometry models by MultiSurf

Two output files from MultiSurf are required for WAMIT input; file with extension '.gdf' and '.ms2' with user specified file names. GDF file is one of essential input file in WAMIT that providing all required geometry information of the model body surface to be analyzed. MS2 represents the geometry during execution of WAMIT by linking to the RGKernel.

The geometry model was developed in a CAD environment in MultiSurf by creating several geometry entities available in MultiSurf; points, curves, and surfaces. In MultiSurf manual, other entities such as bead, magnet, and ring are also available. However, the floating breakwater body was represented by a simple geometry which requires only the first three entities mentioned above.

WAMIT recognizes several types of surface patches with different characteristics for analysis which is distinguished by color coding. Surface colors can be selected in the properties manager in MultiSurf. Some colors are reserved for specific patches; bright cyan (color 11) and bright white (color 15) are reserved for dipole patches and exterior free surface patches, respectively. Body patches and interior free surface patches can be any other color besides 11 and 15.

Since approach 2 of radii of gyration calculation was used in Molo and Maere model analysis (Section 3.3.1), the model geometry was represented in MultiSurf by a rectangular cuboid with small dipole panel at the bottom. The body patches was colored green (color 2) and the dipole patches was colored bright cyan (color 11).

Specifically for 2D model, the breakwater model geometry was represented by a very long cuboid in order to eliminate the wave diffraction effect on the lee side and to achieve the 2D wave flume environment.

Snapshot of body geometry of 2D model, Molo model, and Maere model are shown in Figure 3.9 to Figure 3.11 below.

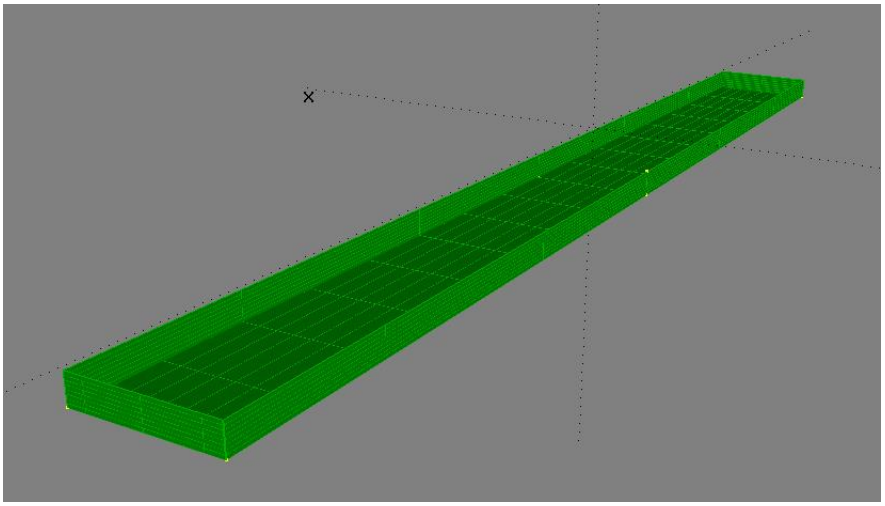

Figure 3.9 2D model MultiSurf snapshot

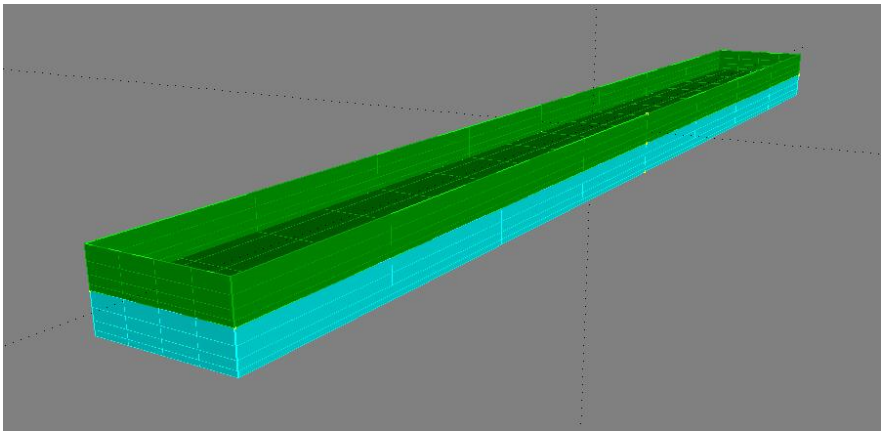

Figure 3.10 Molo model MultiSurf snapshot

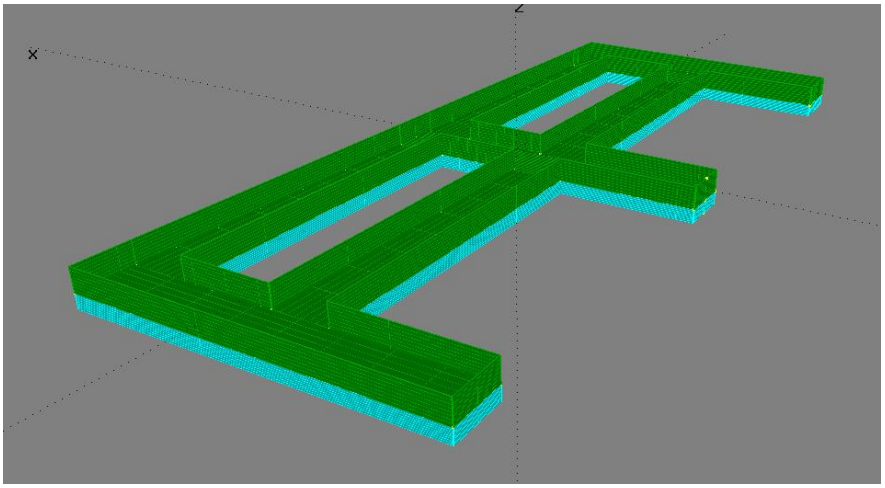

Figure 3.11 Maere model MultiSurf snapshot

The origin of the body coordinate system is located at the center of gravity. Using a plane of symmetry at y=0, only the first half of the breakwater was modeled in MultiSurf. The characteristic length is set to 1. Decimal place was set to 7 places in order to get more accurate results.

Help and tutorial to prepare input files for WAMIT is available in MultiSurf manual. Example output files from MultiSurf are given in Appendix B.

3.3.4 Computation by WAMIT

To execute WAMIT computation, there were several input files prepared. All input files were ASCII files. The first line of most files was reserved for header, consisting of up to 72 characters which may be used to identify the file. The precise format of the input files is not important, provided at least one blank space is used to separate data on the same line of the file.

The geometry of the body was specified by a Geometric Data File (GDF) which included the Cartesian coordinates of each vertex of each panel, listed sequentially. In addition the GDF file specified the characteristics length ULEN used to non-dimensionalize outputs, the value of the gravitational acceleration constant GRAV in the same units of measurement, the number of panels NPAN, and two symmetry indices ISX and ISY.

The Potential Control File (POT) was used to input various parameters to the POTEN subprogram. The name of the POT file can be any legal filename accepted by the operating system, with a maximum length of 16 ASCII characters, followed by the extension ‘,pot’. Two alternatives format for the POT files are available. Either Form 1 or Form 2 of POT file can be used irrespective of whether low-order or high-order method is used. The only distinction is that the Form 2 is particularly convenient for the analysis of multiple bodies. Optional parameter IALTPOT in the CFG file is used to specify which alternative form of the POT is used for the computation.

The Force Control File (FRC) was used to input various parameters to the FORCE subprogram. The name of the FRC file can be any legal filename accepted by the operating system, with a maximum length of 16 ASCII characters, followed by the extension ‘.frc’. Two alternatives format for the FRC files are also available. Alternative Form 1 of FRC file may be used for a rigid body which is freely floating and not subject to external constraints. In this Form 1, the inertia matrix of the body specified in terms of a 3 x 3 matrix of radii of gyration. Alternative Form 2 permits input of up to three 6 x 6 mass, damping and stiffness matrices to allow for a more general body inertia matrix, and for any linear combination of external forces and moments. Another alternative format may also be used for multiple bodies.

An array of option indices IOPTN was included in FRC file. These indicate which hydrodynamics parameters are to be evaluated and output from the program. In this analysis, IOPTN(4) and IOPTN(6) were activated to evaluate the response amplitude operator and free-surface elevation, respectively.

A configuration file CFG was used to specify various parameters and option in WAMIT. As recommended by manual, an optional input file was also used to specify the filenames of the primary input files CFG, POT, FRC, and GDF.

3.3.5 Output processing

Several output files were created by WAMIT with assigned filenames. The final output was saved in a file with the extension OUT which included extensive text, labels, and summaries of the input data. A separate numeric output file for the data corresponding to each requested option was also created in a more suitable form for post-processing. These files were distinguished by their extension, which correspond to the option numbers.

3.3.5.1 Transmission coefficient

The effectiveness of the floating breakwater is analyzed in terms of *Ct* or coefficient. The wave elevation was calculated for all cases and for all frequencies considered in the locations of wave gauges used in the experiments, behind the breakwaters. For each frequency and each case, the wave elevation due to both and radiation was computed. Coordinates of wave gauge locations relative to origin body coordinate system are given in

Table 3.4 below.

The free surface elevation output was given in non-dimensional form as following.

$$\bar{\eta} = \frac{\eta}{A} \tag{3.3}$$

where $\bar{\eta}$ is a non-dimensional free surface elevation, η is dimensional free surface elevation, and A is dimensional incoming wave amplitude.

From Equation 3.3, transmitted wave height was calculated by multiplying the non-dimensional free surface elevation with the incoming wave amplitude. And the transmission coefficient was calculated as a ratio between the transmitted wave height and incoming wave height.

Table 3.4 Wave gauges coordinates behind the breakwaters

Cases	Wave Gauge	*x*	*y*	*z*
1. 2D model - fixed (draft = 0.4 m) 2. 2D model - fixed (draft = 0.5 m) 3. 2D model - fixed (draft = 0.65 m)	#1	2.3	0	0
	#2	2.1	0	0
4. Molo model - free floating 5. Molo model - vertical restrained 6. Molo model - fixed 7. Molo model - heave only 8. Molo model - anchored	#1	0.82	1.9	0
	#2	0.82	0.95	0
	#3	0.82	0	0
	#4	1.88	0	0
9. Maere model - free floating 10. Maere model - vertical restrained 11. Maere model - fixed 12. Maere model - heave only 13. Maere model - anchored	#1	1.47	1.8	0
	#2	1.47	0.9	0
	#3	1.47	0	0
	#4	2.47	0	0

3.3.5.2 Body motions

The non-dimensional definitions of the body motions are given below.

$$\bar{\xi}_i = \frac{\xi_i}{A/{L_c}^n} \tag{3.4}$$

where $\bar{\xi}_i$ and ξ_i are the non-dimensional and dimensional translational motion for i = 1, 2, 3 (surge, sway, heave) and rotational motion for i = 4, 5, 6 (roll, pitch, yaw). Values of n = 0 for i = 1, 2, 3 and n = 1 for i = 4, 5, 6. The translational motions (ξ_1, ξ_2, ξ_3) and rotational motions (ξ_4, ξ_5, ξ_6) are measured in meters and radians, respectively. The diagrams of body motions of Molo and Maere models are shown in Figure 3.12 and Figure 3.13 below.

The response amplitude operators were simply calculated by multiplying the non-dimensional translational and rotational motion with the incoming wave amplitude divided by characteristic length (L_c) to the power of n.

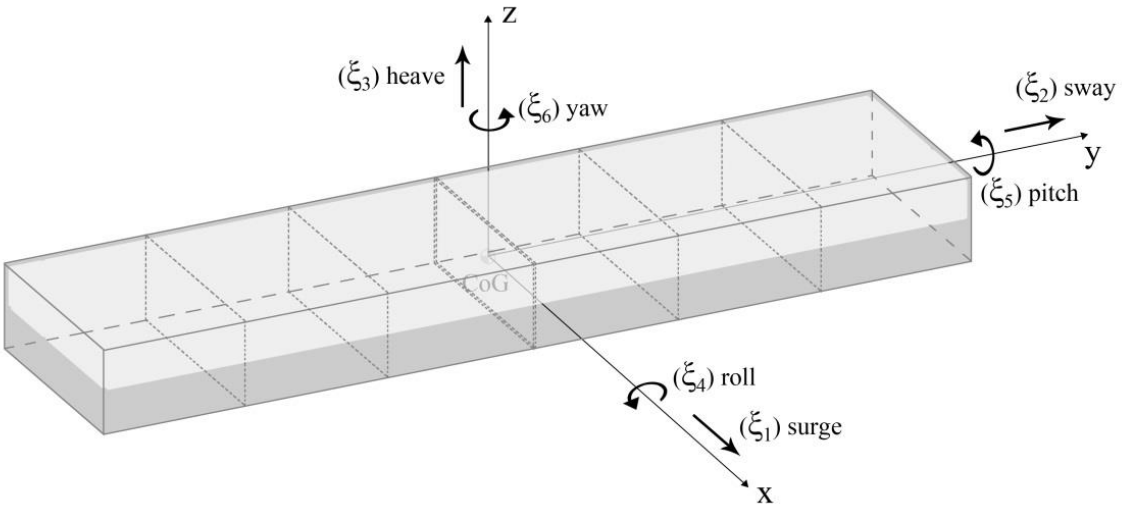

Figure 3.12 Molo model body motions diagram

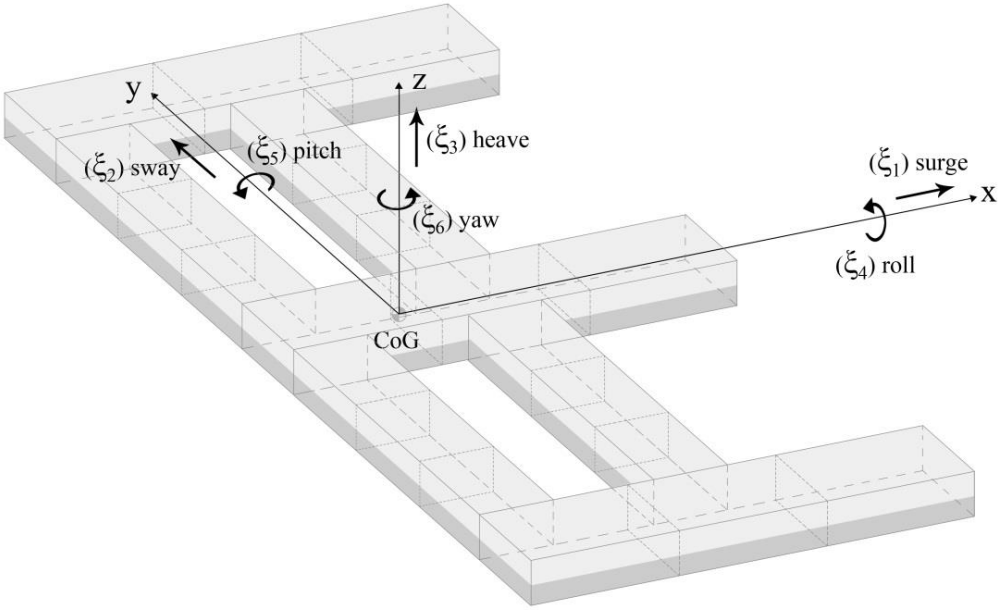

Figure 3.13 Maere model body motions diagram

3.3.5.3 Model natural frequencies

Model natural frequencies ω_{ni} were calculated for assessing the amplitude of motions. The decoupled and un-damped natural frequencies were calculated by using below Equation 3.5 and 3.6 (Faltinsen, 1990).

$$\omega_{ni} = \frac{2\pi}{T_{ni}} \tag{3.5}$$

$$T_{ni} = 2\pi\left(\frac{M_{ii} + A_{ii}}{C_{ii}}\right)^{1/2} \tag{3.6}$$

where T_{ni} is natural periods for each motion mode, A_{ii} and M_{ii} C_{ii} are added mass, mass, and restoring coefficient for each motion mode, respectively.

There are no (uncoupled) natural frequency in surge, sway, and yaw for unmoored structure (Faltinsen, 1990). For a moored structure the natural periods in surge, sway and yaw are much longer relative to incoming wave periods occurring in the sea. The breakwater is symmetrical about the longitudinal plane *x*=0 and transverse *y*=0, thus heave is uncoupled from pitch and roll. Natural frequencies of the breakwater were calculated as un-damped since the natural frequencies are usually shifted less than 1% when damping is added (Fossen, 2011). Calculated natural frequencies in heave and pitch are given below.

Table 3.5 Natural frequencies in heave and pitch

Incoming Wave		Molo Model		Maere Model	
T (s)	ω (rad/s)	ω_{n3} (rad/s)	ω_{n5} (rad/s)	ω_{n3} (rad/s)	ω_{n5} (rad/s)
1.00	6.28	5.26	4.99	5.03	5.78
1.05	5.97	5.30	4.99	5.28	5.82
1.11	5.65	5.33	4.99	5.47	5.83
1.18	5.34	5.36	4.99	5.63	5.84
1.25	5.02	5.37	4.99	5.79	5.85
1.33	4.71	5.38	4.99	5.89	5.83
1.43	4.40	5.38	4.99	5.91	5.77
1.54	4.08	5.39	4.99	5.90	5.70
1.67	3.77	5.40	4.99	5.87	5.61
1.82	3.45	5.40	4.98	5.83	5.52
2.00	3.14	5.38	4.98	5.73	5.42
2.22	2.83	5.31	4.98	5.55	5.32
2.50	2.51	5.18	4.98	5.29	5.23
2.86	2.20	4.98	4.98	4.94	5.15
3.33	1.88	4.71	4.98	4.54	5.09
4.00	1.57	4.41	4.98	4.13	5.05
5.00	1.26	4.07	4.98	3.71	5.04
6.67	0.94	3.70	4.98	3.28	5.04
10.00	0.63	3.31	4.98	2.84	5.07
20.00	0.31	2.85	4.98	2.35	5.10

4. RESULTS ANALYSIS AND DISCUSSIONS

4.1 Output plots

For each case, output plots are presented for two properly selected frequencies which gave the low and high transmission coefficients (*Ct*). Remain plots for complete cases are given in separated CD. Table of content of the CD is given in the Table 4.1 below.

Table 4.1 CD table of contents

No.	Contents	Remarks
01	**Final report**	*.doc* and *.pdf* files
02	**Sketches**	Including *.psd* files
	01 2D model	
	02 Molo model	
	03 Maere model	
03	**WAMIT and MultiSurf models**	with 13 cases, including *.ms2* files
	01 2D model	
	02 Molo model	
	03 Maere model	
04	**Selected output plot**	matlab plots and *.tiff*
05	**Calculation and tables**	*.xlsx* calculation spreadsheets
	01 Cases & CD contents	
	02 Center of gravity	
	03 Mass moment of inertia	
	04 Mooring stiffness	
	05 Wave gauge location	
	06 Transmission coefficients *Ct*	
	07 RAOs plot	
	08 Natural frequencies	

From figures of plots with low *Ct*, effectiveness of floating breakwater for wave attenuation can be clearly observed. Wave diffraction phenomena on the lee side of the breakwaters Molo and Maere model are also clearly shown on these figures by the bent wave crests around the breakwaters. Variation of transmitted wave heights behind the breakwaters is also noticeable. The transmission wave heights were quantified by varying *Ct* values presented on Section 4.2.

Whereas on figures of plots with high *Ct*, it can be inferred that the wave lengths are relatively larger compare to the breakwater width and the waves are transmitted without

any attenuation. The incoming wave lengths, of which the attenuations started to be practically unacceptable, were quantified by ratio between the wave length and breakwater width (*W/L*) given on Section 4.2.

4.1.1 2D model

4.1.1.1 2D model (draft = 0.4 m)

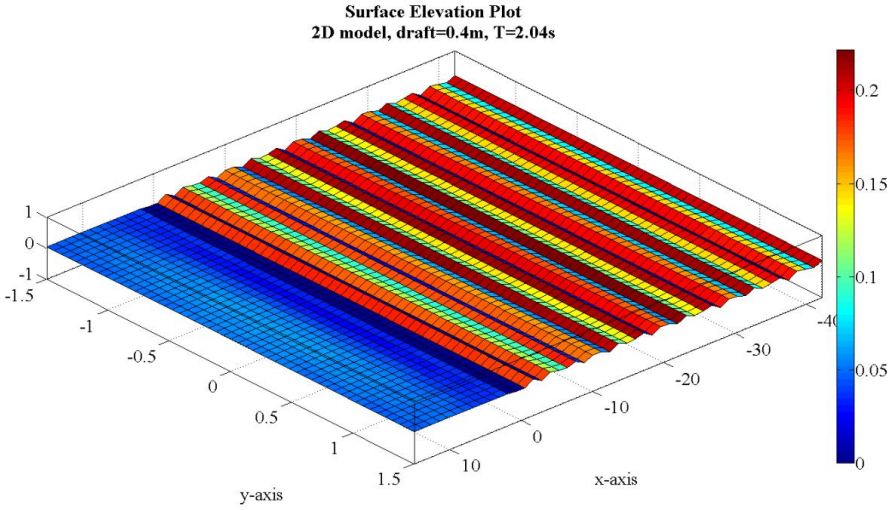

Figure 4.1 Free surface elevation of 2D model (draft=0.4m) with low *Ct*

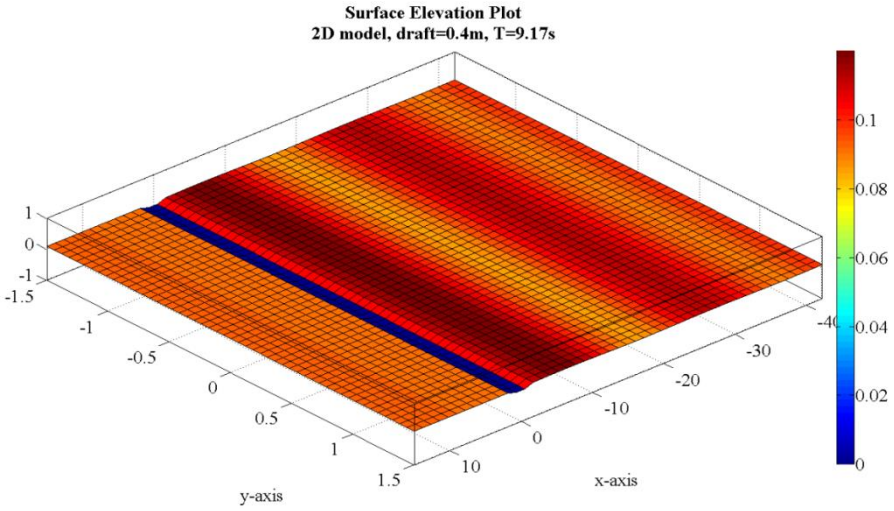

Figure 4.2 Free surface elevation of 2D model (draft=0.4m) with high *Ct*

Above Figure 4.1 shows clearly the incoming wave attenuation on lee side of the breakwater. Only small amount of incoming waves were transmitted and most of it were reflected back in front of the breakwater. The *Ct* resulted by this case is the lowest with

value of 0.31. Whereas Figure 4.2 shows lower ratio between the breakwater width and the wave length (*W/L*) and less effective wave attenuation indicated by relatively larger wave height on lee side of the breakwater.

4.1.1.2 2D model (draft = 0.5 m)

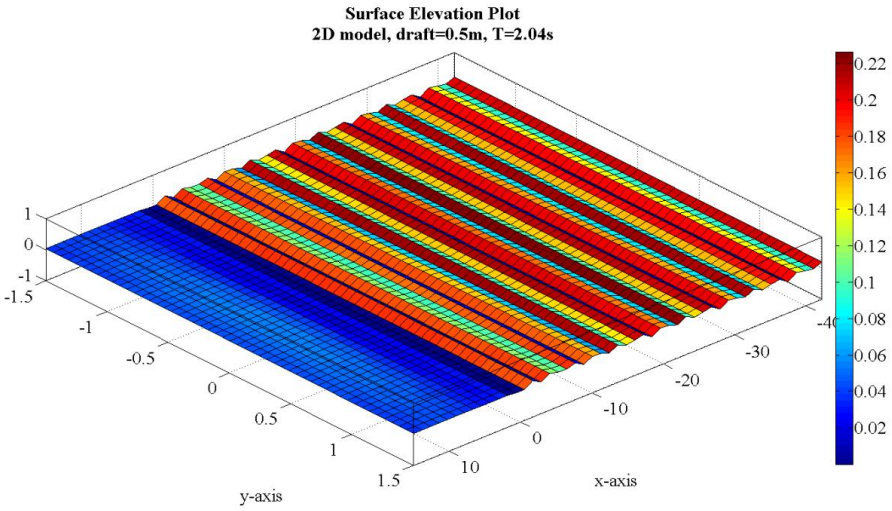

Figure 4.3 Free surface elevation of 2D model (draft=0.5m) with low *Ct*

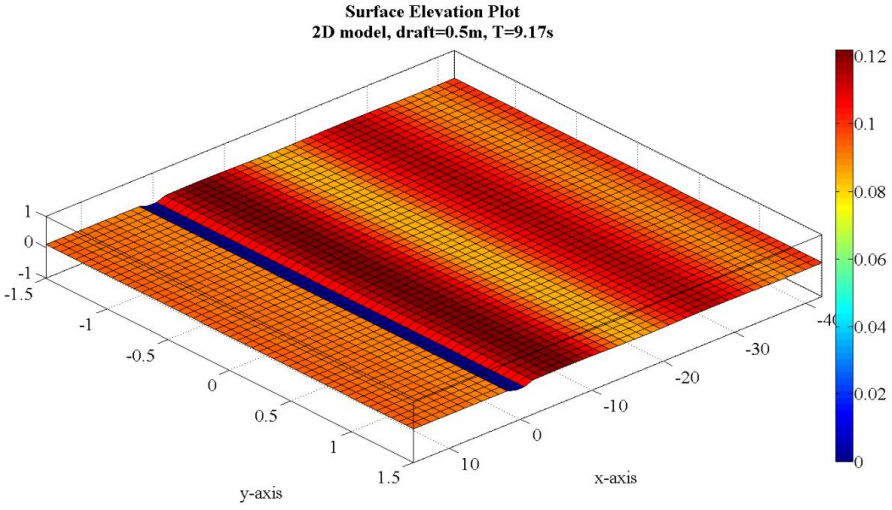

Figure 4.4 Free surface elevation of 2D model (draft=0.5m) with high *Ct*

Similar phenomenon as previous configuration (draft = 0.4m) is shown by above Figure 4.3 and Figure 4.4. The lowest *Ct* of 0.23 is given by top figure, indicating more effective wave attenuation, and highest *Ct* of 0.9 is given by bottom figure, indicating the opposite.

4.1.1.3 2D model (draft = 0.65 m)

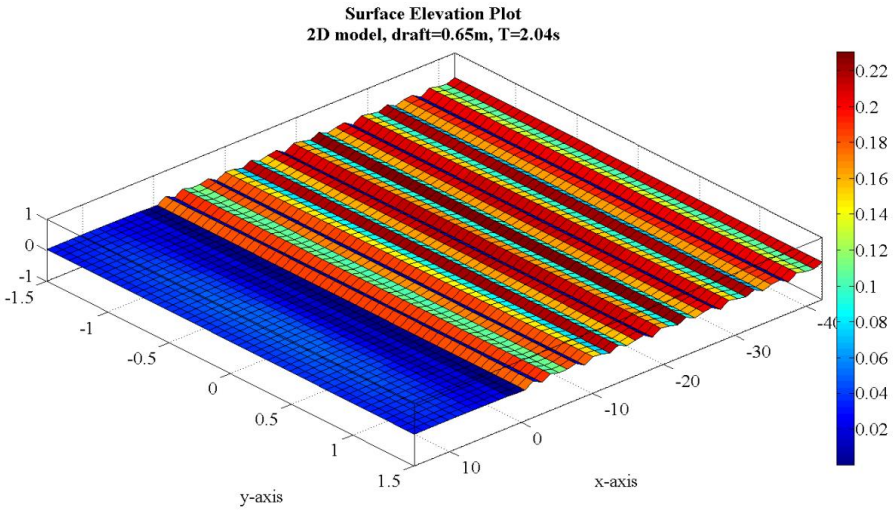

Figure 4.5 Free surface elevation of 2D model (draft=0.65m) with low *Ct*

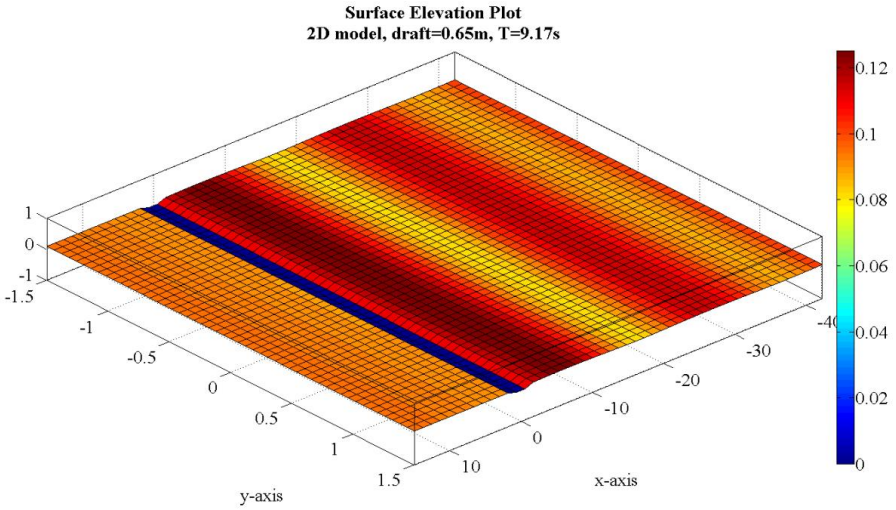

Figure 4.6 Free surface elevation of 2D model (draft=0.65m) with high *Ct*

Similar to both previous configurations, for breakwater with draft of 0.65 m, the lowest *Ct* of 0.13 is given by the shortest wave periods and is illustrated by above Figure 4.5. While the highest *Ct* of 0.9 is given by the longest wave periods and is illustrated by Figure 4.6.

4.1.2 Molo model

In general for Molo model, the effects of wave diffraction and reflection wave is clearly observed behind and in front of the breakwater. From presented figures, it can be

quantitatively determined that for the short wave periods, the fixed configuration (Figure 4.11) gives the best performance as the wave height behind the breakwater is relatively lower than the other configurations, indicating the lower *Ct* value. While for the long wave periods, the wave length is relatively larger than the breakwater width and the wave attenuation is no longer noticeable.

4.1.2.1 Molo model - free floating

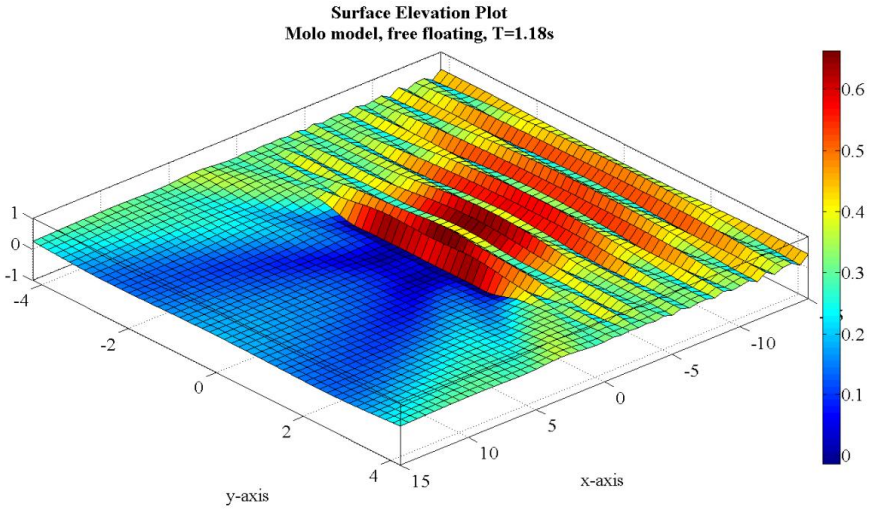

Figure 4.7 Free surface elevation of Molo model (free floating) with low *Ct*

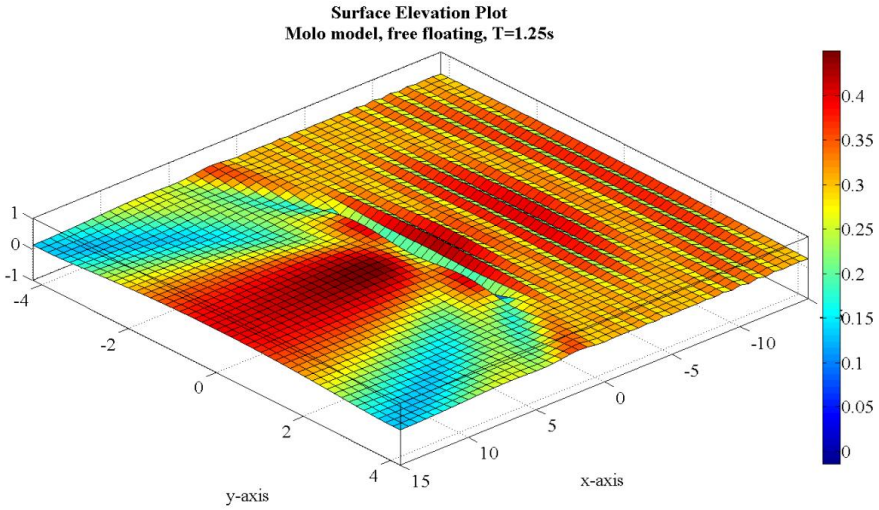

Figure 4.8 Free surface elevation of Molo model (free floating) with high *Ct*

4.1.2.2 Molo model - vertical restrained

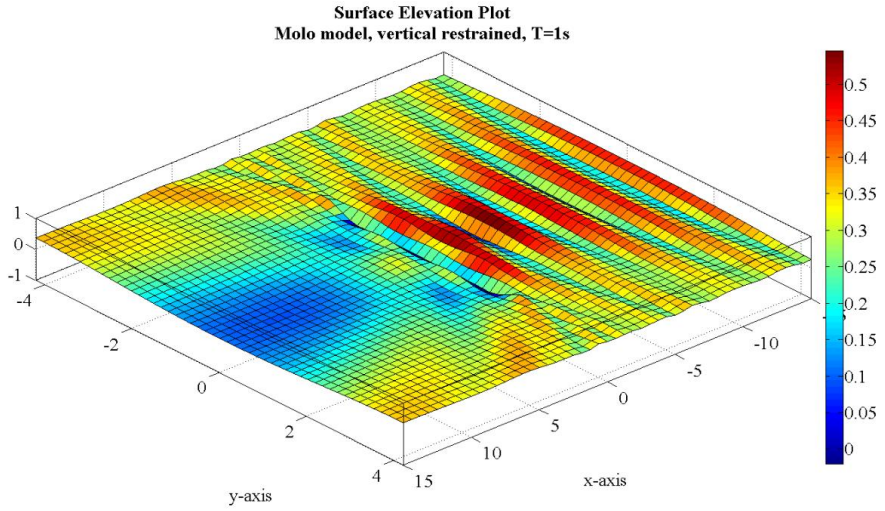

Figure 4.9 Free surface elevation of Molo model (vertical restrained) with low *Ct*

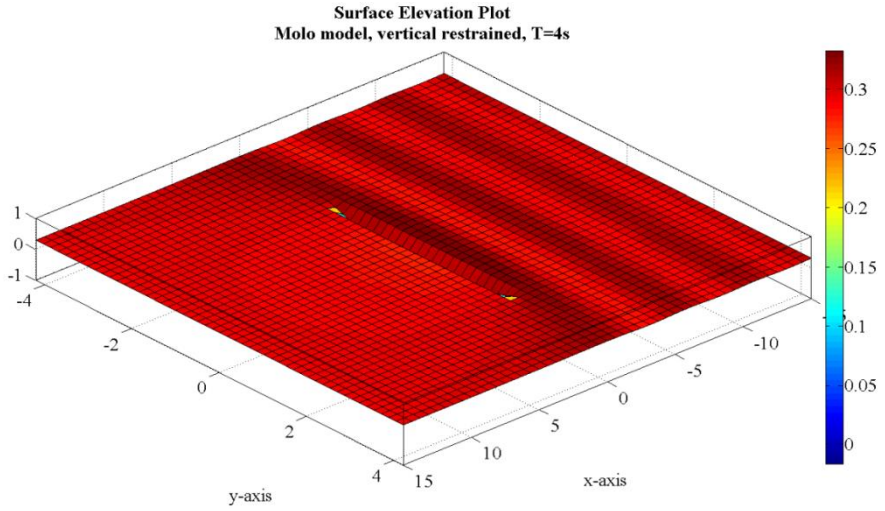

Figure 4.10 Free surface elevation of Molo model (vertical restrained) with high *Ct*

4.1.2.3 Molo model - fixed

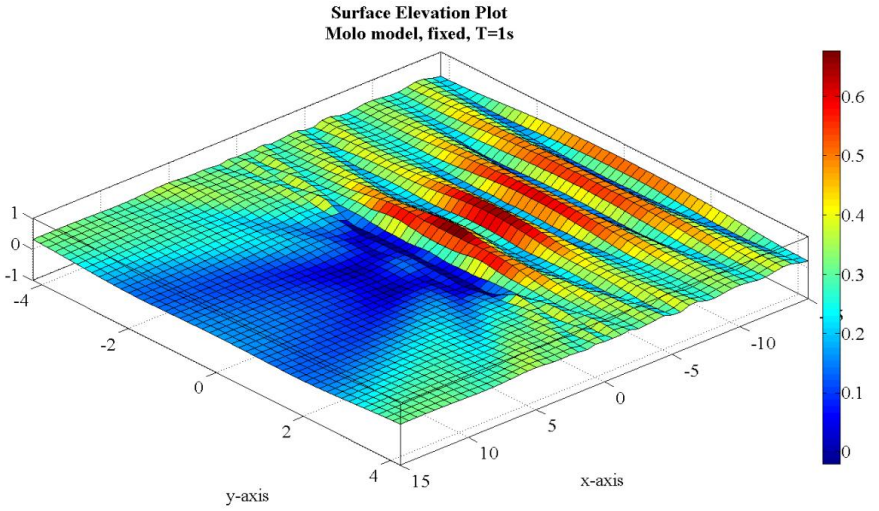

Figure 4.11 Free surface elevation of Molo model (fixed) with low *Ct*

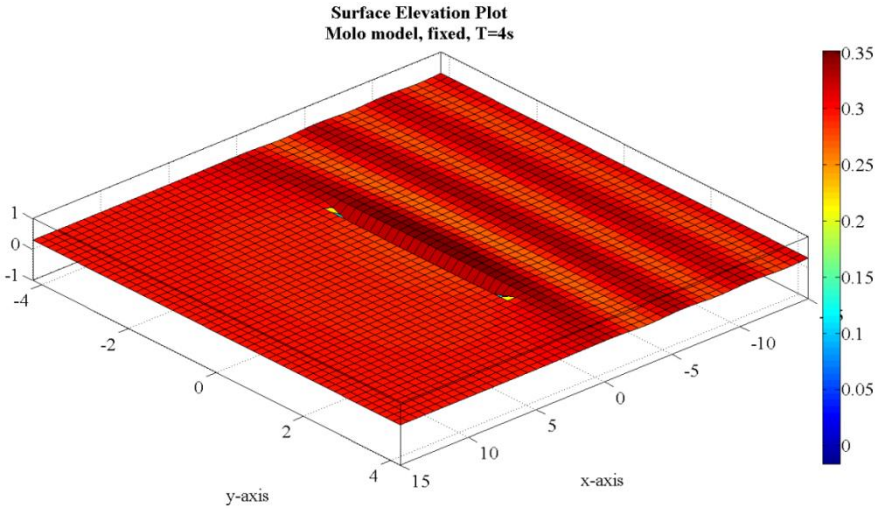

Figure 4.12 Free surface elevation of Molo model (fixed) with high *Ct*

4.1.2.4 *Molo model - heave only*

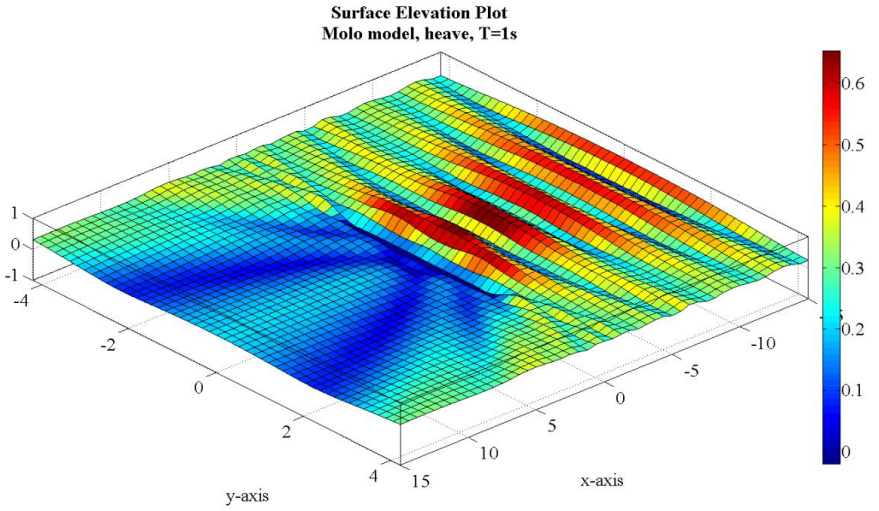

Figure 4.13 Free surface elevation of Molo model (heave only) with low *Ct*

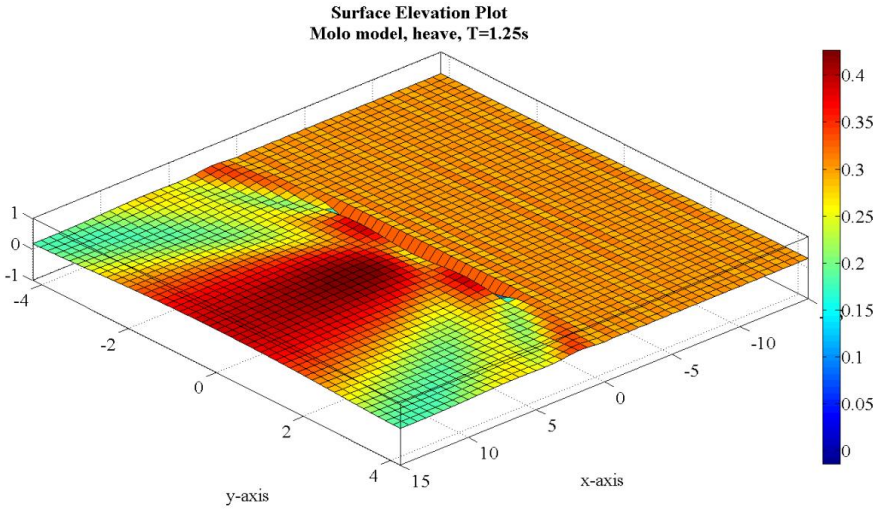

Figure 4.14 Free surface elevation of Molo model (heave only) with high *Ct*

4.1.2.5 Molo model – moored

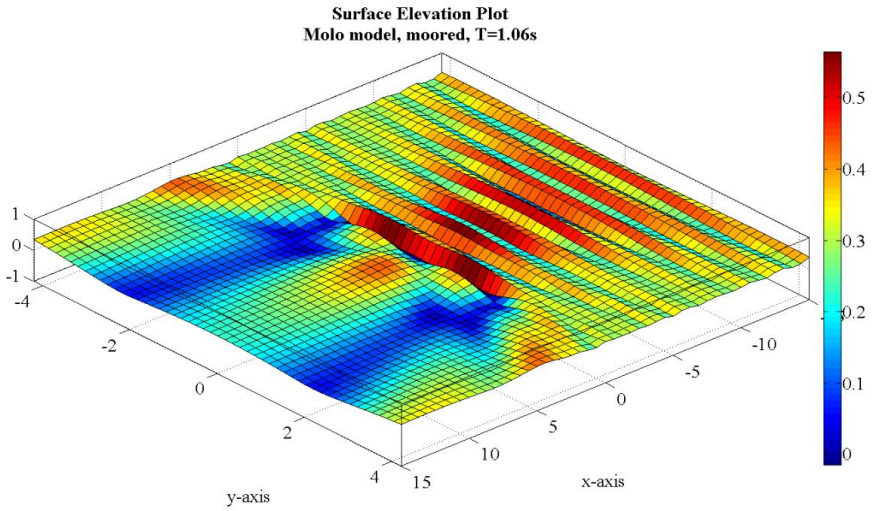

Figure 4.15 Free surface elevation of Molo model (moored) with low *Ct*

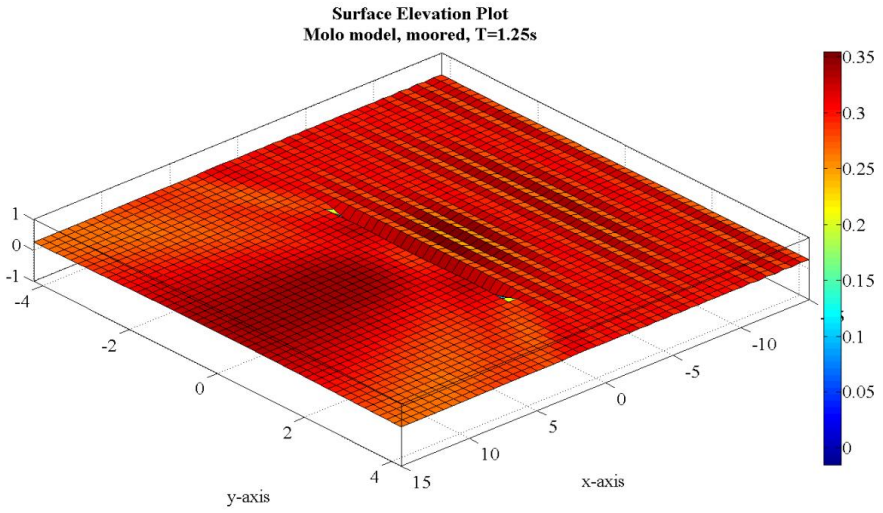

Figure 4.16 Free surface elevation of Molo model (moored) with high *Ct*

4.1.3 Maere model

Similar to Molo model, generally the effects of wave diffraction and reflection wave is clearly observed behind and in front of the breakwater Maere model. Quantitatively, it can also be determined figures that for the short wave periods, the fixed configuration (Figure 4.21) gives the best performance as the wave height behind the breakwater is relatively lower than the other configurations, indicating the lower *Ct* value. And for long wave

periods, the wave length is relatively larger than the breakwater width and the wave attenuation is no longer noticeable.

4.1.3.1 Maere model - free floating

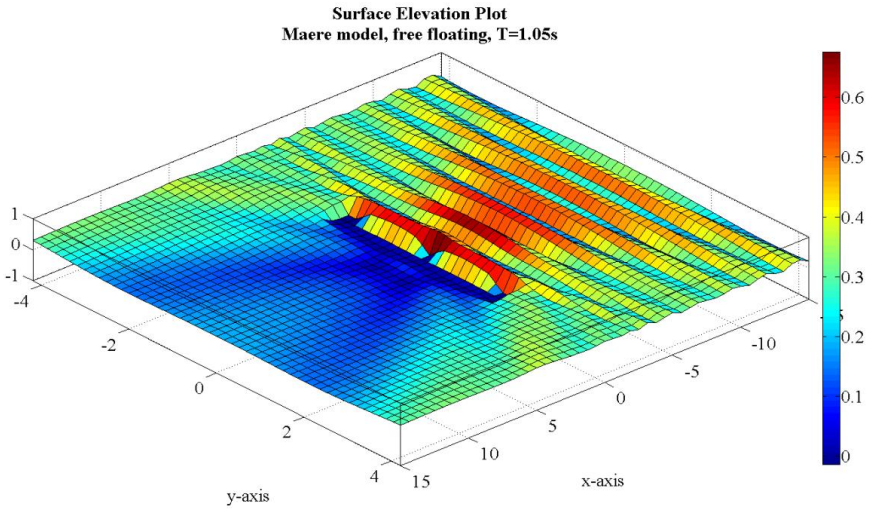

Figure 4.17 Free surface elevation of Maere model (free floating) with low *Ct*

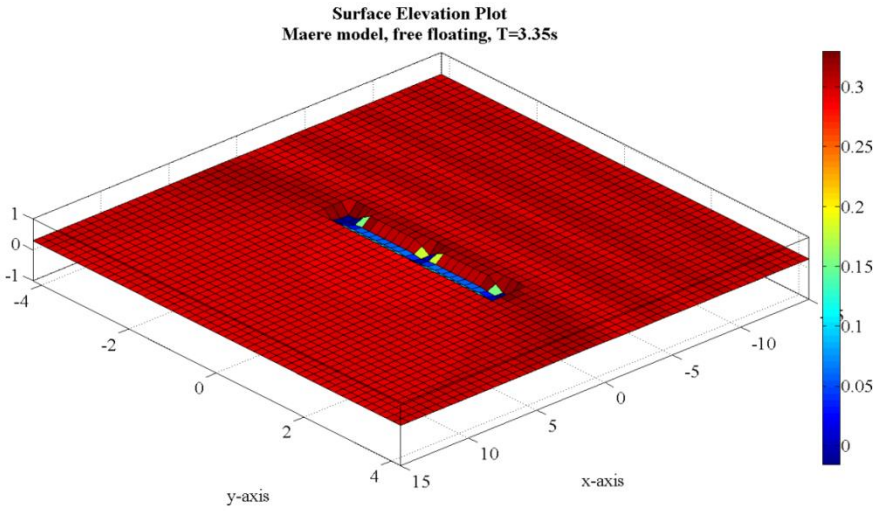

Figure 4.18 Free surface elevation of Maere model (free floating) with high *Ct*

4.1.3.2 Maere model - vertical restrained

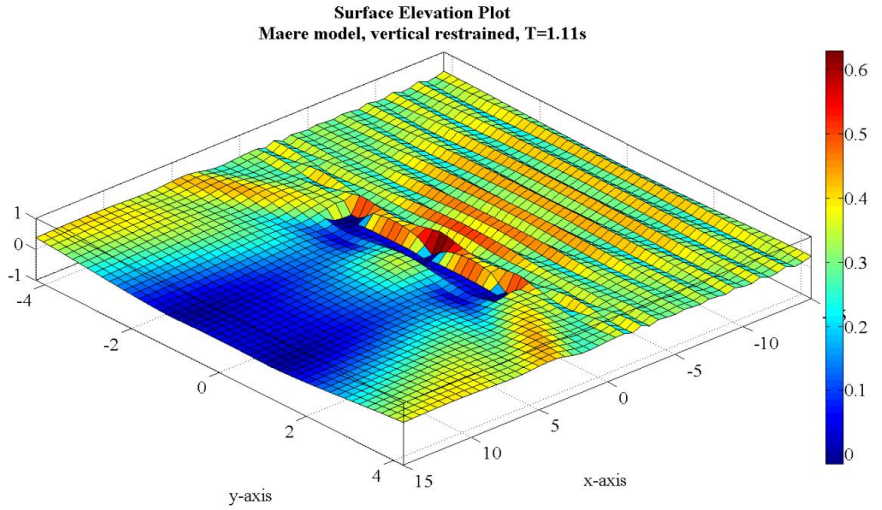

Figure 4.19 Free surface elevation of Maere model (vertical restrained) with low *Ct*

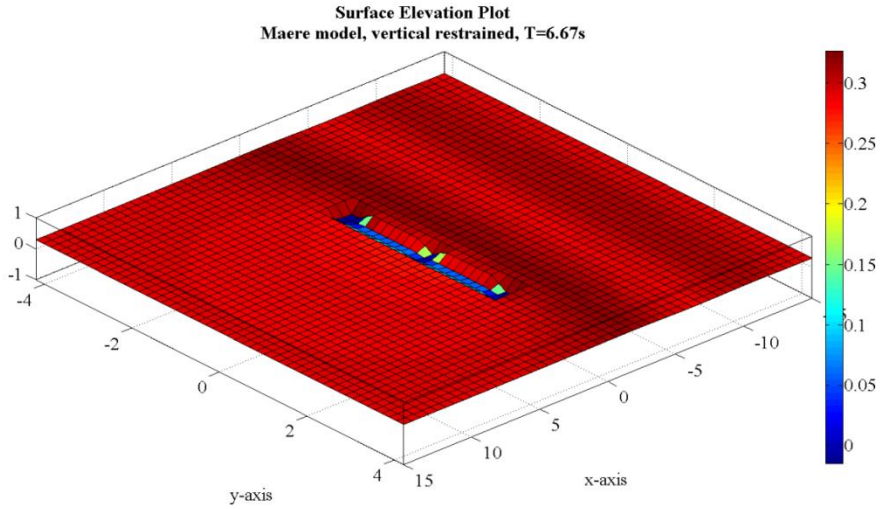

Figure 4.20 Free surface elevation of Maere model (vertical restrained) with high *Ct*

4.1.3.3 Maere model - fixed

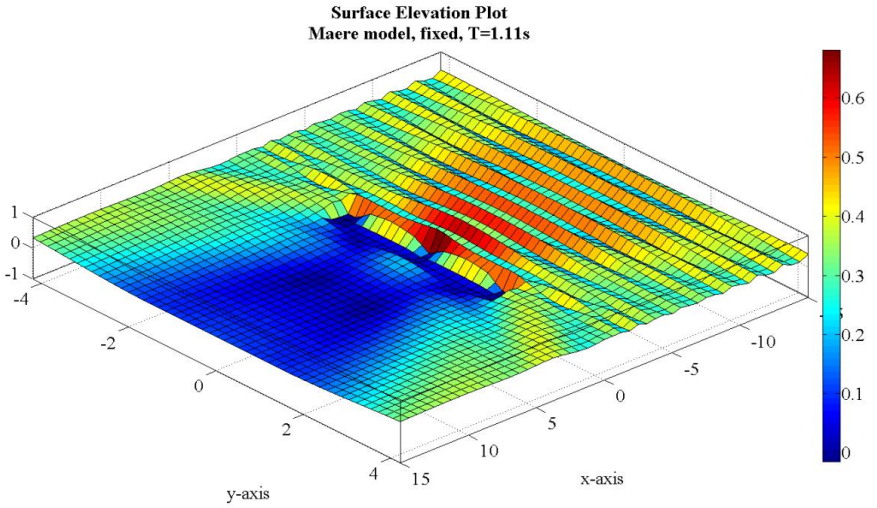

Figure 4.21 Free surface elevation of Maere model (fixed) with low *Ct*

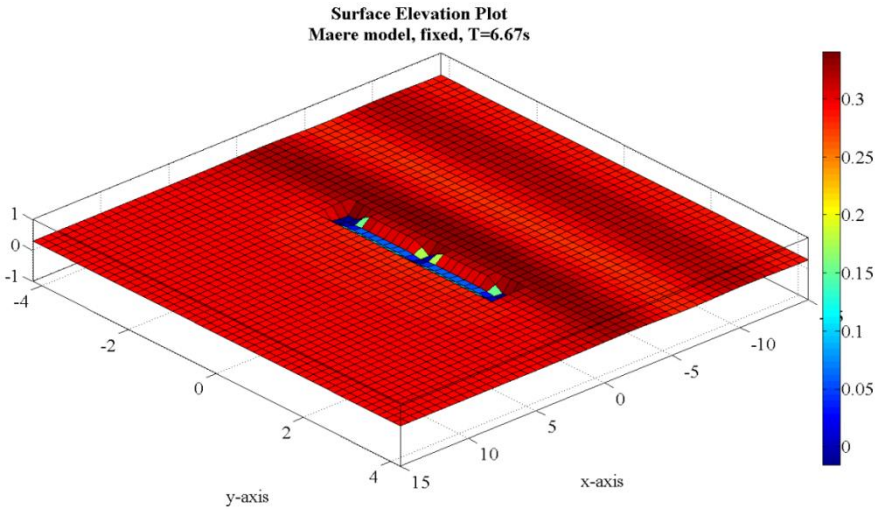

Figure 4.22 Free surface elevation of Maere model (fixed) with high *Ct*

4.1.3.4 Maere model - heave only

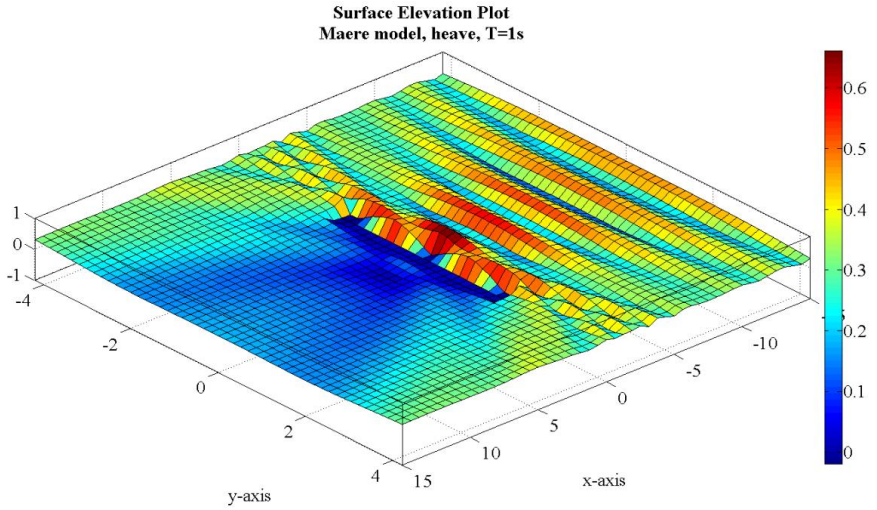

Figure 4.23 Free surface elevation of Maere model (heave only) with low *Ct*

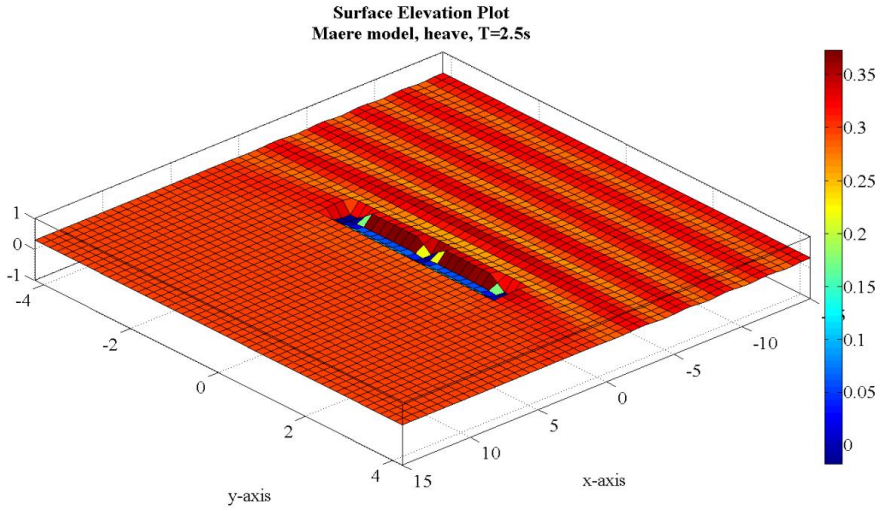

Figure 4.24 Free surface elevation of Maere model (heave only) with high *Ct*

4.2 Transmission coefficients

4.2.1 2D model

The result of transmission coefficient calculation for 2D model is presented in Figure 4.25. The influence of *W/L* on the wave attenuation by the breakwaters is shown, as well as the influence of varies breakwater drafts. The *Ct* values presented here are the average of *Ct* calculated on two locations of the wave gauges positions. *Ct* value of each wave gauge location is given in the result comparison Section 4.4.1.

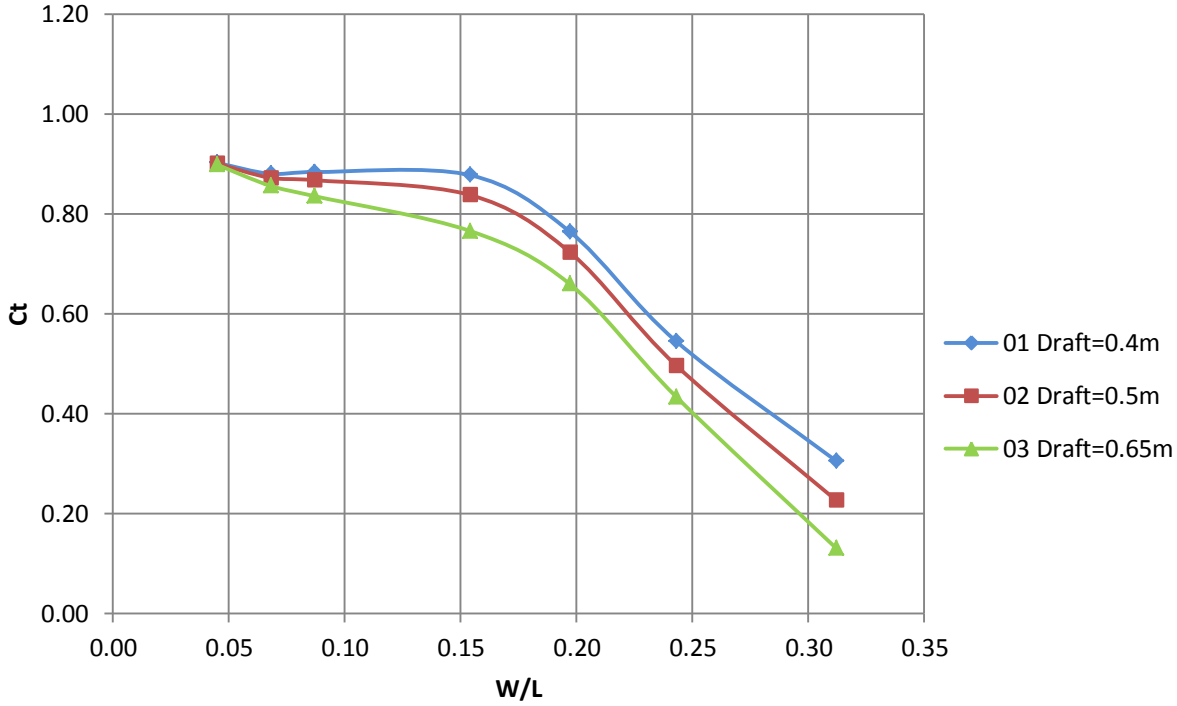

Figure 4.25 Transmission coefficients of 2D model

Quantitative comparison between the result and the laboratory experiment measured data is given in Section 4.4.1. Comparing the presented results with the corresponding one of Koutandos, et al. (2005), the tendency of the *Ct* values as a function of *W/L* is accordingly match. The transmission coefficient decreases with a decrease of wave period, that is to say a decrease of wave length, indicating an increase of wave attenuation for short wave period.

Though not significant, it can also be inferred that the transmission coefficients are lower for breakwater with larger draft. It indicates that the incoming wave is less transmitted through the breakwater. It is reasonable since the larger the draft the larger the damping effect in surge motion resulting more wave energy dissipated and less transmitted.

The performance of the breakwater with draft of 0.65 m is considered to be practically acceptable when the *W/L* is greater than or approximately 0.25, since *Ct* is less than 0.5. The breakwaters work more effectively with short periods of incoming waves.

4.2.2 Molo model

The result of transmission coefficient calculation for Molo model is presented in Figure 4.26. The influence of *W/L* on the wave attenuation is shown, as well as different degree of freedom defined to the model motions.

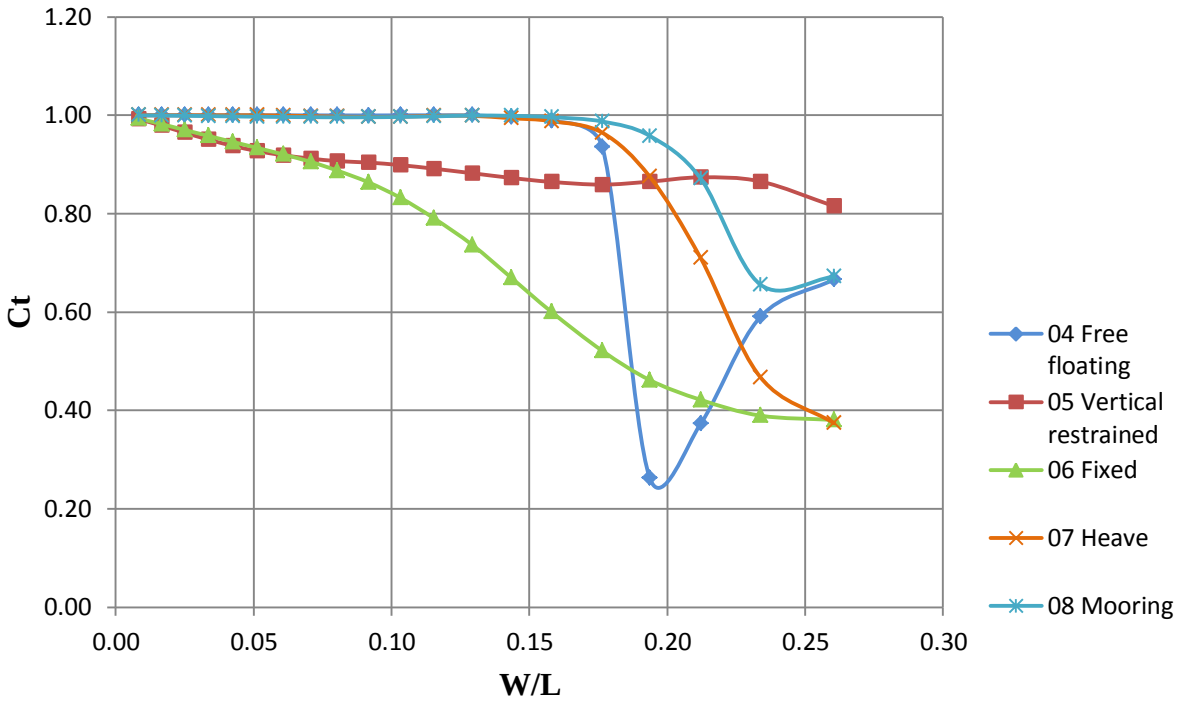

Figure 4.26 Transmission coefficients of Molo model

The free floating Molo model only gives a low *Ct* on a very narrow range of wave periods. Though the lowest *Ct* is really low at *W/L* = 0.19 (wave period of 1.18 s), indicating a very effective wave attenuation on the lee side of breakwater, when the model is exposed to incoming wave periods greater than 1.18 s and lower than 1.11 s the performance is drastically decreased. The model started to ride the wave without any attenuation when the incoming wave period is equal to 1.33 s.

In analysis of model with vertical restrained configuration, the model motions in horizontal modes are free (surge, sway, and yaw) and the vertical modes are fixed (heave, pitch, and roll). Over a wide range of incoming wave periods the wave attenuation is not noticeable with the lowest *Ct* value of only 0.8. Clearly the configuration is not considerable for

floating breakwaters due to its poor ability in wave attenuation. These high *Ct* values are also understandable since the breakwater acts similar to a vertical wave paddle that oscillating and generating waves which effecting the transmitted and reflected waves.

Relative to other configurations, the fixed configuration gives lower *Ct* over the whole range of incoming wave periods. Considering *Ct* lower than 0.5 as an acceptable value, this configuration performs relatively well for periods range 1 s to 1.18 s (*W/L* of 0.38 to 0.46). For an increase of wave period, or decrease of *W/L*, the *Ct* increase gradually and reach the value of 1 at wave period of 20 s.

On the next model configuration, heave is the only allowed motion. The *Ct* tends to be similar to the fixed configuration, unless the increase of its value is more immoderate on wave period range of 1.05 s to 1.18 s. On the wave periods greater than this range, the model started to ride the incoming wave without any attenuation.

Molo model with moored configuration surprisingly gives high *Ct* values. According to Yamamoto et al., (1980) if the mooring system is properly arranged, the wave attenuation by a small draft breakwater can be improved several times compared to the same floating breakwater conventionally moored (Sannasiraj, et al., 1998). In this case, the cause of this high *Ct* might be due to the mooring system or some other uncertainties of the numerical model. A more thorough analysis and comparison with experiment result is given in Section 4.4.2.

4.2.3 Maere model

The result of transmission coefficient calculation for Maere model is presented in Figure 4.27. The influence of *W/L* on the wave attenuation is shown, as well as different degree of freedom defined to the model motions.

The free floating Maere model performance relatively more effective compare to Molo model with the same configuration due to the increase of breakwater width. For incoming waves with periods lesser than 1.18 s (*W/L* = 0.42), free floating model works the most effective and gives the lowest *Ct* which values lower than 0.5. However with period greater than that, the *Ct* increases drastically.

The Maere model with vertical restrained configuration performs in a similar way as Molo model to some degree. The *Ct* values are ranging from 0.75 to 0.82 over a wide range of incoming wave periods, and approaching the value of 1 rapidly when the incoming wave periods are greater than 2.86 s (*W/L* = 0.13).

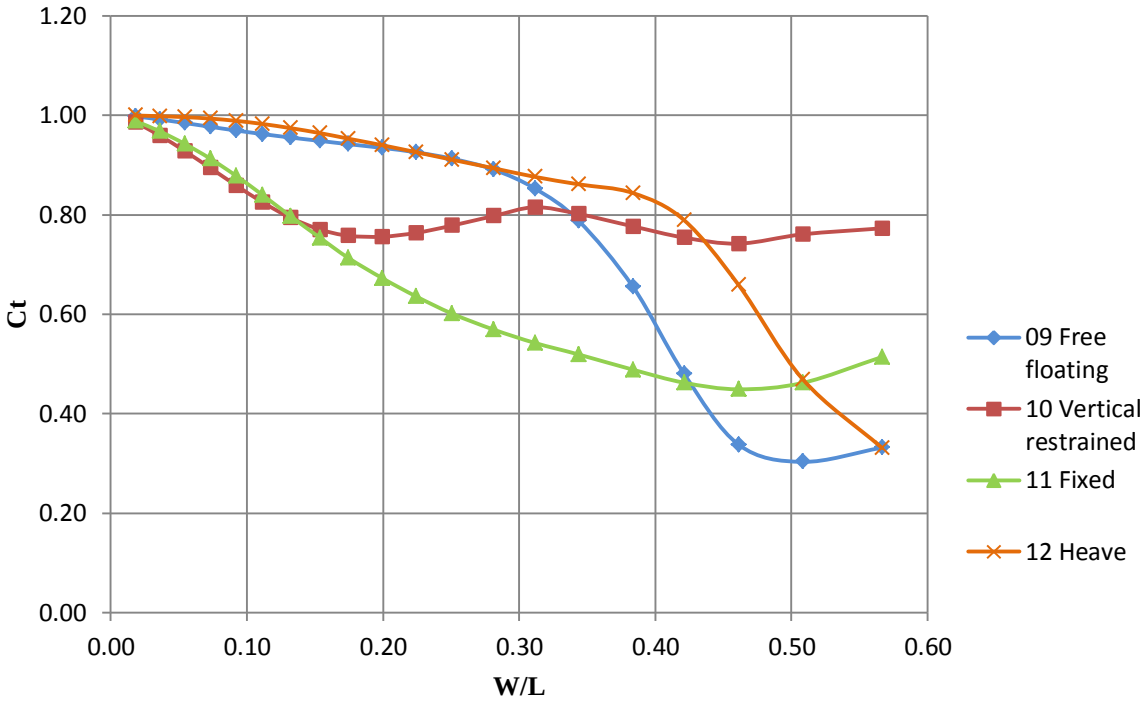

Figure 4.27 Transmission coefficients of Maere model

Similar to Molo model, Maere model with fixed configuration gives considerably *Ct* values for periods range 1 s to 1.18 s (*W/L* of 0.38 to 0.46). For an increase of wave period, or decrease of *W/L*, the *Ct* increase gradually and reach the value of 1 at wave period of 20 s.

Maere model with heave configuration give acceptable *Ct* values lower than 0.5 only on the wave periods lesser than 1.05 s (*W/L* = 0.51). Greater than this, the model gives unnoticeable wave attenuation.

4.3 Response motions of floating breakwaters model

4.3.1 Molo model

The response amplitude operators, RAOs, of the motion responses of Molo and Maere models are presented as a function of normalized frequency, $\omega^2 W/2g$, where ω is the wave excitation frequency. Figure 4.28 and Figure 4.29 contain the variation of RAOs for both translational and rotational motions responses, and Figure 4.30 shows corresponding natural frequencies for Molo model. The dependence of the added mass, A_{ij}, on the wave excitation frequency, ω, results to natural frequency in each degree of freedom dependent upon ω. Therefore, resonance occurs at wave frequencies where the absolute differences between the excitation and the natural frequency tend to zero.

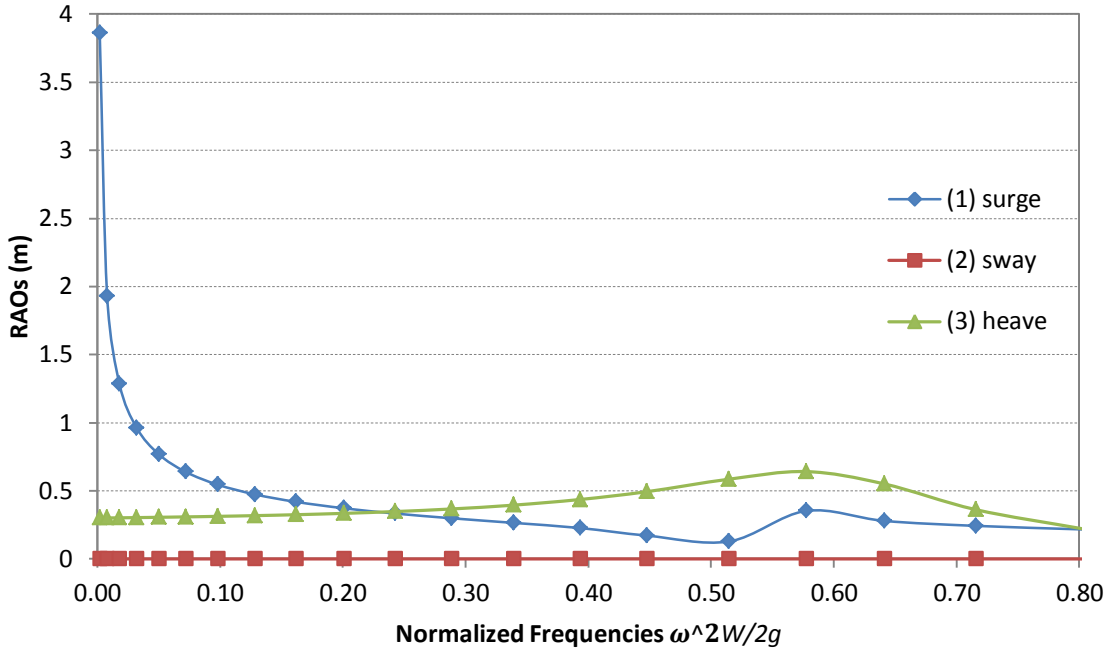

Figure 4.28 Variation of RAOs (translational motions) – Molo model

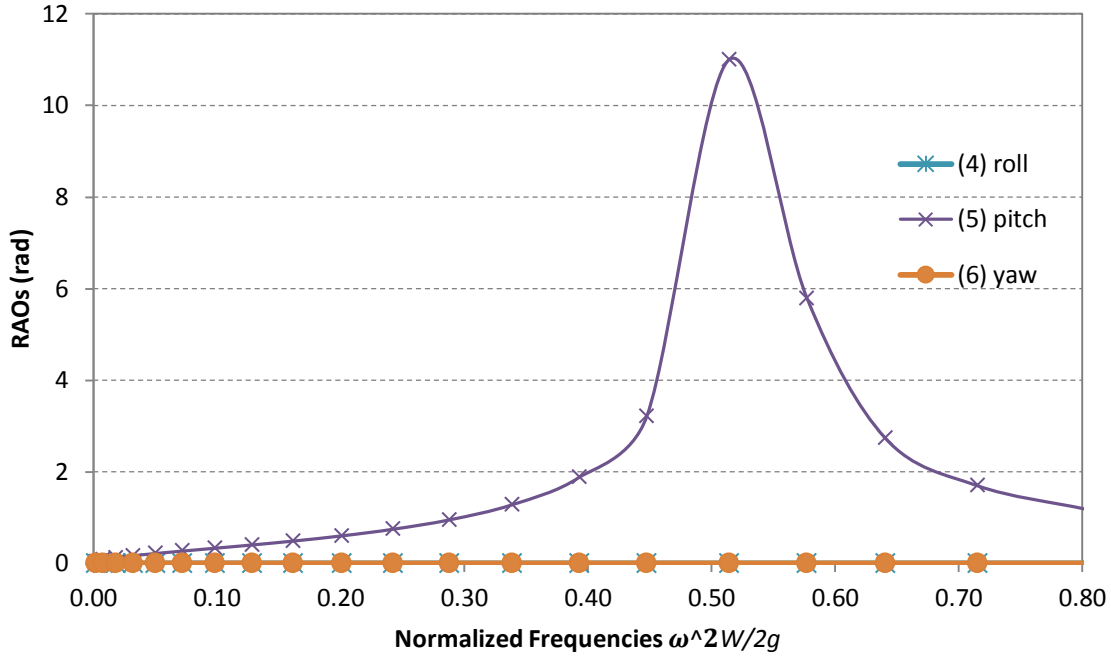

Figure 4.29 Variation of RAOs (rotational motions) – Molo model

In the case of heave response (Figure 4.28), resonance is observed at normalized frequency of 0.58 where the difference ω- ω_{n3} tends to zero, and then the heave RAO gradually decreases.

In the case of pitch response (Figure 4.29), resonance is observed at normalized frequency of 0.51where the difference ω- ω_{n5} tends to zero, and then the pitch RAO rapidly decreases.

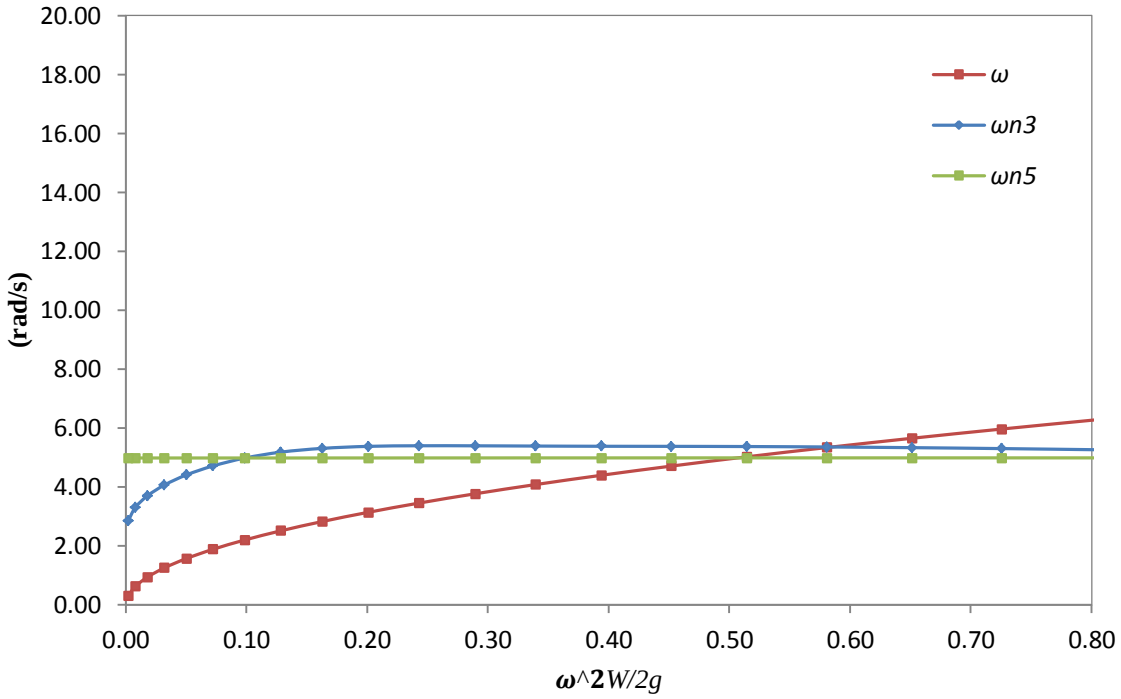

Figure 4.30 Molo model natural frequencies

4.3.2 Maere model

Figure 4.31 and Figure 4.33 contain the variation of RAOs for both translational and rotational motions responses, and Figure 3.31 shows corresponding natural frequencies for Maere model. Similar to Molo model, the dependence of the added mass, A_{ij}, on the wave excitation frequency, ω, results to natural frequency in each degree of freedom dependent upon ω. Therefore, resonance occurs at wave frequencies where the absolute differences between the excitation and the natural frequency tend to zero.

In the case of heave response (Figure 4.31), resonance is observed at normalized frequency of 1.42 where the difference ω- ω_{n3} tends to zero (Figure 3.31). However, the peak value is observed at normalized frequency of 0.63.

Similar for the case of pitch response (Figure 4.32), resonance is observed at normalized frequency of 1.58 where the difference ω- ω_{n5} tends to zero (Figure 4.33), but the peak value is observed at normalized frequency of 1.12.

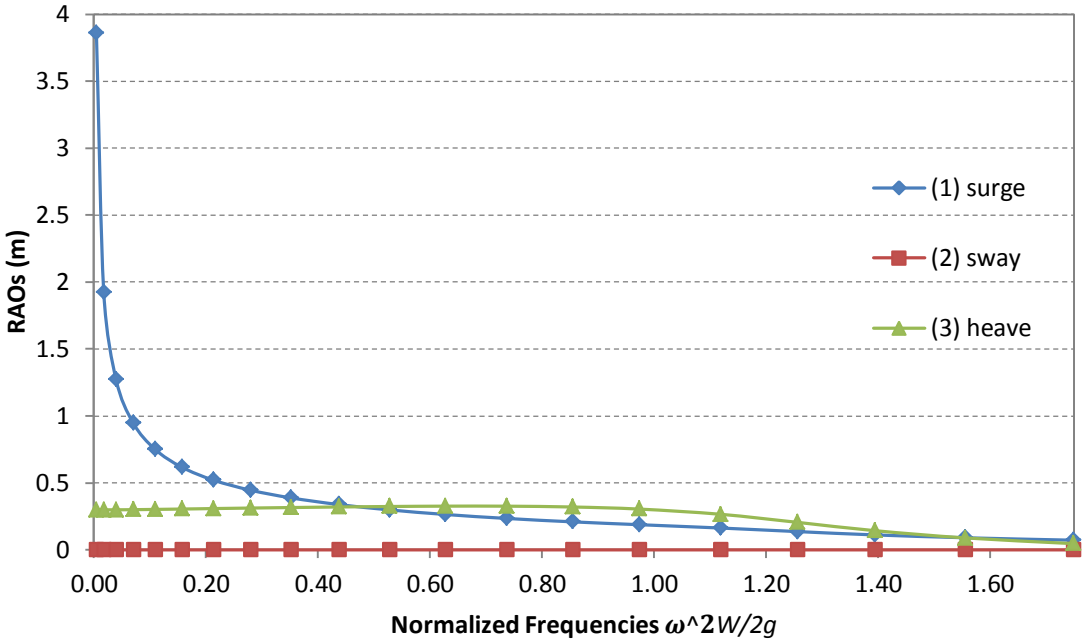

Figure 4.31 Variation of RAOs (translational motions) – Maere model

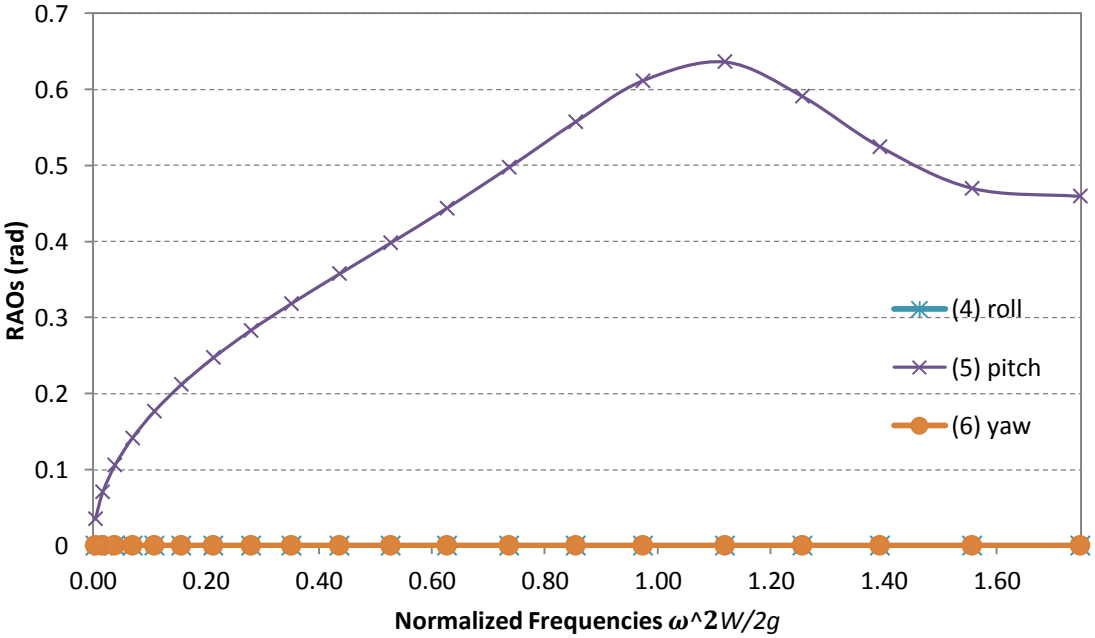

Figure 4.32 Variation of RAOs (rotational motions) – Maere model

Initially, the unconformity was suspected due to the breakwater natural frequency of each degree of freedom was calculated by using decoupled formulation. However, according to Fossen (2011), the values of natural frequencies computed by coupled and decoupled equations are close to each other. Therefore the unconformity is considered due to

uncertainties in input parameter of numerical model and further study for improvement is recommended for future work.

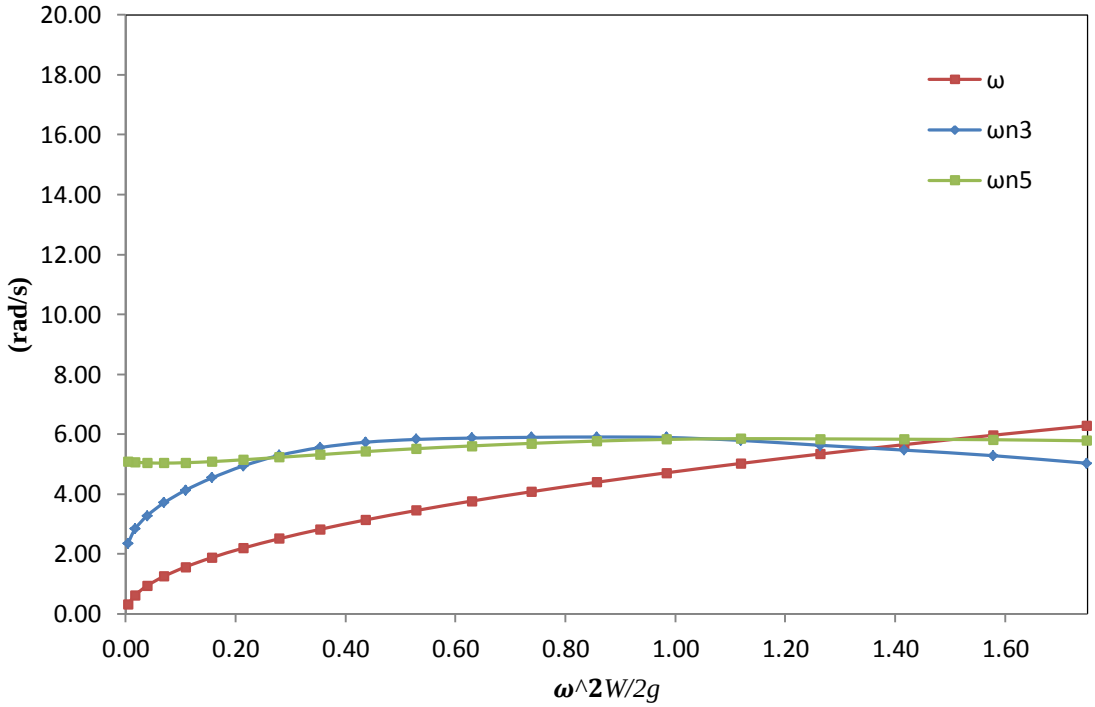

Figure 4.33 Maere model natural frequencies

4.4 Model validation

4.4.1 2D model

Transmission coefficients comparison of 2D models with the laboratory experiments data by Koutandos, et al. (2005) are given in Figure 4.34 to Figure 4.36 below. *Ct* of numerical model was calculated on two different locations of installed wave gauges WG6 and WG7.

Comparing the presented results with the corresponding one of Koutandos, et al. (2005), the tendency of the *Ct* values as a function of *W/L* is accordingly match. The transmission coefficient decreases with a decrease of wave period, that is to say a decrease of wave length, indicating an increase of wave attenuation for short wave period. However, the *Ct* values for incoming wave periods greater than 2.04 s (*W/L*=0.31) are generally larger than the laboratory experiment data. Whereas the *Ct* values for incoming wave periods of 2.04 s (*W/L*=0.31) are lower than the laboratory experiment data for all three cases.

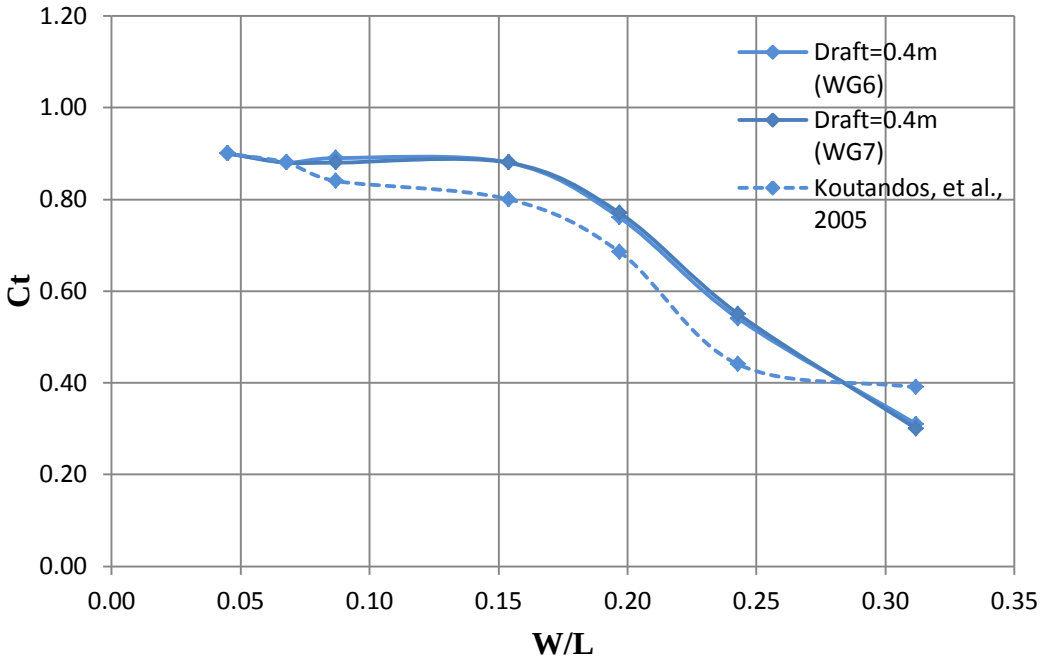

Figure 4.34 2D model *Ct* comparison (draft=0.4m)

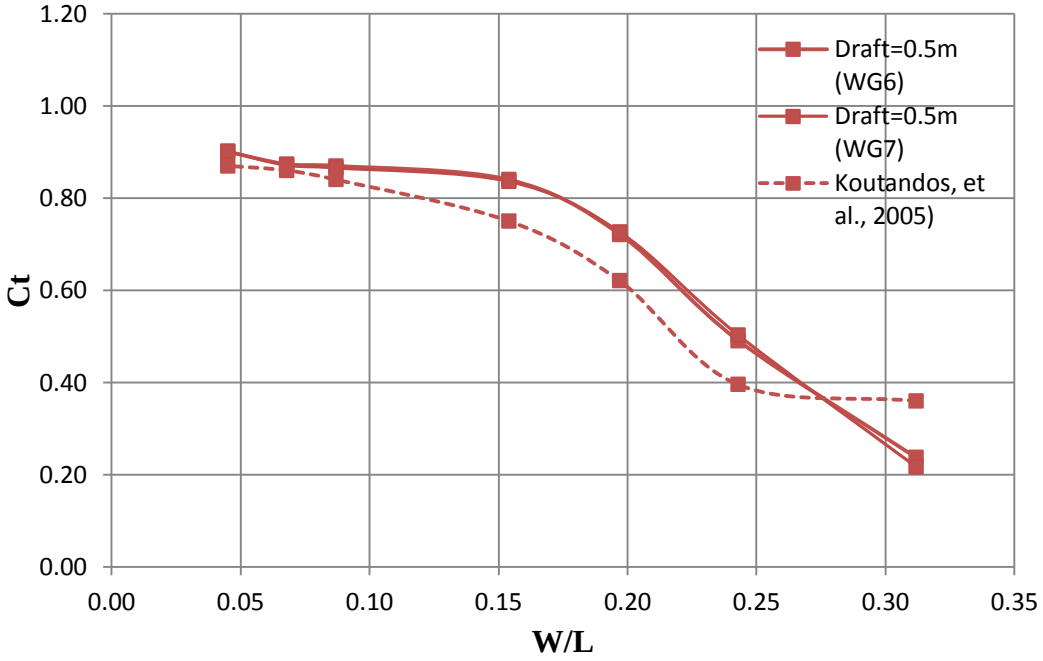

Figure 4.35 2D model *Ct* comparison (draft=0.5m)

Initially these unconformities were suspected due to different locations of where the transmitted wave heights were calculated. However from further observation, the above comparisons of *Ct* on those two different locations show that the differences are not

significant. Therefore, some improvement on the numerical model may be considered in the future work. The starting point of the improvement would be revisiting the WAMIT model and simulating several different parameters to see the sensitivity of the result. Other possibility is performing a deeper study of how the *Ct* values were calculated in the laboratory experiment.

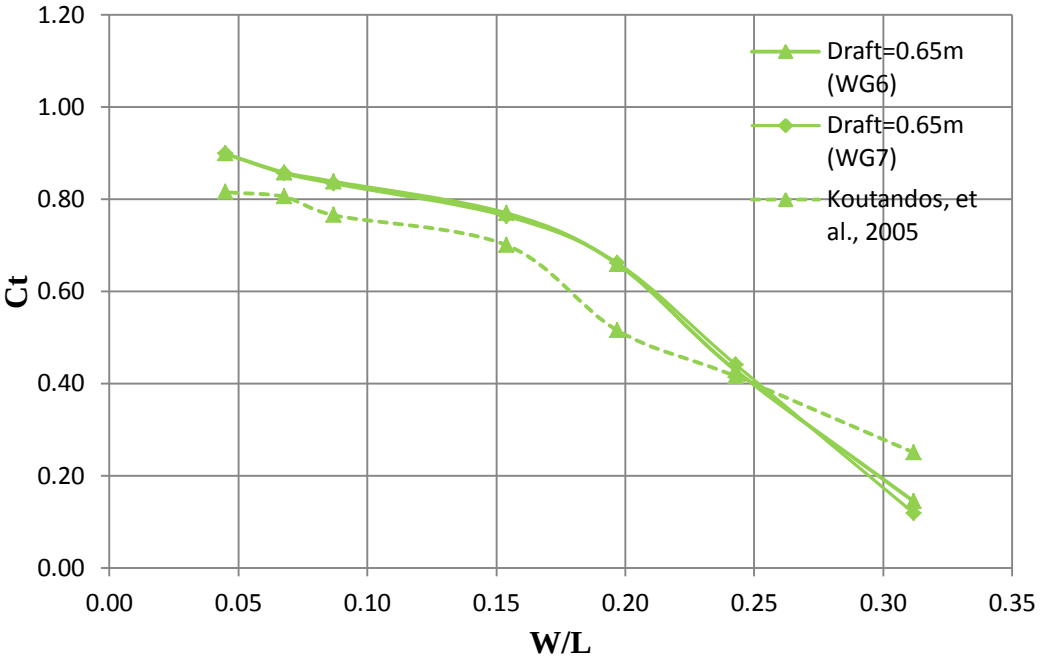

Figure 4.36 2D model *Ct* comparison (draft=0.65m)

A remarkable peculiarity of numerical model was also observed within the range of short wave periods. For incoming wave periods shorter than 2.34 s (*W/L* greater than 0.25), the experiment results show that the effect of decreasing wave length on the *Ct* values is less and even none for breakwater with draft 0.4 m and 0.5 m. This is due to the breakwater performance in a more reflective manner for shorter wave periods. It is also clarified by comparison of reflection coefficient *Cr* of breakwater (draft = 0.4 m) below. As opposed to this, the numerical model result still shows the decrease of *Ct* values on this range.

In Figure 4.37, on the same range of incoming wave periods (shorter than 2.34 s, W/L greater than 0.25), the decreasing of wave length on the experiment result is less effecting the reflection coefficients. While on the numerical model result, the effect is still noticeable. It is shown by the increasing *Cr* that indicating the increasing of wave height reflected by breakwater. Upon this observation, it could be concluded that WAMIT model has a limitation in analyzing the floating breakwater 2D model subjected to shorter incoming wave periods.

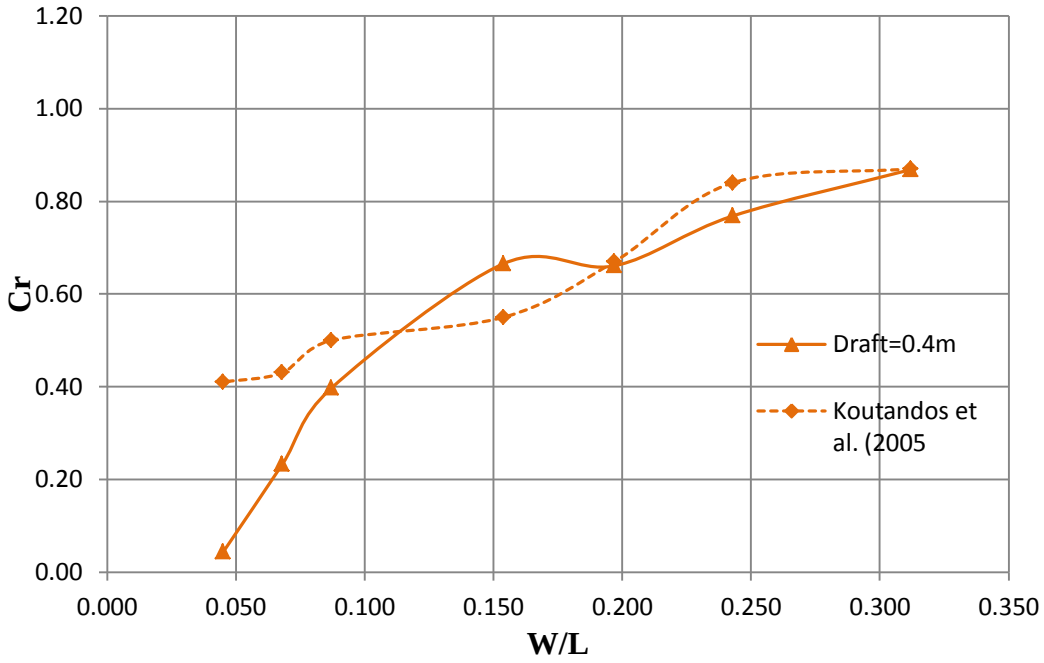

Figure 4.37 2D model *Cr* comparison (draft=0.65m)

4.4.2 Molo model

Transmission coefficients comparison of moored Molo models with the laboratory experiments data by Syltern (2005) are presented in Figure 4.38 below. *Ct* of numerical model was calculated on four different locations of installed wave gauges WG4 to WG6.

From the graph, it can be clearly noticed that the numerical model result is far from satisfactorily describing the experiment result. The great difference of the *Ct* resulted from this configuration can hardly be explained.

An improvement method has been carried out by changing the mooring stiffness matrix several times, but the results were still the same. All the results show that for the same incoming wave periods as tested on the experiment, the *Ct* values resulted from numerical model are equal to 1 indicating that the incoming waves are relatively longer compare to the breakwater width and wave attenuation was not performed by the breakwater.

These erroneous results are considered due to uncertainties in numerical model. Further investigation and improvement are recommended to be done in future work. Modification on the breakwater geometry representation by trying out different panels configurations (i.e. no-dipole with existing draft and/or no-dipole with increasing draft) in the MultiSurf geometry development is one of possible approach for the improvement. More detail study of how the laboratory experiment was performed and adapting more comparable cases from the experiment can also be considered for future work i.e. combination floating

breakwater with parabolic beach, increasing draft and width, and changing the incoming wave direction.

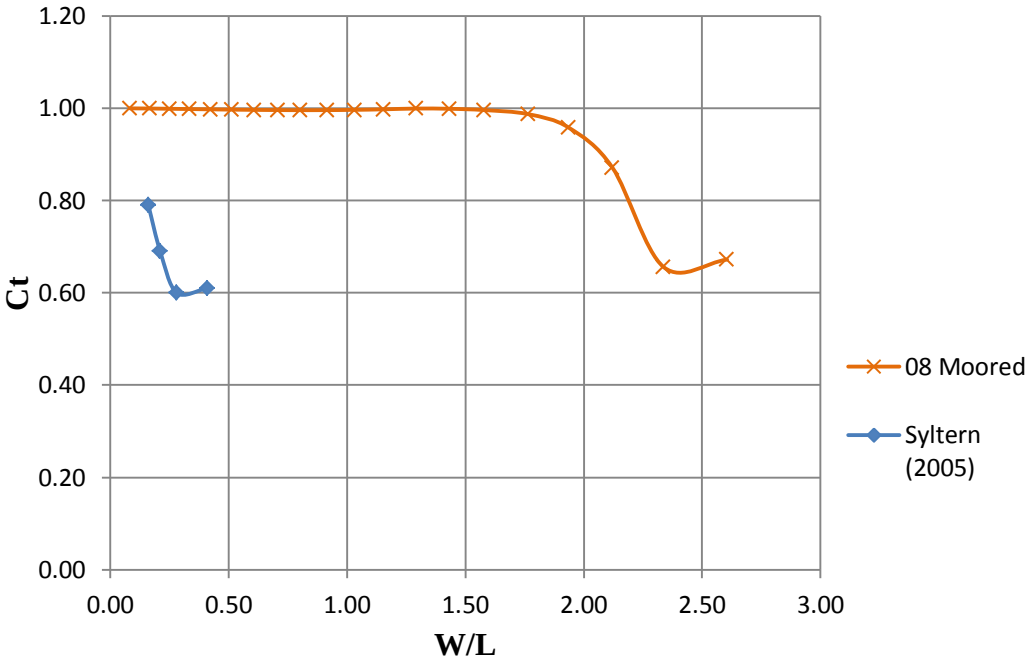

Figure 4.38 Moored Molo model *Ct* comparison

5. CONCLUSIONS AND RECOMMENDATIONS FOR FUTURE WORK

5.1 Conclusions

In this master thesis twelve out of total 13 cases of floating breakwater with different configurations has been analyzed numerically by using WAMIT and MultiSurf. The cases were based on physical models which were tested in a laboratory experiments. Measurement data from the experiments were available for numerical model validation. The study was focused on the transmitted wave behind the floating breakwaters and response motions of the breakwater.

The main conclusions from this study are as following:

- Numerical analysis for 2D floating breakwater model can be satisfactorily performed by WAMIT.
  - Approaching the condition of two-dimensional wave flume by eliminating the diffraction effect on the lee side of breakwater is considered to be appropriate.
  - The tendencies of resulted *Ct* were accordingly match to the experiment data, with only small deviation of the *Ct* magnitude.
  - A limitation of WAMIT performance was observed on the short incoming wave periods where WAMIT was not indicating the reflective manner of the breakwater performance in the experiment.
- Numerical analysis for Molo model with moored configuration is still far from perfect.
  - The RAOs predicted by WAMIT was clarified by calculated natural frequencies i.e. resonances occurred at wave frequencies in the vicinity of the natural frequencies.
  - A remarkable erroneous result of *Ct* was obtained from this case and the cause could hardly be explained.
  - Initial presumption that the error was caused by incorrect mooring line stiffness matrix was proven wrong since the same results were obtained by using different values of the mooring stiffness. Few possible approaches for numerical model improvement might be considered for future work.
- Numerical analysis for Maere model is not validated and further improvement for the analysis is required.
  - The RAOs predicted by WAMIT was not clarified since there were differences between the calculated natural frequencies and the peak response motions.
  - Comparable cases for this model are recommended for improvement and model validation.

5.2 RecommendationS for future work

Recommendations for future work are as following:

- Improving the numerical model result by trying out different structure geometry representation, i.e. no-dipole with existing draft and/or no dipole with increasing draft, and determining the best one for the analysis
- Simulating more cases which are comparable to the laboratory experiment i.e. combination floating breakwater with parabolic beach, increasing draft and width, and changing the incoming wave direction
- deeper and more thorough study on how the laboratory experiment were carried out including detail on how the results were processed and final outputs were calculated in order to have a better approach for the numerical model.

REFERENCES

Faltinsen, O. M., 1990. *Sea Loads on Ships and Offshore Structures.* Cambridge: The Press Syndicate of University of Cambridge.

Fossen, T. I., 2011. *Handbook of Marine Craft Hydrodynamics and Motion Control.* s.l.:John Wiley & Sons, Ltd.

Koutandos, E., Prinos, P. & Gironella, X., 2005. Floating breakwaters under regular and irregular wave forcing: reflection and transmission characteristics. *Journal of Hydraulic Research,* Vol. 43(Iss. 2), pp. 174-188.

Ozeren, Y. et al., 2011. Experimental Investigation of Cylindrical Floating Breakwater Performance with Various Mooring Configurations. *Journal of Waterway, Port, Coastal, and Ocean Engineering,* 137(6), pp. 300-309.

Ruol, P., 2008. *Vlaams Instituut voor de Zee.* [Online]
Available at: http://www.vliz.be/wiki/Floating_breakwaters
[Accessed 2 December 2012].

Sannasiraj, S. A., Sundar, V. & Sundaravadivelu, R., 1998. Mooring Forces and Motion Responses of Pontoon-Type Floating Breakwater. *Ocean Engineering,* 25(1), pp. 27-48.

Syltern, J. A., 2005. *Experimental Studies of the OMS Floating Breakwater,* Trondheim: NTNU.

Tørum, A., 2011. *Coastal Structure, Lecture notes distributed in Department of Civil and Transport, NTNU.* Trondheim: s.n.

W., 1998-2006. *WAMIT User Manual Versions 6.4, 6.4PC, 6.3S, 6.3S-PC,* Massachusetts: s.n.

Zidan, A. R., Rageh, O. S., Sarhan, T. E. & El-Sharabasy, M. M., 2012. *Wave Interaction with Single and Twin Pontoon.* Istanbul, Turkey, IWTC 16.

APPENDICES

TABLES

FIGURES

A. CENTER OF GRAVITY AND RADII OF GYRATION

Calculation of center of gravity (CoG) and radii of gyration of Molo and Maere models are detailed in this section. Two approaches of body representation are used in Molo model calculation to check its effect on the analysis results. In the first approach (Section A.1) the model is considered as one rigid composite body consists of steel plate, polystyrene, and amount of water filled the open compartment on the bottom model which moves along with the model. Whereas in the second approach (Section A.2) the amount of water filled the bottom open compartment is no longer considered.

Comparing the analysis results using both approaches, it found that the results are qualitatively comparable in terms of wave diffraction, wave attenuation, and wave riding breakwater occurrence on certain incident wave conditions. Consequently, the second approach is used in Maere model calculation (Section A.3) and further analysis since it is representing the model more accurately. Summary table of calculated radii of gyration is given in Section A.4.

A.1 Molo model (approach 1)

Molo model is constructed from 2 units of pontoons type I with total dimensions of 4 m length, 0.4 m width, and 0.2 m height. It is constructed as bottomless boxes of steel plate with thickness of 3 mm and polystyrene as the floating element. Two internal plates were installed on each pontoon dividing the pontoon into three equal spaces.

After being submerged for a long time, pontoons weight on air is approximately each 50 kg, indicating the polystyrene saturated with water.

In this approach, the model is considered as one rigid composite body. It consists of steel plate, polystyrene, and amount of water filled the open compartment on the bottom part which moves along with the model. Figure A.1 and Figure A.2 show the sketch of the model perspective and cross section.

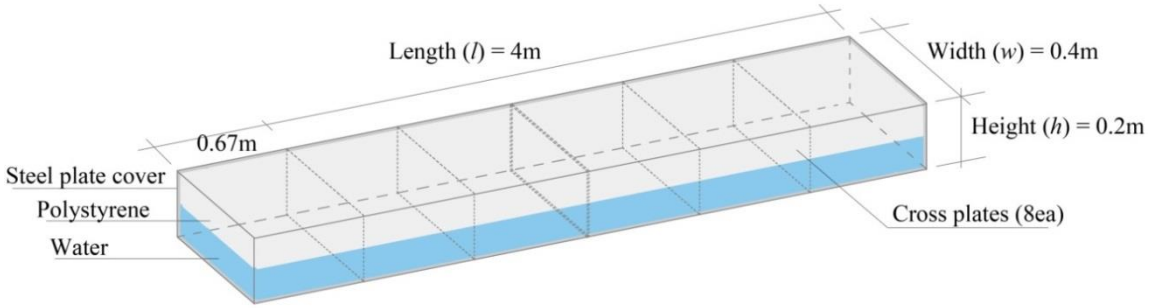

Figure A.1 Molo model perspective

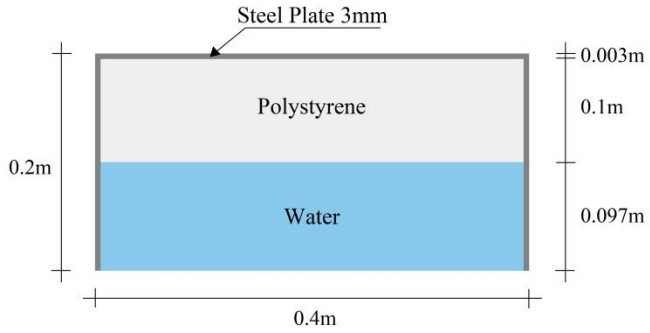

Figure A.2 Molo model cross section

Body properties are given below.

$$Total\ mass\ (m_{Steel} + m_{Polystyrene}) = 100kg$$
$$Length\ (l) = 4m$$
$$Height\ (h) = 0.2m$$
$$Width\ (w) = 0.4m$$
$$Cross\ plate = 8ea\ (4\ internal\ plates\ and\ 4\ side\ plates)$$
$$Area_{Steel} = 2(0.2m \times 4m) + (4m \times 0.4m) + 8(0.2m \times 0.4m) = 3.84m^2$$
$$Unit\ weight = 7.85kg/m^2mm \times 3mm = 23.6\,kg/m^2$$
$$Steel\ Mass\ (m_{Steel}) = 3.84m^2 \times 23.6\,kg/m^2 = 90.6kg$$
$$Polystyrene\ Mass\ (m_{Polystyrene)}) = 100kg - 90.6kg = 9.4kg$$
$$Polystyrene\ Height = 0.1m$$

A.1.1 Component mass calculation

To ease the calculation of pontoon-center of gravity (pontoon-CoG) and mass moment of inertia, the pontoon is divided into components consists of cross-plates and body-sections as shown in following Figure A.3. The cross-plates and body-sections are marked by c1 to c8 and s1 to s6, respectively.

A.1.1.1 Cross-plates mass (c1 to c8)

$$Area = 0.4m \times 0.2m = 0.08m^2$$
$$Unit\ weight = 7.85kg \times 3mm = 23.6\,kg/m^2$$
$$Mass\ (m_{Cross-plate}) = 0.08m^2 \times 23.6\,kg/m^2 = 1.89kg$$

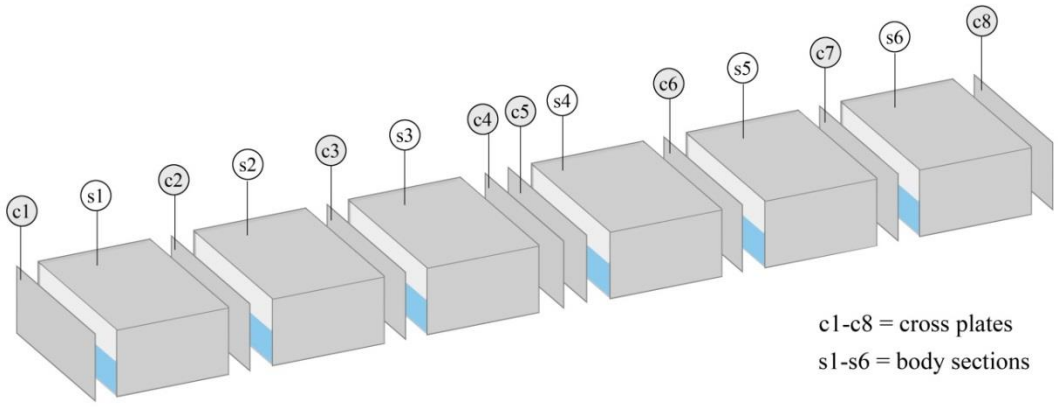

Figure A.3 Molo model divisions

A.1.1.2 Body-sections mass (s1 to s6)

$$Steel\ mass\ (m_{Steel-bs}) = \left(m_{Steel} - 8\left(m_{Cross-plate}\right)\right)/6 = 12.58kg$$

$$Polystyrene\ mass\ \left(m_{Polystyrene-bs}\right) = m_{Polystyrene}/6 = 1.57kg$$

$$Water\ mass\ (m_{Water-bs}) = Volume_{Water} \times \rho_{Water}$$
$$= (0.663 \times 0.394 \times 0.097)m^3 \times 1000\,kg/m^3 = 25.34kg$$

$$Mass\ \left(m_{Body-section}\right) = m_{Steel-bs} + m_{Polystyrene-bs} + m_{Water-bs} = 39.49kg$$

A.1.2 Calculation of component-CoG and pontoon-CoG

Cross-plates are component with uniform density. Therefore the component-CoG of cross-plates is right in the center of the cross-plates.

In other hand, body-section is a composite component with various densities which is symmetrical about the plane x=0 and y=0. Following is the calculation of component-CoG of the body-sections relative to reference point placed on the center of top plate with ź-axis positive upward. The position of calculated component-CoG is shown in Figure A.4.

$$\bar{x}_{Body-section} = 0m$$

$$\bar{y}_{Body-section} = 0m$$

$$\bar{z}_{Body-section} = \frac{(\bar{z} \times m)_{Steel-bs} + (\bar{z} \times m)_{Polystyrene-bs} + (\bar{z} \times m)_{Water-bs}}{m_{Steel-bs} + m_{Polystyrene-bs} + m_{Water-bs}}$$

$$\bar{z}_{Steel-bs} = \frac{2\left(-0.1m(23.6\,kg/m^2 \times 0.2m \times 0.663m)\right)}{12.58kg} = -0.05m$$

$$\bar{z}_{Polystyrene-bs} = \frac{-0.05m \times 1.57kg}{1.57kg} = -0.05m$$

$$\bar{z}_{Water-bs} = \frac{-0.15m \times 25.34kg}{25.34kg} = -0.15m$$

$$\bar{z}_{Body-section} = \frac{(-0.05m \times 12.58kg) + (-0.05m \times 1.57kg) + (-0.15 \times 25.34kg)}{12.58kg + 1.57kg + 25.34kg}$$
$$= -0.11m$$

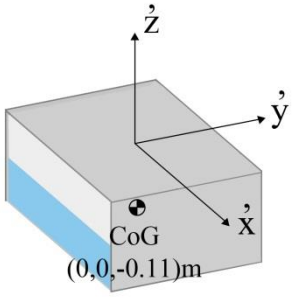

Figure A.4 Position of body-sections CoG

Pontoon is symmetrical about the plane x=0 and y=0. Therefore;

$$\bar{x}_{Pontoon} = 0m$$
$$\bar{y}_{Pontoon} = 0m$$

Calculation of pontoon-CoG on the ẑ-axis is given below. A new reference point is placed on the center of pontoon top plate with ẑ-axis positive upward. Figure A.5 illustrates the reference point placement and the calculated pontoon-CoG position.

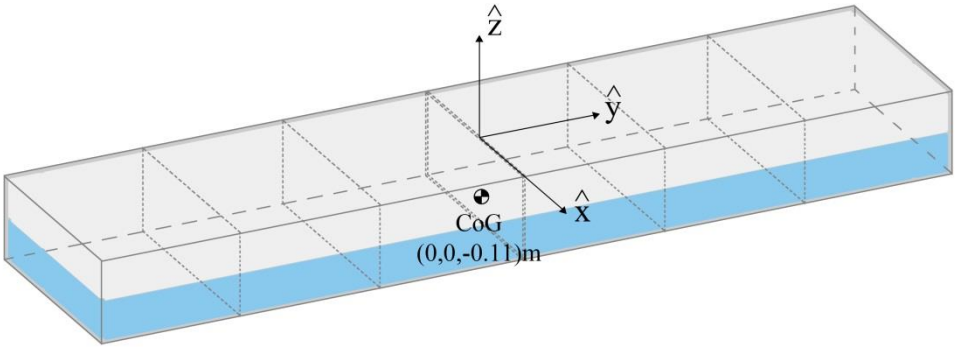

Figure A.5 Position of pontoon CoG

$$\bar{z}_{Pontoon} = \frac{\sum_{n=1}^{8}(\bar{z}_n \times m_n)_{Cross-plate} + \sum_{m=1}^{6}(\bar{z}_m \times m_m)_{Body-section}}{m_{Cross-plate} + m_{Body-section}}$$

$$\bar{z}_{Pontoon} = \frac{8(-0.1m \times 1.89kg) + 6(-0.11m \times 39.49kg)}{8(1.89) + 6(39.49)} = -0.11m$$

A.1.3 Calculation of mass moment of inertia

A.1.3.1 Cross-plates mass moment of inertia

Mass moment of inertia of cross plates relative to its CoG is calculated below.

$$I_{xx-Cross-plate} = \frac{1}{12}m(h^2 + l^2) = \frac{1}{12}1.89kg(0.2^2 + 0.003^2)m^2 = 0.0063kgm^2$$

$$I_{yy-Cross-plate} = \frac{1}{12}m(w^2 + h^2) = \frac{1}{12}1.89kg(0.4^2 + 0.2^2)m^2 = 0.0315kgm^2$$

$$I_{zz-Cross-plate} = \frac{1}{12}m(w^2 + l^2) = \frac{1}{12}1.89kg(0.4^2 + 0.003^2)m^2 = 0.0252kgm^2$$

A.1.3.2 Body-section mass moment of inertia

Mass moment of inertia of steel plates covering the body-section is done by calculating mass moment of inertia of steel solid rectangular cuboid then subtracted by mass moment of inertia of center portion in order to obtain the mass moment of inertia of bottomless hollow steel cuboid.

$$Unit\ weight\ solid = 7.85kg/m^2mm \times 200mm = 1570\,kg/m^2$$

$$Area\ solid = 0.663m \times 0.4m = 0.2652m^2$$

$$m_{Solid} = 0.2652m^2 \times 1570\,kg/m^2 = 416.36kg$$

$$I_{xx-Solid} = \frac{1}{12}m_{Solid}(h^2 + l^2) = \frac{1}{12}416.36kg(0.2^2 + 0.663^2)m^2 = 16.64kgm^2$$

$$I_{yy-Solid} = \frac{1}{12}m_{Solid}(w^2 + h^2) = \frac{1}{12}416.36kg(0.4^2 + 0.2^2)m^2 = 6.94kgm^2$$

$$I_{zz-Solid} = \frac{1}{12}m_{Solid}(w^2 + l^2) = \frac{1}{12}416.36kg(0.4^2 + 0.663^2)m^2 = 20.8kgm^2$$

$$Unit\ weight\ center = 7.85kg/m^2mm \times 197mm = 1546.45\,kg/m^2$$

$$Area\ center = 0.663m \times 0.394m = 0.261m^2$$

$$m_{Center} = 0.261m^2 \times 1546.45\,kg/m^2 = 403.62kg$$

$$I_{xx-Center} = \frac{1}{12} m_{Center}(h^2 + l^2) = \frac{1}{12} 403.62kg(0.197^2 + 0.663^2)m^2 = 16.1kgm^2$$

$$I_{yy-Center} = \frac{1}{12} m_{Center}(w^2 + h^2) = \frac{1}{12} 403.62kg(0.394^2 + 0.197^2)m^2 = 6.53kgm^2$$

$$I_{zz-Center} = \frac{1}{12} m_{Center}(w^2 + l^2) = \frac{1}{12} 403.62kg(0.394^2 + 0.663^2)m^2 = 20kgm^2$$

$$I_{xx-Steel} = I_{xx-Solid} - I_{xx-Center} = 16.64kgm^2 - 16.1kgm^2 = 0.54kgm^2$$
$$I_{yy-Steel} = I_{yy-Solid} - I_{yy-Center} = 6.94kgm^2 - 6.53kgm^2 = 0.41kgm^2$$
$$I_{zz-Steel} = I_{zz-Solid} - I_{zz-Center} = 20.8kgm^2 - 20kgm^2 = 0.8kgm^2$$

Above mass moment of inertia is relative to the solid cuboid CoG. To get the correct mass moment inertia of bottomless hollow steel cuboid, it should be translated to the hollow cuboid CoG. According to parallel axis theorem, mass moment of inertia about the new axis is given by Equation A.1 below.

$$I_{xx} = I_{xx} + md^2 \quad \textbf{(A.1)}$$

where d is the perpendicular distance between the axis of rotation. The same equation is also applied to other axis.

$$I_{xx-Steel} = I_{xx-Steel} + m_{Steel-bs}d^2 = 0.54kgm^2 + (12.58kg \times 0^2m^2) = 0.54kgm^2$$
$$I_{yy-Steel} = I_{yy-Steel} + m_{Steel-bs}d^2 = 0.41gm^2 + (12.58kg \times 0^2m^2) = 0.41kgm^2$$
$$I_{zz-Steel} = I_{zz-Steel} + m_{Steel-bs}d^2 = 0.8kgm^2 + (12.58kg \times 0.05^2m^2) = 0.83kgm^2$$

Mass moment of inertia of polystyrene in the body-section is calculated below.

$$I_{xx-Polystyrene} = \frac{1}{12} m_{Polystyrene-bs}(h^2 + l^2) = \frac{1}{12} 1.57kg(0.1^2 + 0.663^2)m^2 = 0.06kgm^2$$

$$I_{yy-Polystyrene} = \frac{1}{12} m_{Polystyrene-bs}(w^2 + h^2) = \frac{1}{12} 1.57kg(0.394^2 + 0.1^2)m^2$$
$$= 0.02kgm^2$$
$$I_{zz-Polystyrene} = \frac{1}{12} m_{Polystyrene-bs}(w^2 + l^2) = \frac{1}{12} 1.57kg(0.394^2 + 0.663^2)m^2$$
$$= 0.08kgm^2$$

Mass moment of inertia of water in the body-section is calculated below.

$$I_{xx-Water} = \frac{1}{12} m_{Water-bs}(h^2 + l^2) = \frac{1}{12} 25.43kg(0.097^2 + 0.663^2)m^2$$
$$= 0.95kgm^2$$
$$I_{yy-Water} = \frac{1}{12} m_{Water-bs}(w^2 + h^2) = \frac{1}{12} 25.43kg(0.394^2 + 0.097^2)m^2$$
$$= 0.35kgm^2$$
$$I_{zz-Water} = \frac{1}{12} m_{Water-bs}(w^2 + l^2) = \frac{1}{12} 25.43kg(0.394^2 + 0.663^2)m^2$$
$$= 1.26kgm^2$$

Total mass moment of inertia of body-section is the sum up of the mass moment of inertia of all elements about the same axis of reference. Parallel axis theorem is used to translate calculated moment of inertia to the body-section CoG. Since the element center of masses are shifted only about the z-axis, the mass moment of inertia of all elements about the x and y-axis will be the same. The mass moment of inertia for new z-axis is given below.

$$I_{zz-Steel} = I_{zz-Steel} + m_{Steel} d^2 = 0.83kgm^2 + (12.58kg \times 0.06^2 m^2) = 0.88kgm^2$$
$$I_{zz-Polystyrene} = I_{zz-Polystyrene} + m_{Polystyrene} d^2$$
$$= 0.08kgm^2 + (1.57kg \times 0.06^2 m^2) = 0.09kgm^2$$
$$I_{zz-Water} = I_{zz-Water} + m_{Water} d^2 = 1.26kgm^2 + (25.43kg \times 0.04^2 m^2)$$
$$= 1.3kgm^2$$

Total mass moment of inertia of each body-section about its CoG is given below.

$$I_{xx-Body-section} = I_{xx-Steel} + I_{xx-Polystyrene} + I_{xx-Water} = 1.55kgm^2$$
$$I_{yy-Body-section} = I_{yy-Steel} + I_{yy-Polystyrene} + I_{yy-Water} = 0.78kgm^2$$
$$I_{zz-Body-section} = I_{zz-Steel} + I_{zz-Polystyrene} + I_{zz-Water} = 2.27kgm^2$$

A.1.3.3 Pontoon mass moment of inertia

Pontoon mass moment of inertia is calculated by translating mass moment of inertia of each cross-plate and body-section to the pontoon-CoG. Parallel axis theorem is also used for the calculation. Table A.1 shows the calculated pontoon mass moment of inertia.

Table A.1 Calculation of pontoon mass moment of inertia

Components	Component mass moment of inertia (kgm^2)			Mass (kg)	Axis distance (m)			Pontoon mass moment of inertia ($kgm2$)		
	I_{xx}	I_{yy}	I_{zz}		d_x	d_y	d_z	I_{xx}	I_{yy}	I_{zz}
Cross-plate c1	0.0063	0.0315	0.0252	1.89	1.9950	0.0000	0.0100	7.53	0.03	0.03
Cross-plate c2	0.0063	0.0315	0.0252	1.89	1.3340	0.0000	0.0100	3.37	0.03	0.03
Cross-plate c3	0.0063	0.0315	0.0252	1.89	0.6680	0.0000	0.0100	0.85	0.03	0.03
Cross-plate c4	0.0063	0.0315	0.0252	1.89	0.0000	0.0000	0.0100	0.01	0.03	0.03
Cross-plate c5	0.0063	0.0315	0.0252	1.89	0.0000	0.0000	0.0100	0.01	0.03	0.03
Cross-plate c6	0.0063	0.0315	0.0252	1.89	0.6680	0.0000	0.0100	0.85	0.03	0.03
Cross-plate c7	0.0063	0.0315	0.0252	1.89	1.3340	0.0000	0.0100	3.37	0.03	0.03
Cross-plate c8	0.0063	0.0315	0.0252	1.89	1.9950	0.0000	0.0100	7.53	0.03	0.03
Body-section s1	1.5500	0.7800	2.2700	39.49	1.6670	0.0000	0.0000	111.29	0.78	2.27
Body-section s2	1.5500	0.7800	2.2700	39.49	1.0000	0.0000	0.0000	41.04	0.78	2.27
Body-section s3	1.5500	0.7800	2.2700	39.49	0.3350	0.0000	0.0000	5.98	0.78	2.27
Body-section s4	1.5500	0.7800	2.2700	39.49	0.3350	0.0000	0.0000	5.98	0.78	2.27
Body-section s5	1.5500	0.7800	2.2700	39.49	1.0000	0.0000	0.0000	41.04	0.78	2.27
Body-section s6	1.5500	0.7800	2.2700	39.49	1.6670	0.0000	0.0000	111.29	0.78	2.27
							Total	**340.13**	**4.93**	**13.82**

A.1.4 Calculation of radii of gyration

Calculation of pontoon radii of gyration is done by Equation A.2 below.

$$r_i = \sqrt{\frac{I_{i-Pontoon}}{m_{Pontoon}}} = \sqrt{\frac{I_{i-Pontoon}}{m_{Steel} + m_{Polystyrene} + m_{Water}}} \quad \textbf{(A.2)}$$

$$r_x = \sqrt{\frac{I_{xx}}{m_{Pontoon}}} = \sqrt{\frac{340.13 kgm^2}{252.06 kg}} = 1.16m$$

$$r_y = \sqrt{\frac{I_{yy}}{m_{Pontoon}}} = \sqrt{\frac{4.93kgm^2}{252.06kg}} = 0.14m$$

$$r_z = \sqrt{\frac{I_{zz}}{m_{Pontoon}}} = \sqrt{\frac{13.82kgm^2}{252.06kg}} = 0.23m$$

A.2 Molo model (approach 2)

In this approach, the model is considered as one rigid composite body. It consists of steel plate and polystyrene placed inside the pontoons with height of 0.1m. The amount of water filled the bottom open compartment is no longer considered. Figure A.6 and Figure A.7 show the sketch of the model perspective and cross section.

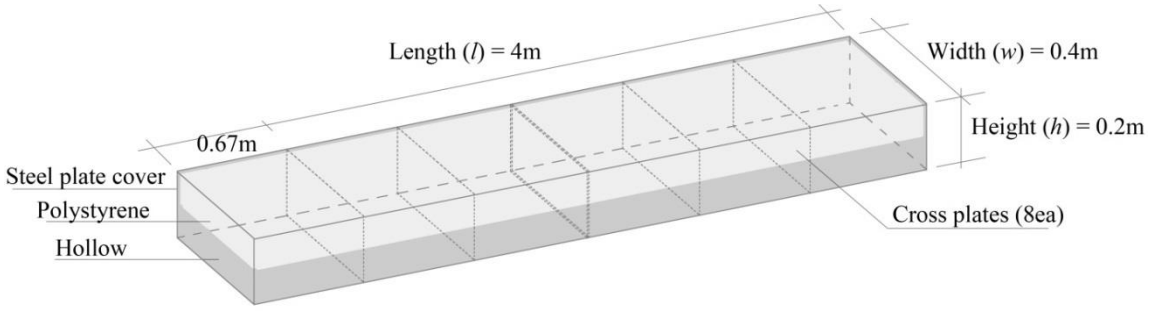

Figure A.6 Molo model perspective (approach 2)

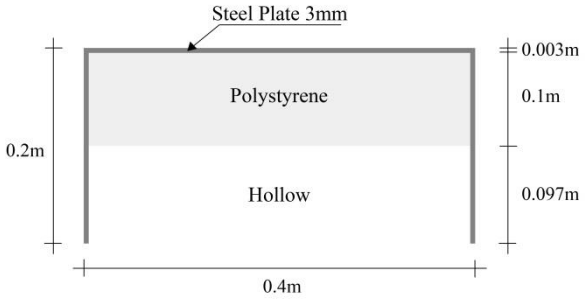

Figure A.7 Molo model cross section (approach 2)

Body properties are given below.

$$Total\ mass\ \left(m_{Steel} + m_{Polystyrene}\right) = 100kg$$

$$Length\ (l) = 4m$$

$$Height\ (h) = 0.2m$$

$$Width\ (w) = 0.4m$$
$$Cross\ plate = 8ea\ (4\ internal\ plates\ and\ 4\ side\ plates)$$
$$Area_{Steel} = 2(0.2m \times 4m) + (4m \times 0.4m) + 8(0.2m \times 0.4m) = 3.84m^2$$
$$Unit\ weight = 7.85kg/m^2mm \times 3mm = 23.6\,kg/m^2$$
$$Steel\ Mass\ (m_{Steel}) = 3.84m^2 \times 23.6\,kg/m^2 = 90.6kg$$
$$Polystyrene\ Mass\ \left(m_{Polystyrene)}\right) = 100kg - 90.6kg = 9.4kg$$
$$Polystyrene\ Height = 0.1m$$

A.2.1 Component mass calculation

Similar to previous approach, the pontoon is divided into components consists of cross-plates and body-sections as shown in following Figure A.8. The cross-plates and body-sections are marked by c1 to c8 and s1 to s6, respectively.

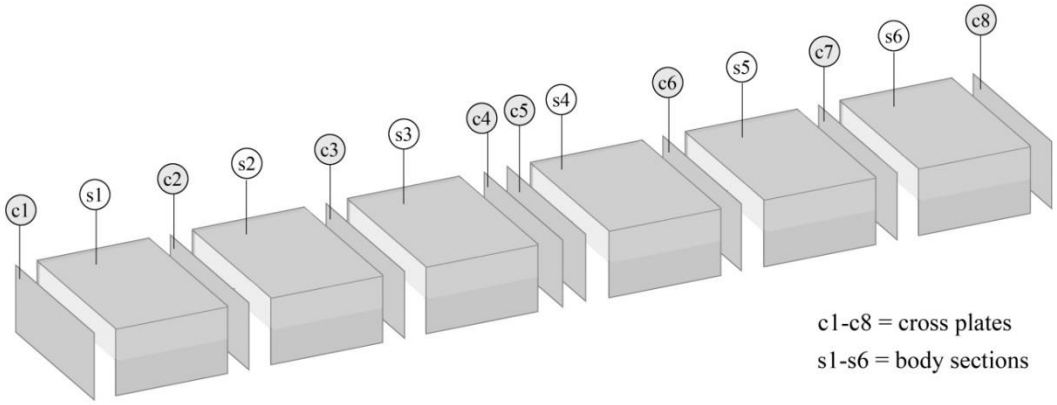

Figure A.8 Molo model divisions (approach 2)

Applying the same calculations as in section A.1.1.1 and A.1.1.2 above, the cross-plate and body-section masses are following.

$$Mass\ \left(m_{Cross-plate}\right) = 1.89kg$$
$$Mass\ \left(m_{Body-section}\right) = 14.15kg$$

A.2.2 Calculation of component-CoG and pontoon-CoG

Cross-plates are component with uniform density. Therefore the component-CoG of cross-plates is right in the center of the cross-plates.

The component-CoG and pontoon-CoG are calculated by employing the same procedures as in Section A.1.2 above. The calculated CoG are given below and illustrated in Figure A.9 and A.10.

$$\bar{x}_{Body-section} = 0m$$
$$\bar{y}_{Body-section} = 0m$$
$$\bar{z}_{Body-section} = -0.05m$$

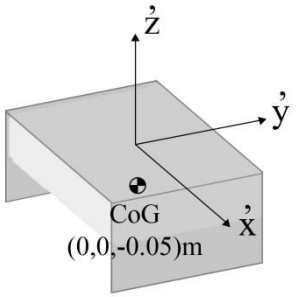

Figure A.9 Position of body-sections CoG (approach 2)

$$\bar{x}_{Pontoon} = 0m$$
$$\bar{y}_{Pontoon} = 0m$$
$$\bar{z}_{Pontoon} = -0.06m$$

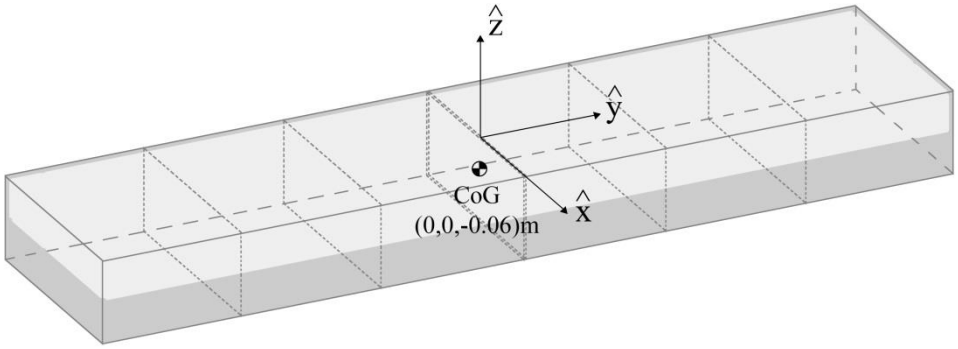

Figure A.10 Position of pontoon CoG (approach 2)

A.2.3 Calculation of mass moment of inertia

Pontoon mass moment of inertia is calculated with the same procedures as in Section A.1.3 above. The calculated moment of inertia is given in Table A.2 below.

Table A.2 Calculation of Pontoon Mass Moment of Inertia (approach 2)

Components	Component mass moment of inertia (kgm^2)			Mass (kg)	Axis distance (m)			Pontoon mass moment of inertia ($kgm2$)		
	I_{xx}	I_{yy}	I_{zz}		d_x	d_y	d_z	I_{xx}	I_{yy}	I_{zz}
Cross-plate c1	0.0063	0.0315	0.0252	1.89	1.9950	0.0000	0.0100	7.53	0.03	0.03
Cross-plate c2	0.0063	0.0315	0.0252	1.89	1.3340	0.0000	0.0100	3.37	0.03	0.03
Cross-plate c3	0.0063	0.0315	0.0252	1.89	0.6680	0.0000	0.0100	0.85	0.03	0.03
Cross-plate c4	0.0063	0.0315	0.0252	1.89	0.0000	0.0000	0.0100	0.01	0.03	0.03
Cross-plate c5	0.0063	0.0315	0.0252	1.89	0.0000	0.0000	0.0100	0.01	0.03	0.03
Cross-plate c6	0.0063	0.0315	0.0252	1.89	0.6680	0.0000	0.0100	0.85	0.03	0.03
Cross-plate c7	0.0063	0.0315	0.0252	1.89	1.3340	0.0000	0.0100	3.37	0.03	0.03
Cross-plate c8	0.0063	0.0315	0.0252	1.89	1.9950	0.0000	0.0100	7.53	0.03	0.03
Body-section s1	0.6000	0.4300	0.9700	39.49	1.6670	0.0000	0.0000	110.34	0.43	0.97
Body-section s2	0.6000	0.4300	0.9700	39.49	1.0000	0.0000	0.0000	40.09	0.43	0.97
Body-section s3	0.6000	0.4300	0.9700	39.49	0.3350	0.0000	0.0000	5.03	0.43	0.97
Body-section s4	0.6000	0.4300	0.9700	39.49	0.3350	0.0000	0.0000	5.03	0.43	0.97
Body-section s5	0.6000	0.4300	0.9700	39.49	1.0000	0.0000	0.0000	40.09	0.43	0.97
Body-section s6	0.6000	0.4300	0.9700	39.49	1.6670	0.0000	0.0000	110.34	0.43	0.97
							Total	**334.43**	**2.83**	**6.02**

A.2.4 Calculation of radii of gyration

$$r_x = \sqrt{\frac{I_{xx}}{m_{Pontoon}}} = \sqrt{\frac{334.43kgm^2}{100kg}} = 1.83m$$

$$r_y = \sqrt{\frac{I_{yy}}{m_{Pontoon}}} = \sqrt{\frac{2.83kgm^2}{100kg}} = 0.17m$$

$$r_z = \sqrt{\frac{I_{zz}}{m_{Pontoon}}} = \sqrt{\frac{6.02kgm^2}{100kg}} = 0.25m$$

A.3 Mære model

Mære model is constructed from 7 units of pontoons type II with configuration of longitudinal and transversal pontoons as shown in Figure 11. The pontoon dimension is 1.5 m length, 0.24 m width, and 0.16 m height. It is constructed as bottomless boxes of steel

plate with thickness of 3 mm and polystyrene as the floating element. Two internal plates were installed on each pontoon dividing the pontoon into three equal spaces.

On this analysis, the model is considered as one rigid composite body. It consists of steel plate and polystyrene placed inside the pontoons with height of 0.1m. Figure A.11 and Figure A.12 show the sketch of the model perspective and cross section.

Body properties of each pontoon are given below.

$$Pontoon\ length\ (l_p) = 1.5m$$

$$Pontoon\ height\ (h_p) = 0.16m$$

$$Pontoon\ width\ (w_p) = 0.24m$$

$$Cross\ plate = 28ea\ (14\ internal\ plates\ and\ 14\ side\ plates)$$

$$Area_{Steel} = 2(0.16m \times 1.5m) + (1.5m \times 0.24m) + 4(0.16m \times 0.24m) = 0.994m^2$$

$$Unit\ weight = 7.85kg/m^2mm \times 3mm = 23.6\ kg/m^2$$

$$Steel\ Mass\ (m_{Steel}) = 0.994m^2 \times 23.6\ kg/m^2 = 23.46kg$$

$$Polystyrene\ Mass\ (m_{Polystyrene}) = 2.35kg\ (10\%\ of\ steel\ mass)$$

$$Polystyrene\ Height\ (assumed) = 0.1m$$

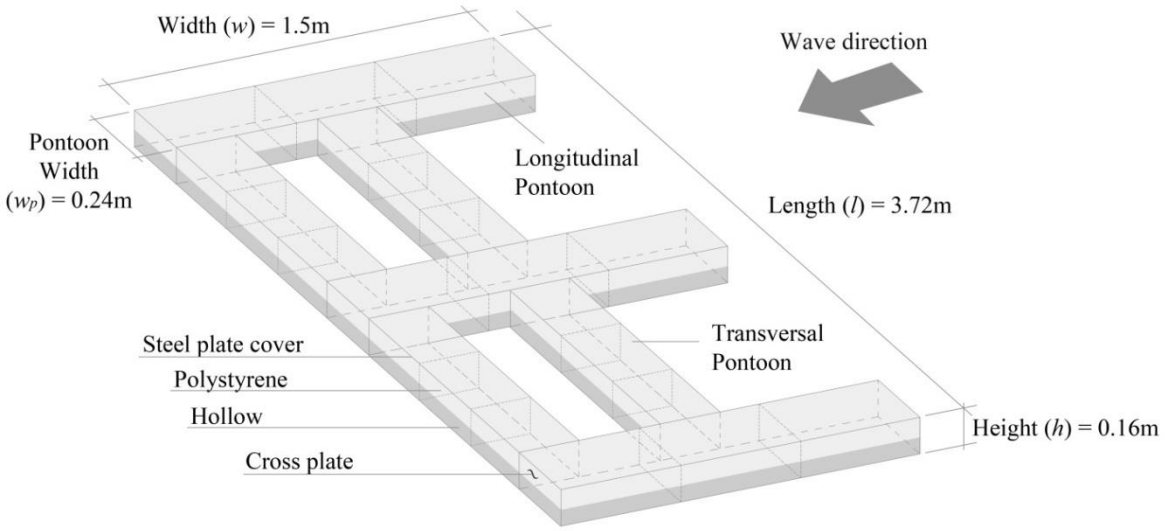

Figure A.11 Maere model perspective

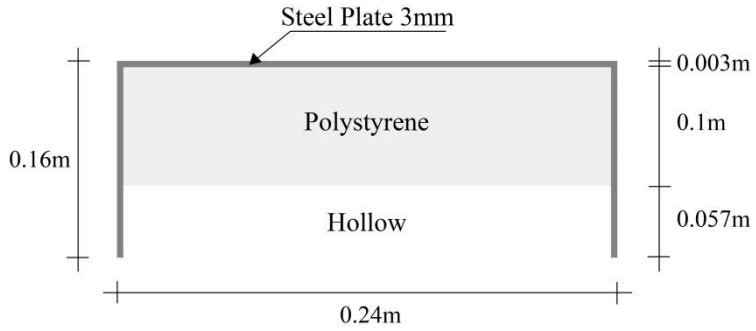

Figure A.12 Maere model cross section

A.3.1 Component mass calculation

Similar to calculation of Molo model in previous section, each pontoon is divided into components consists of cross-plates and body-sections. Figure A.13 and A.14 show the cross-plates and body-sections of longitudinal and transversal pontoon division.

A.3.1.1 Cross-plates mass

$$Area = 0.24m \times 0.16m = 0.0384m^2$$

$$Unit\ weight = 7.85kg \times 3mm = 23.6\,kg/m^2$$

$$Mass\left(m_{Cross-plate}\right) = 0.0384m^2 \times 23.6\,kg/m^2 = 0.91kg$$

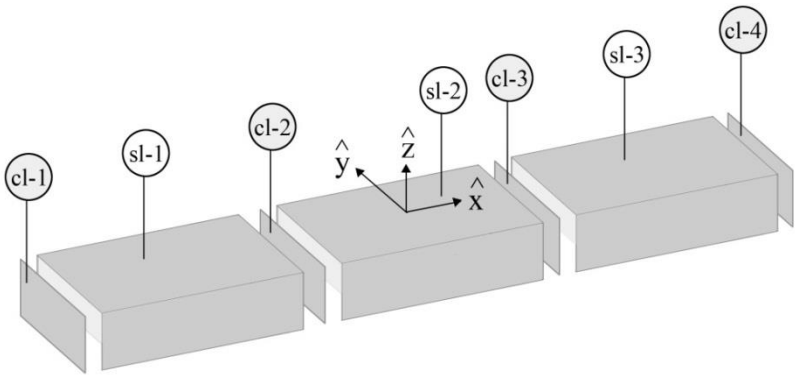

Figure A.13 Mære model longitudinal pontoon divisions

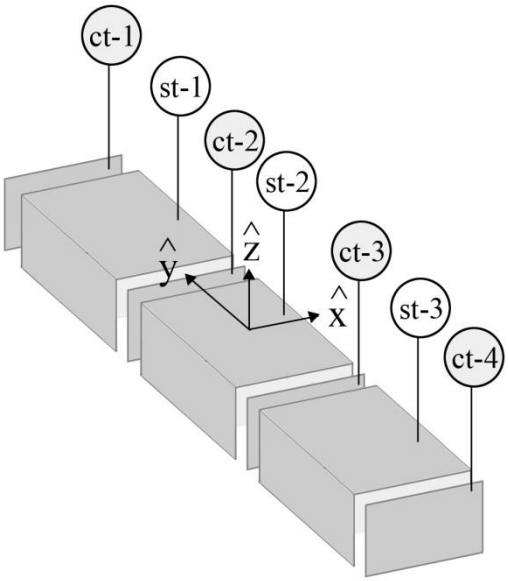

Figure A.14 Mære mdel transversal pontoon divisions

A.3.1.2 Body-sections mass

$$Steel\ mass\ (m_{Steel-bs}) = \left(m_{Steel} - 4\left(m_{Cross-plate}\right)\right)/3 = 6.61kg$$

$$Polystyrene\ mass\ \left(m_{Polystyrene-bs}\right) = m_{Polystyrene}/3 = 0.78kg$$

$$Mass\ \left(m_{Body-section}\right) = m_{Steel-bs} + m_{Polystyrene-bs} = 7.39kg$$

A.3.2 Calculation of component-CoG and pontoon-CoG

Cross-plates are component with uniform density. Therefore the component-CoG of cross-plates is right in the center of the cross-plates.

In other hand, body-section is a composite component with various densities which is symmetrical about the plane x=0 and y=0. Following is the calculation of component-CoG of the body-sections relative to reference point placed on the center of top plate with ź-axis positive upward.

$$\bar{x}_{Body-section} = 0m$$

$$\bar{y}_{Body-section} = 0m$$

$$\bar{z}_{Body-section} = \frac{(\bar{z} \times m)_{Steel-bs} + (\bar{z} \times m)_{Polystyrene-bs}}{m_{Steel-bs} + m_{Polystyrene-bs}}$$

$$\bar{z}_{Steel-bs} = \frac{2\left(-0.08m(23.6\,kg/m^2 \times 0.16m \times 0.496m)\right)}{6.61kg} = -0.045m$$

$$\bar{z}_{Polystyrene-bs} = \frac{-0.05m \times 0.78kg}{0.78kg} = -0.05m$$

$$\bar{z}_{Body-section} = \frac{(-0.045m \times 6.61kg) + (-0.05m \times 0.78kg)}{6.61kg + 0.78kg} = -0.046m$$

Pontoon is symmetrical about the plane x=0 and y=0. Therefore;

$$\bar{x}_{Pontoon} = 0m$$

$$\bar{y}_{Pontoon} = 0m$$

Calculation of pontoon-CoG on the ẑ-axis is given below. A new reference point is placed on the center of pontoon top plate with ẑ-axis positive upward. Figure A.15 illustrates the reference point placement and the calculated pontoon-CoG position.

$$\bar{z}_{Pontoon} = \frac{\sum_{n=1}^{4}(\bar{z}_n \times m_n)_{Cross-plate} + \sum_{m=1}^{3}(\bar{z}_m \times m_m)_{Body-section}}{m_{Cross-plate} + m_{Body-section}}$$

$$\bar{z}_{Pontoon} = \frac{4(-0.08m \times 0.91kg) + 3(-0.046m \times 7.39kg)}{4(0.91) + 3(7.39)} = -0.05m$$

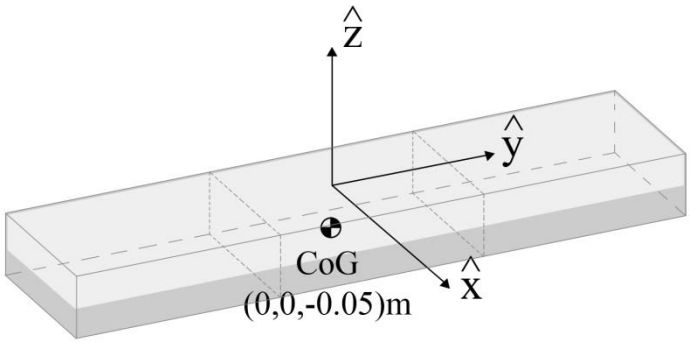

Figure A.15 Position of Pontoon CoG

A.3.3 Calculation of breakwater-CoG

Calculation of breakwater-CoG is given on the Table A.3 below. A new reference point is placed on the center of middle pontoon top plate with ż-axis positive upward. Figure A.15 illustrates the reference point placement and the breakwater division for CoG calculation.

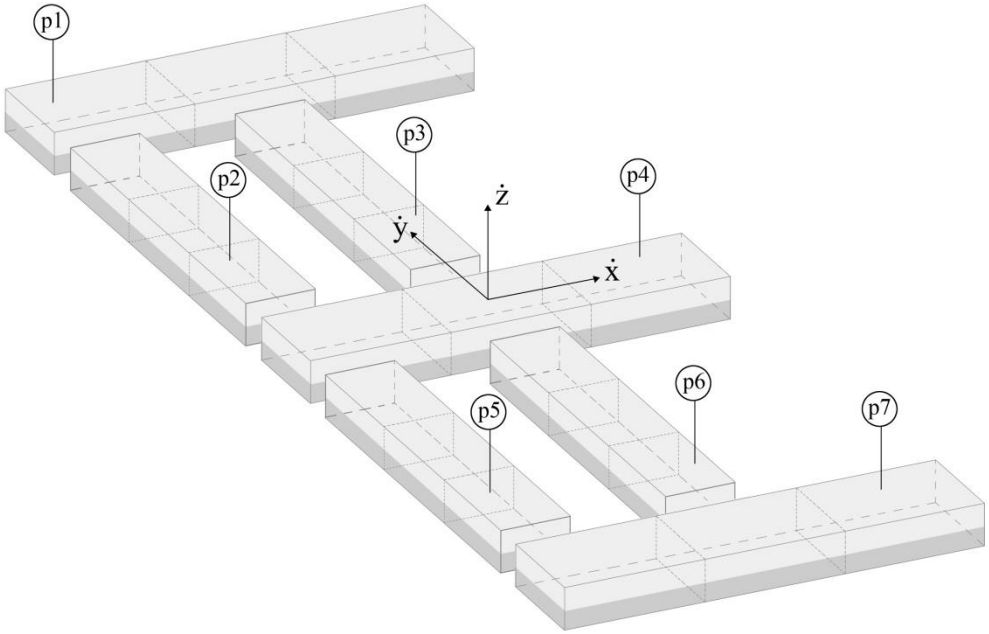

Figure A.16 Mære Model Divisions

Table A.3 Calculation of Breakwater-CoG

Pontoon	Mass (kg)	Distance to Reference Point (m)			Mass X Distance		
		x	y	z	x	y	z
p1	25.81	0.00	1.74	-0.05	0.00	44.91	-1.29
p2	25.81	-0.63	0.87	-0.05	-16.26	22.45	-1.29
p3	25.81	0.00	0.87	-0.05	0.00	22.45	-1.29
p4	25.81	0.00	0.00	-0.05	0.00	0.00	-1.29
p5	25.81	-0.63	-0.87	-0.05	-16.26	-22.45	-1.29
p6	25.81	0.00	-0.87	-0.05	0.00	-22.45	-1.29
p7	25.81	0.00	-1.74	-0.05	0.00	-44.91	-1.29
Σ	**180.67**			**Σ**	**-32.52**	**0.00**	**-9.03**
				CoG (m)	**-0.18**	**0.00**	**-0.05**

A.3.4 Calculation of mass moment of inertia of longitudinal pontoon

A.3.4.1 Cross-plates mass moment of inertia

Mass moment of inertia of cross-plates relative to its CoG is calculated below.

$$I_{xx-Cross-plate} = \frac{1}{12} m(h^2 + l^2) = \frac{1}{12} 0.91kg(0.16^2 + 0.24^2)m^2 = 0.0063kgm^2$$

$$I_{yy-Cross-plate} = \frac{1}{12} m(w^2 + h^2) = \frac{1}{12} 0.91kg(0.003^2 + 0.16^2)m^2 = 0.0019kgm^2$$
$$I_{zz-Cross-plate} = \frac{1}{12} m(w^2 + l^2) = \frac{1}{12} 0.91kg(0.24^2 + 0.003^2)m^2 = 0.0044kgm^2$$

A.3.4.2 Body-section mass moment of inertia

Mass moment of inertia of steel plates covering the body-section is done by calculating mass moment of inertia of steel solid rectangular cuboid then subtracted by mass moment of inertia of center portion in order to obtain the mass moment of inertia of bottomless hollow steel cuboid.

$$Unit\ weight\ solid = 7.85kg/m^2mm \times 160mm = 1256\,kg/m^2$$
$$Area\ solid = 0.496m \times 0.24m = 0.119m^2$$
$$m_{Solid} = 0.119m^2 \times 1256\,kg/m^2 = 149.46kg$$

$$I_{xx-Solid} = \frac{1}{12} m_{Solid}(h^2 + l^2) = \frac{1}{12} 149.46(0.16^2 + 0.24^2)m^2 = 1.04kgm^2$$
$$I_{yy-Solid} = \frac{1}{12} m_{Solid}(w^2 + h^2) = \frac{1}{12} 149.46kg(0.496^2 + 0.16^2)m^2 = 3.38kgm^2$$
$$I_{zz-Solid} = \frac{1}{12} m_{Solid}(w^2 + l^2) = \frac{1}{12} 149.46kg(0.24^2 + 0.496^2)m^2 = 3.78kgm^2$$

$$Unit\ weight\ center = 7.85kg/m^2mm \times 157mm = 1232.45\,kg/m^2$$
$$Area\ center = 0.496m \times 0.234m = 0.116m^2$$
$$m_{Center} = 0.116m^2 \times 1232.45\,kg/m^2 = 142.96kg$$

$$I_{xx-Center} = \frac{1}{12} m_{Center}(h^2 + l^2) = \frac{1}{12} 142.96kg(0.157^2 + 0.234^2)m^2$$
$$= 0.95kgm^2$$
$$I_{yy-Center} = \frac{1}{12} m_{Center}(w^2 + h^2) = \frac{1}{12} 142.96kg(0.496^2 + 0.157^2)m^2$$
$$= 3.23kgm^2$$
$$I_{zz-Center} = \frac{1}{12} m_{Center}(w^2 + l^2) = \frac{1}{12} 142.96kg(0.234^2 + 0.496^2)m^2$$
$$= 3.58kgm^2$$

$$I_{xx-Steel} = I_{xx-Solid} - I_{xx-Center} = 1.04kgm^2 - 0.95kgm^2 = 0.09kgm^2$$

$$I_{yy-Steel} = I_{yy-Solid} - I_{yy-Center} = 3.38kgm^2 - 3.23kgm^2 = 0.15kgm^2$$
$$I_{zz-Steel} = I_{zz-Solid} - I_{zz-Center} = 3.78kgm^2 - 3.58kgm^2 = 0.2kgm^2$$

Above mass moment of inertia is relative to the solid cuboid CoG. To get the correct mass moment inertia of bottomless hollow steel cuboid, it should be translated to the hollow cuboid CoG by employing parallel axis theorem given in Equation 1 above.

$$I_{xx-Steel} = I_{xx-Steel} + m_{Steel-bs}d^2 = 0.09kgm^2 + (6.61kg \times 0^2m^2) = 0.09kgm^2$$
$$I_{yy-Steel} = I_{yy-Steel} + m_{Steel-bs}d^2 = 0.15gm^2 + (6.61kg \times 0^2m^2) = 0.15kgm^2$$
$$I_{zz-Steel} = I_{zz-Steel} + m_{Steel-bs}d^2 = 0.2kgm^2 + (6.61kg \times 0.034^2m^2) = 0.21kgm^2$$

Mass moment of inertia of polystyrene in the body-section is calculated below.

$$I_{xx-Polystyrene} = \frac{1}{12}m_{Polystyrene-bs}(h^2 + l^2) = \frac{1}{12}0.78kg(0.1^2 + 0.234^2)m^2 = 0.0042kgm^2$$
$$I_{yy-Polystyrene} = \frac{1}{12}m_{Polystyrene-bs}(w^2 + h^2) = \frac{1}{12}0.78kg(0.496^2 + 0.1^2)m^2 = 0.017kgm^2$$
$$I_{zz-Polystyrene} = \frac{1}{12}m_{Polystyrene-bs}(w^2 + l^2) = \frac{1}{12}0.78kg(0.234^2 + 0.496^2)m^2 = 0.02kgm^2$$

Total mass moment of inertia of body-section is the sum up of the mass moment of inertia of all elements about the same axis of reference. Parallel axis theorem is used to translate calculated moment of inertia to the body-section CoG. Since the element center of masses are shifted only about the z-axis, the mass moment of inertia of all elements about the x and y-axis will be the same. The mass moment of inertia for new z-axis is given below.

$$I_{zz-Steel} = I_{zz-Steel} + m_{Steel}d^2 = 0.21kgm^2 + (6.61kg \times 0.001^2m^2) = 0.21kgm^2$$
$$I_{zz-Polystyrene} = I_{zz-Polystyrene} + m_{Polystyrene}d^2 = 0.02kgm^2 + (0.78kg \times 0.004^2m^2) = 0.02kgm^2$$

Total mass moment of inertia of each body-section about its CoG is given below.

$$I_{xx-Body-section} = I_{xx-Steel} + I_{xx-Polystyrene} = 0.094kgm^2$$
$$I_{yy-Body-section} = I_{yy-Steel} + I_{yy-Polystyrene} = 0.167kgm^2$$
$$I_{zz-Body-section} = I_{zz-Steel} + I_{zz-Polystyrene} = 0.23kgm^2$$

A.3.4.3 Longitudinal pontoon mass moment of inertia

Longitudinal pontoon mass moment of inertia is calculated by translating mass moment of inertia of each cross-plate and body-section to the pontoon-CoG. Parallel axis theorem is also used for the calculation. Table A.4 shows the calculated pontoon mass moment of inertia.

Table A.4 Calculation of Longitudinal Pontoon Mass Moment of Inertia

Components	Component mass moment of inertia (kgm^2)			Mass (kg)	Axis distance (m)			Pontoon mass moment of inertia ($kgm2$)		
	I_{xx}	I_{yy}	I_{zz}		d_x	d_y	d_z	I_{xx}	I_{yy}	I_{zz}
Cross-plate cl-1	0.0063	0.0019	0.0044	0.91	0.0000	0.7490	0.0300	0.01	0.51	0.01
Cross-plate cl-2	0.0063	0.0019	0.0044	0.91	0.0000	0.2500	0.0300	0.01	0.06	0.01
Cross-plate cl-3	0.0063	0.0019	0.0044	0.91	0.0000	0.2500	0.0300	0.01	0.06	0.01
Cross-plate cl-4	0.0063	0.0019	0.0044	0.91	0.0000	0.7490	0.0300	0.01	0.51	0.01
Body-section sl-1	0.0940	0.1670	0.2300	7.39	0.0000	0.4990	0.0040	0.09	2.01	0.23
Body-section sl-2	0.0940	0.1670	0.2300	7.39	0.0000	0.0000	0.0040	0.09	0.17	0.23
Body-section sl-3	0.0940	0.1670	0.2300	7.39	0.0000	0.4990	0.0040	0.09	2.01	0.23
							Total	**0.31**	**5.32**	**0.71**

A.3.5 Calculation of mass moment of inertia of transversal pontoon

A.3.5.1 Cross-plates mass moment of inertia

Mass moment of inertia of cross-plates relative to its CoG is calculated below.

$$I_{xx-Cross-plate} = \frac{1}{12} m(h^2 + l^2) = \frac{1}{12} 0.91kg(0.16^2 + 0.003^2)m^2 = 0.0019kgm^2$$

$$I_{yy-Cross-plate} = \frac{1}{12} m(w^2 + h^2) = \frac{1}{12} 0.91kg(0.24^2 + 0.16^2)m^2 = 0.0063kgm^2$$

$$I_{zz-Cross-plate} = \frac{1}{12} m(w^2 + l^2) = \frac{1}{12} 0.91kg(0.24^2 + 0.003^2)m^2 = 0.0044kgm^2$$

A.3.5.2 Body-section mass moment of inertia

Mass moment of inertia of steel plates covering the body-section is done by calculating mass moment of inertia of steel solid rectangular cuboid then subtracted by mass moment of inertia of center portion in order to obtain the mass moment of inertia of bottomless hollow steel cuboid.

$$Unit\ weight\ solid = 7.85kg/m^2mm \times 160mm = 1256\,kg/m^2$$
$$Area\ solid = 0.496m \times 0.24m = 0.119m^2$$
$$m_{Solid} = 0.119m^2 \times 1256\,kg/m^2 = 149.46kg$$

$$I_{xx-Solid} = \frac{1}{12} m_{Solid}(h^2 + l^2) = \frac{1}{12} 149.46(0.16^2 + 0.496^2)m^2 = 3.38kgm^2$$
$$I_{yy-Solid} = \frac{1}{12} m_{Solid}(w^2 + h^2) = \frac{1}{12} 149.46kg(0.24^2 + 0.16^2)m^2 = 1.04kgm^2$$
$$I_{zz-Solid} = \frac{1}{12} m_{Solid}(w^2 + l^2) = \frac{1}{12} 149.46kg(0.24^2 + 0.496^2)m^2 = 3.78kgm^2$$

$$Unit\ weight\ center = 7.85kg/m^2mm \times 157mm = 1232.45\,kg/m^2$$
$$Area\ center = 0.496m \times 0.234m = 0.116m^2$$
$$m_{Center} = 0.116m^2 \times 1232.45\,kg/m^2 = 142.96kg$$

$$I_{xx-Center} = \frac{1}{12} m_{Center}(h^2 + l^2) = \frac{1}{12} 142.96kg(0.157^2 + 0.496^2)m^2 = 3.23kgm^2$$
$$I_{yy-Center} = \frac{1}{12} m_{Center}(w^2 + h^2) = \frac{1}{12} 142.96kg(0.234^2 + 0.157^2)m^2 = 0.95kgm^2$$
$$I_{zz-Center} = \frac{1}{12} m_{Center}(w^2 + l^2) = \frac{1}{12} 142.96kg(0.234^2 + 0.496^2)m^2 = 3.58kgm^2$$

$$I_{xx-Steel} = I_{xx-Solid} - I_{xx-Center} = 3.38kgm^2 - 3.23kgm^2 = 0.15kgm^2$$
$$I_{yy-Steel} = I_{yy-Solid} - I_{yy-Center} = 1.04kgm^2 - 0.95kgm^2 = 0.09kgm^2$$
$$I_{zz-Steel} = I_{zz-Solid} - I_{zz-Center} = 3.78kgm^2 - 3.58kgm^2 = 0.2kgm^2$$

Above mass moment of inertia is relative to the solid cuboid CoG. To get the correct mass moment inertia of bottomless hollow steel cuboid, it should be translated to the hollow cuboid CoG. According to parallel axis theorem, mass moment of inertia about the new axis is given by Equation 3 below.

$$I_{xx} = I_{xx} + md^2 \quad (3)$$

where d is the perpendicular distance between the axis of rotation. The same equation is also applied to other axis.

$$I_{xx-Steel} = I_{xx-Steel} + m_{Steel-bs}d^2 = 0.15kgm^2 + (6.61kg \times 0^2m^2) = 0.15kgm^2$$
$$I_{yy-Steel} = I_{yy-Steel} + m_{Steel-bs}d^2 = 0.09gm^2 + (6.61kg \times 0^2m^2) = 0.09kgm^2$$
$$I_{zz-Steel} = I_{zz-Steel} + m_{Steel-bs}d^2 = 0.2kgm^2 + (6.61kg \times 0.034^2m^2) = 0.21kgm^2$$

Mass moment of inertia of polystyrene in the body-section is calculated below.

$$I_{xx-Polystyrene} = \frac{1}{12}m_{Polystyrene-bs}(h^2 + l^2) = \frac{1}{12}0.78kg(0.1^2 + 0.496^2)m^2 = 0.017kgm^2$$
$$I_{yy-Polystyrene} = \frac{1}{12}m_{Polystyrene-bs}(w^2 + h^2) = \frac{1}{12}0.78kg(0.234^2 + 0.1^2)m^2 = 0.0042kgm^2$$
$$I_{zz-Polystyrene} = \frac{1}{12}m_{Polystyrene-bs}(w^2 + l^2) = \frac{1}{12}0.78kg(0.234^2 + 0.496^2)m^2 = 0.02kgm^2$$

Total mass moment of inertia of body-section is the sum up of the mass moment of inertia of all elements about the same axis of reference. Parallel axis theorem is used to translate calculated moment of inertia to the body-section CoG. Since the element center of masses are shifted only about the z-axis, the mass moment of inertia of all elements about the x and y-axis will be the same. The mass moment of inertia for new z-axis is given below.

$$I_{zz-Steel} = I_{zz-Steel} + m_{Steel}d^2 = 0.21kgm^2 + (6.61kg \times 0.001^2m^2) = 0.21kgm^2$$
$$I_{zz-Polystyrene} = I_{zz-Polystyrene} + m_{Polystyrene}d^2 = 0.02kgm^2 + (0.78kg \times 0.004^2m^2) = 0.02kgm^2$$

Total mass moment of inertia of each body-section about its CoG is given below.

$$I_{xx-Body-section} = I_{xx-Steel} + I_{xx-Polystyrene} = 0.167kgm^2$$
$$I_{yy-Body-section} = I_{yy-Steel} + I_{yy-Polystyrene} = 0.094kgm^2$$
$$I_{zz-Body-section} = I_{zz-Steel} + I_{zz-Polystyrene} = 0.23kgm^2$$

A.3.5.3 Transversal pontoon mass moment of inertia

Transversal pontoon mass moment of inertia is calculated by translating mass moment of inertia of each cross-plate and body-section to the pontoon-CoG. Parallel axis theorem is also used for the calculation. Table A.5 shows the calculated pontoon mass moment of inertia.

Table A.5 Calculation of Transversal Pontoon Mass Moment of Inertia

Components	Component mass moment of inertia (kgm^2)			Mass (kg)	Axis distance (m)			Pontoon mass moment of inertia ($kgm2$)		
	I_{xx}	I_{yy}	I_{zz}		d_x	d_y	d_z	I_{xx}	I_{yy}	I_{zz}
Cross-plate cl-1	0.0019	0.0063	0.0044	0.91	0.7490	0.0000	0.0300	0.51	0.01	0.01
Cross-plate cl-2	0.0019	0.0063	0.0044	0.91	0.2500	0.0000	0.0300	0.06	0.01	0.01
Cross-plate cl-3	0.0019	0.0063	0.0044	0.91	0.2500	0.0000	0.0300	0.06	0.01	0.01
Cross-plate cl-4	0.0019	0.0063	0.0044	0.91	0.7490	0.0000	0.0300	0.51	0.01	0.01
Body-section sl-1	0.1670	0.0940	0.2300	7.39	0.4990	0.0000	0.0040	2.01	0.09	0.23
Body-section sl-2	0.1670	0.0940	0.2300	7.39	0.0000	0.0000	0.0040	0.17	0.09	0.23
Body-section sl-3	0.1670	0.0940	0.2300	7.39	0.4990	0.0000	0.0040	2.01	0.09	0.23
							Total	**5.32**	**0.31**	**0.71**

A.3.6 Calculation of mass moment of inertia of Mære breakwater

Calculation of breakwater mass moment of inertia relative to breakwater-CoG is given on the Table A.6 below.

Table A.6 Calculation of Mære breakwater Mass Moment of Inertia

Components	Component mass moment of inertia (kgm^2)			Mass (kg)	CoG distance (m)			Pontoon mass moment of inertia ($kgm2$)		
	I_{xx}	I_{yy}	I_{zz}		d_x	d_y	d_z	I_{xx}	I_{yy}	I_{zz}
Pontoon p1	0.3100	5.3200	0.7100	25.81	1.7400	0.1800	0.0000	78.45	6.16	0.71
Pontoon p2	5.3200	0.3100	0.7100	25.81	0.8700	0.4500	0.0000	24.86	5.54	0.71
Pontoon p3	5.3200	0.3100	0.7100	25.81	0.8700	0.1800	0.0000	24.86	1.15	0.71
Pontoon p4	0.3100	5.3200	0.7100	25.81	0.0000	0.1800	0.0000	0.31	6.16	0.71
Pontoon p5	5.3200	0.3100	0.7100	25.81	0.8700	0.4500	0.0000	24.86	5.54	0.71
Pontoon p6	5.3200	0.3100	0.7100	25.81	0.8700	0.1800	0.0000	24.86	1.15	0.71
Pontoon p7	0.3100	5.3200	0.7100	25.81	1.7400	0.1800	0.0000	78.45	6.16	0.71
							Total	**256.64**	**31.83**	**4.97**

A.3.7 Calculation of radii of gyration

$$r_x = \sqrt{\frac{I_{xx}}{m_{Pontoon}}} = \sqrt{\frac{256.64kgm^2}{180.67kg}} = 1.19m$$

$$r_y = \sqrt{\frac{I_{yy}}{m_{Pontoon}}} = \sqrt{\frac{31.83kgm^2}{180.67kg}} = 0.42m$$

$$r_z = \sqrt{\frac{I_{zz}}{m_{Pontoon}}} = \sqrt{\frac{4.97kgm^2}{180.67kg}} = 0.012m$$

A.4 Summary of radii of gyration

Summary of calculated radii of gyration is given in Table A.7 below.

Table A.7 Summary of calculated radii of gyration

Model	Radii of gyration relative to CoG		
	r_x (m)	r_y (m)	r_z (m)
Molo model (approach 1)	1.16	0.14	0.23
Molo model (approach 2)	1.83	0.17	0.25
Maere model	1.19	0.42	0.012

B. MOORING STIFFNESS MATRIX

Calculation of mooring stiffness matrix for Molo model is detailed in this section. To simplify the analysis, solutions of the inelastic mooring line (catenary) equations are used (Faltinsen, 1990). The mooring lines are assumed to have constant weight per unit length.

Figure B.1 and Figure B.2 show the mooring configuration and spread mooring system of the breakwater Molo model.

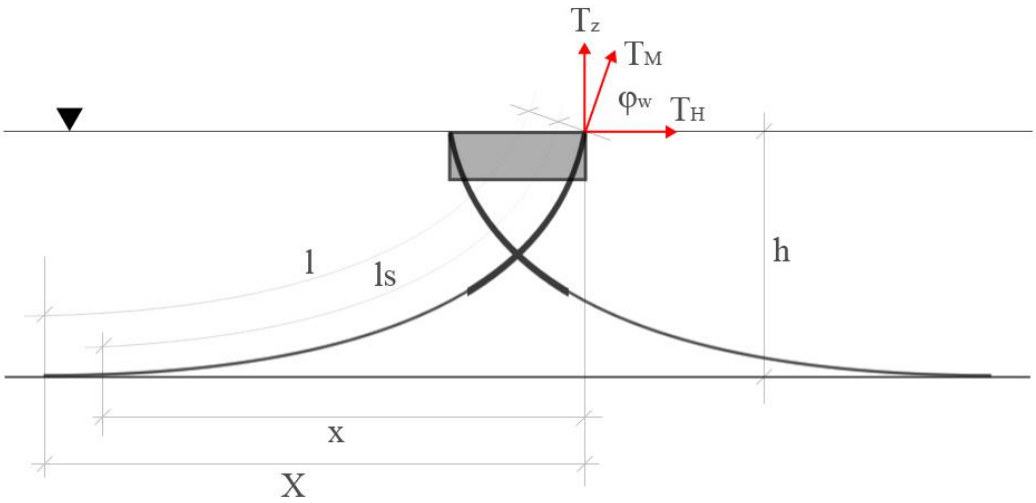

Figure B.1 Molo model mooring configuration

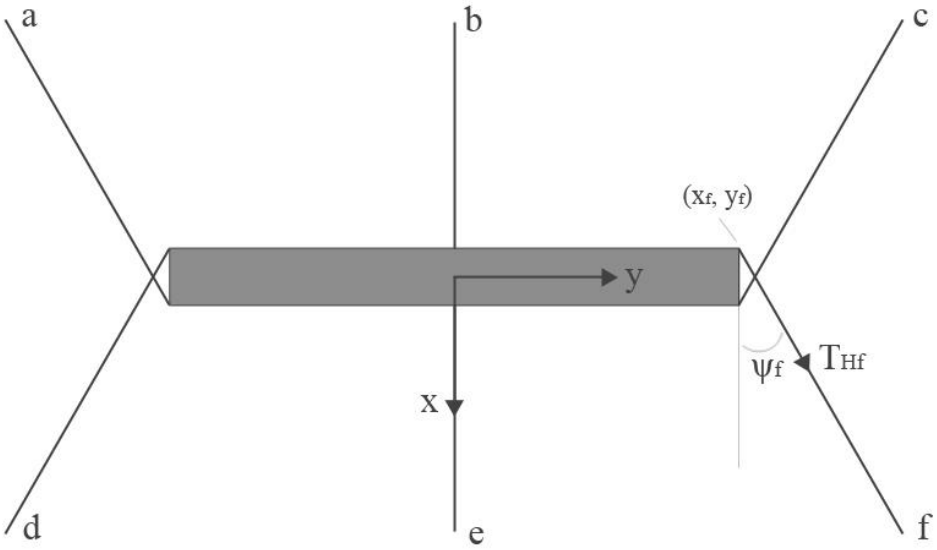

Figure B.2 Molo model spread mooring system

B.1 Middle mooring lines (line b and e)

Middle mooring lines parameters are given below.

$X = 2m$

$l = 2.01m$

$h = 0.6m$

$unit\ weight\ (w) = 80.7gr/m$

Equation B.1 below expresses relation between *X* and the horizontal force T_H.

$$X = l - h\left(1 + 2\frac{a}{h}\right)^{1/2} + a\cosh^{-1}\left(1 + \frac{h}{a}\right) \quad \textbf{(B.1)}$$

where $a = T_H/w$.

Calculation results based on Equation B.1 is illustrated in Figure B.3 where the horizontal force from a mooring line on breakwater model is a function of the horizontal distance *X* between the mooring and the point where the mooring line is connected to the model.

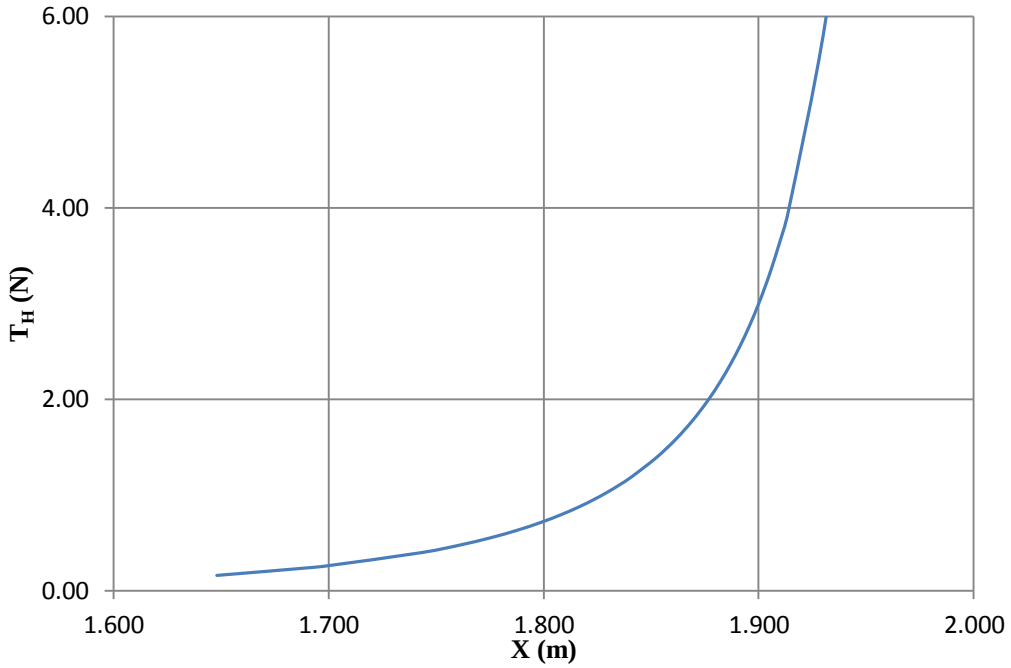

Figure B.3 Middle mooring horizontal forces

Line tension and vertical force at the model is given by Equation B.2 and B.3 below.

$$T = T_H + wh \tag{B.2}$$

$$\varphi_w = \cos^{-1}\left(\frac{T_H}{T}\right) \tag{B.3}$$

Using both equations above, the vertical force from a mooring line on breakwater model then can be calculated. The calculation result is illustrated in Figure B.4 where the vertical force is a function of the horizontal distance *X*.

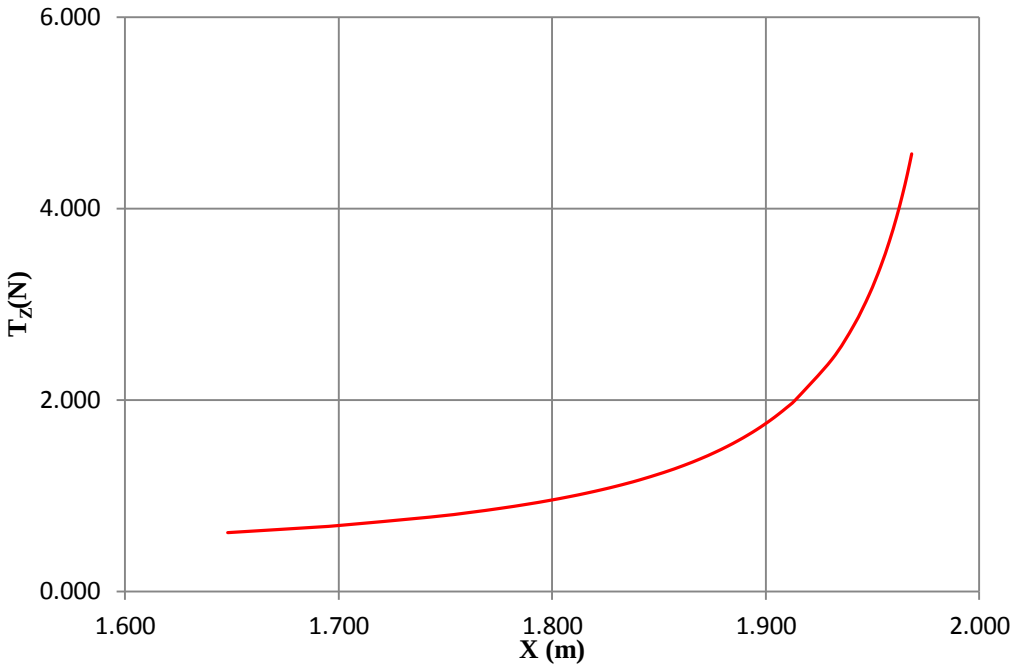

Figure B.4 Middle mooring vertical forces

Since WAMIT is not able to predict model with non-linear mooring tension line, the model horizontal motions are restricted to only small motions and the average model position was selected at distance *X* within the linear region. In this case, the distance *X* is selected at 1.7m, indicating the model horizontal motions oscillate around amplitude of 0.3m. From Figure B.3 and B.4 the average horizontal force for the distance *X* is $T_H = 0.26N$, vertical force $T_Z = 0.688N$, $a_H = 0.33m$, and $a_Z = T_Z/w = 0.869m$.

The analytical expression of mooring line restoring coefficient is given by Equation B.4 below.

$$k = w\left[\frac{-2}{\left(1+2\frac{a}{h}\right)^{1/2}} + \cosh^{-1}\left(1+\frac{h}{a}\right)\right]^{-1} \quad \textbf{(B.4)}$$

Using above equation, the restoring coefficients of mooring line b and e are calculated as $k_{Hb} = k_{He} = 0.25\,N/m$ and $k_{Zb} = k_{Ze} = 0.085\,N/m$.

B.2 End mooring lines (line a, c, d, and f)

End mooring lines parameters are given below.

$X = 2.24m$

$l = 2.37m$

$h = 0.6m$

$unit\ weight\ (w) = 70.7gr/m$

Calculation results based on Equation B.1to B.3 is illustrated in Figure B.5 and B.6 where the horizontal and vertical force from a mooring line on breakwater model is a function of the horizontal distance *X* between the mooring and the point where the mooring line is connected to the model.

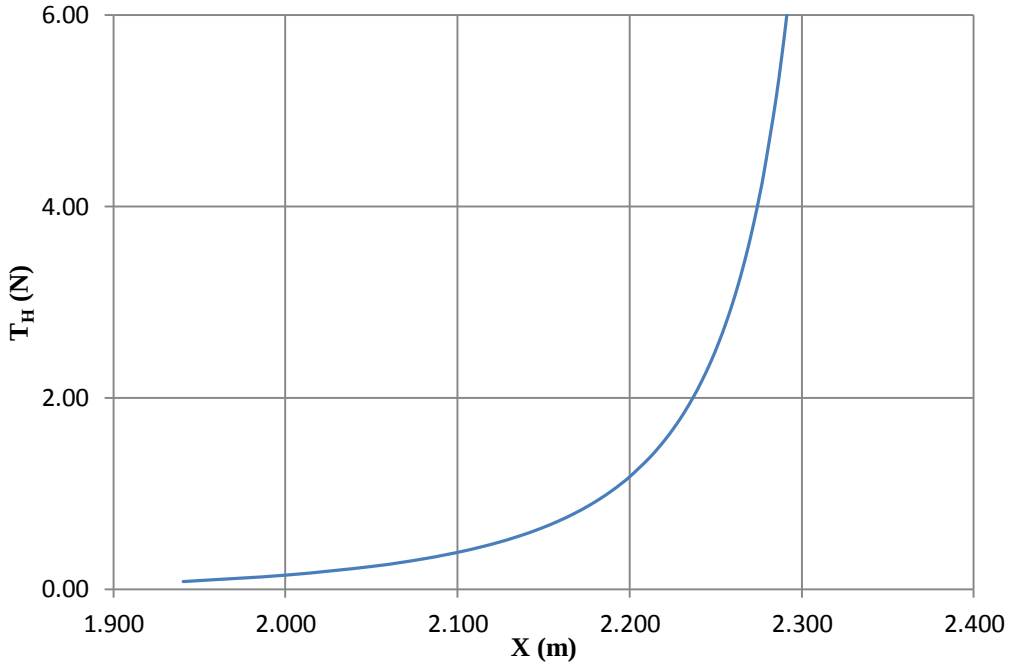

Figure B.5 End mooring horizontal forces

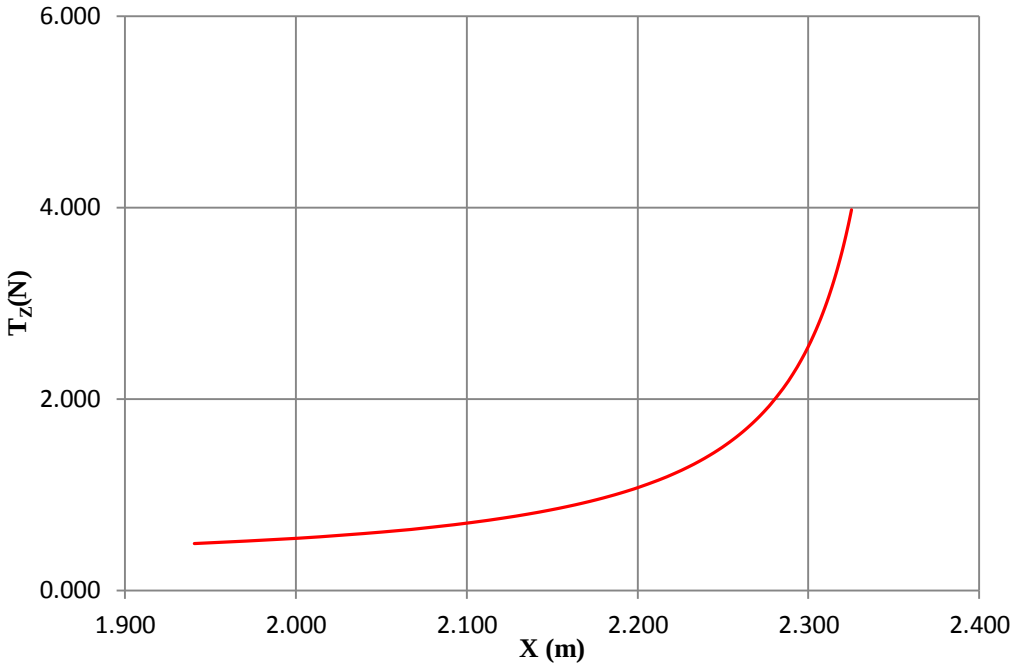

Figure B.6 End mooring vertical forces

Similar to the middle mooring line, since WAMIT is not able to predict model with non-linear mooring tension line, the model horizontal motions are restricted to only small motions and the average model position was selected at distance X within the linear region. In this case, the distance X is selected at 2m, indicating the model horizontal motions oscillate around amplitude of 0.24m. From Figure B.5 and B.6 the average horizontal force for the distance X is $T_H = 0.15N$, vertical force $T_Z = 0.543N$, and , $a_H = 0.185m$, and $a_Z = T_Z/w = 0.783m$.

Using Equation B.4, the restoring coefficients of mooring line a, c, d and f are calculated as $k_{Ha} = k_{Hc} = k_{Hd} = k_{Hf} = 0.13\,N/m$ and $k_{Za} = k_{Zc} = k_{Zd} = k_{Zf} = 0.081\,N/m$.

B.3 Analysis of spread mooring system

To find the linear restoring effect of the mooring lines of a spread mooring system in the equation of motion, the procedure can be generalized by following Equation B.5 to B.9.

$$K_{11} = \sum_{i=a}^{f} k_{Hi} \cos^2 \psi_i \tag{B.5}$$

$$K_{22} = \sum_{i=a}^{f} k_{Hi} \sin^2 \psi_i \tag{B.6}$$

$$K_{33} = \sum_{i=a}^{f} k_{Zi} \tag{B.7}$$

$$K_{66} = \sum_{i=a}^{f} k_{Hi} \left(x_i \sin \psi_i - y_i \cos \psi_i\right)^2 \tag{B.8}$$

$$K_{26} = C_{62} = \sum_{i=a}^{f} k_{Hi} \left(x_i \sin \psi_i - y_i \cos \psi_i\right) \sin \psi_i \tag{B.9}$$

The coupling coefficients K_{16}, K_{61}, K_{12}, and K_{21} are zero since the mooring arrangement is symmetric about the x-z plane.

Calculated linear restoring coefficients are presented in Table B.1 below.

Table B.1 Mooring restoring coefficients

Mooring Line	x_i	y_i	ψ_i (deg)	k_H (N/m)	k_Z (N/m)	K_{11} (N/m)	K_{22} (N/m)	K_{33} (N/m)	K_{66} (N/m)	K_{26} (N/m)	K_{62} (N/m)
a	-0.1	-1	206.57	0.13	0.081	0.104	0.026	0.081	0.094	0.049	0.049
b	-0.1	0	180.00	0.25	0.085	0.250	0.000	0.085	0.000	0.000	0.000
c	-0.1	1	153.43	0.13	0.081	0.104	0.026	0.081	0.094	0.049	0.049
d	0.1	-1	333.43	0.13	0.081	0.104	0.026	0.081	0.093	-0.050	-0.050
e	0.1	0	0.00	0.25	0.085	0.250	0.000	0.085	0.000	0.000	0.000
f	0.1	1	26.57	0.13	0.081	0.104	0.026	0.081	0.094	-0.049	-0.049
					Σ	**0.916**	**0.104**	**0.494**	**0.375**	**0.000**	**0.000**

Complete 6 X 6 mooring stiffness matrix which is used for WAMIT input file is given below.

$$K = \begin{pmatrix} 0.916 & 0 & 0 & 0 & 0 & 0 \\ 0 & 0.104 & 0 & 0 & 0 & 0 \\ 0 & 0 & 0.494 & 0 & 0 & 0 \\ 0 & 0 & 0 & 0 & 0 & 0 \\ 0 & 0 & 0 & 0 & 0 & 0 \\ 0 & 0 & 0 & 0 & 0 & 0.375 \end{pmatrix}$$

C. MULTISURF AND WAMIT FILES

Examples of MultiSurf output files and WAMIT input files of 2D model (draft = 0.4 m), Molo model (free floating), and Mare model (free floating) are given below. Snapshot of model geometry model are shown in Figure C.1 to Figure C.3. Explanation of WAMIT input files and each command can be found in WAMIT manual. Complete files are given in separated CD.

C.1 2D model (draft = 0.4m)

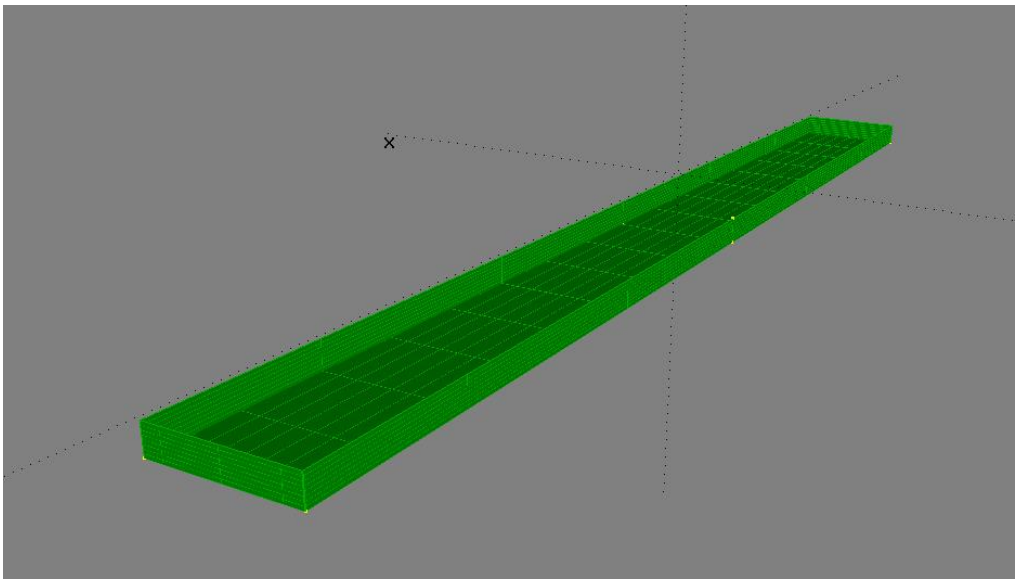

Figure C.1 2D model MultiSurf snapshot

C3.GDF:

```
c3 draft=0.4m
   1.000000  9.806650    ULEN, GRAV
   0 1                   ISX, ISY
   0  2                  NPATCH  IGDEF
   3                     NLINES
   C3.MS2
   *
   0  0  0               Fast/acc  DivMult  Inward_normals
```

C3.POT

```
c3 draft=0.4m
    2
    1         1          IRAD, IDIFF
```

```
    7                       NPER (array PER follows)
    2.04 2.34 2.67 3.16 5.04 6.23 9.17
    1                       NBETA (array BETA follows)
    0.
    1                       NBODY
    c3.gdf
    0. 0. 0.6 0.            XBODY
    1  1  0  0  0  1        IMODE(1-6)
    0                       NEWMDS
```

C3.FRC:

c3 draft=0.4m

```
    1    0    0    -1    0    1  0  0 0     IOPTN(1-9)
    6                       NDFR
    0 0 0 0 0 0             IMODE
    1000                    RHO
    0. 0. 0.                XCG
    0                       IMASS
    0                       IDAMP
    0                       ISTIFF
    0                       (NBETAH)
    0                       (NFIELD -- no individual field points)
    3                       (NFIELD_ARRAYS -- number of arrays)
    0                       (Array is in exterior fluid domain)
    30   1.2   0.2          (NFX, X1, DELX)
    11   0.0   0.15         (NFY, Y1, DELY)
    1    0.0   0.0          (NFZ, Z1, DELZ)
    0                       (Array is in exterior fluid domain)
    35   -8    0.2          (NFX, X2, DELX)
    11   0.0   0.15         (NFY, Y2, DELY)
    1    0.0   0.0          (NFZ, Z2, DELZ)
    1                       (Array is in interior fluid domain)
    11   -1  0.2           (NFX, X4, DELX)
    11   0.0   0.15         (NFY, Y4, DELY)
    1    0.0   0.0          (NFZ, Z4, DELZ)
```

C3.CFG:

```
   ILOWHI=1
   IALTPOT=2
   IRR=0
   ISOLVE=2
   KSPLIN=3
```

IALTFRC=2
IQUADO=3
IQUADI=4
IPERIO=1
ITANKFPT=1
MONITR=0
NUMHDR=1
NOOUT= 1 1 1 1 0 1 1 1 1
IFIELD_ARRAYS=1 (field points input in array format in .frc file)
USERID_PATH=\WAMITv6 (directory for *.exe, *.dll, and userid.wam)
ipltdat=5

C.2 Maere model (free floating)

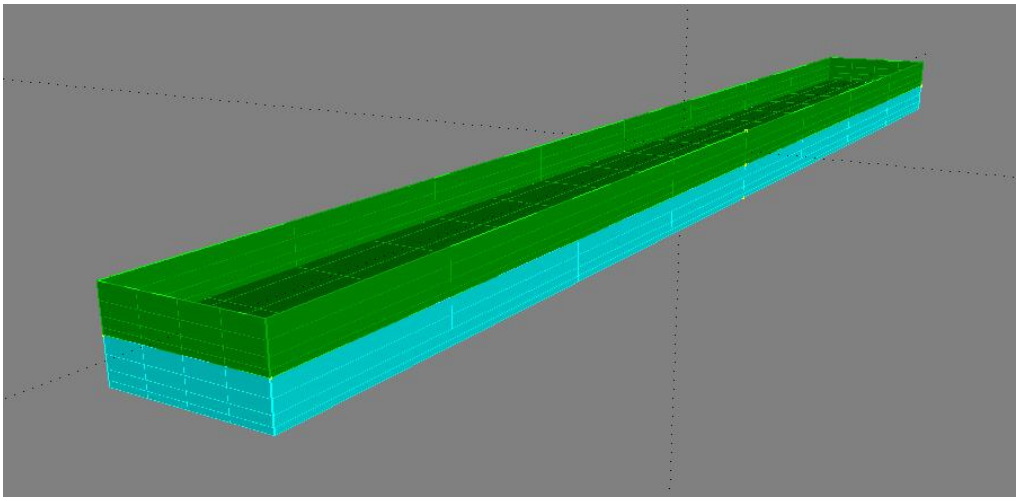

Figure C.2 Molo model MultiSurf snapshot

C1.GDF:
c1, s1, free floating, high-order, dipole
1.000000 9.806650 ULEN, GRAV
0 1 ISX, ISY
0 2 N PATCH IGDEF
3 NLINES
C1.MS2
*
0 0 0 Fast/acc DivMult Inward_normals

C1.POT:
c1, s1, free floating, high-order, dipole
```
   0.6                    HBOT
   1          1           IRAD, IDIFF
   20                     NPER (array PER follows)
   1 1.06 1.12 1.18 1.25 1.34 1.43 1.54 1.67 1.82 2 2.23 2.5 2.86 3.34 4 5 6.67
10 20
   1                      NBETA (array BETA follows)
   0.                     BETA
   1                      NBODY
   c1.gdf
   0. 0. -0.06 0.         XBODY
   1  1  1  1  1  1       IMODE(1-6)
   0                      NEWMDS
```

C1.FRC:
c1, s1, free floating, high-order, dipole
```
    1    0    0    1    0    1  0  0 0     IOPTN(1-9)
    0.000000                               VCG
    1.830000      .0000000      .0000000
    .0000000      0.170000      .0000000
    .0000000      .0000000      0.250000       XPRDCT
    0                          (NBETAH)
    0                          (NFIELD -- no individual field points)
    4                          (NFIELD_ARRAYS -- number of arrays)
    0                          (Array is in exterior fluid domain)
    10   0.4   0.2             (NFX, X1, DELX)
    11   0.0   0.2             (NFY, Y1, DELY)
    1    0.0   0.0             (NFZ, Z1, DELZ)
    0                          (Array is in exterior fluid domain)
    10   -2.2  0.2             (NFX, X2, DELX)
    11   0.0   0.2             (NFY, Y2, DELY)
    1    0.0   0.0             (NFZ, Z2, DELZ)
    0                          (Array is in exterior fluid domain)
    23   -2.2  0.2             (NFX, X3, DELX)
    11   2.2   0.2             (NFY, Y3, DELY)
    1    0.0   0.0             (NFZ, Z3, DELZ)
    1                          (Array is in interior fluid domain)
    5   -0.2  0.1              (NFX, X4, DELX)
    5   0.   0.4               (NFY, Y4, DELY)
    1    0.0   0.0             (NFZ, Z4, DELZ)
```

C1.CFG:

```
   ILOWHI=1
   IALTPOT=2
   IRR=0
   ISOLVE=2
   KSPLIN=3
   IQUADO=3
   IQUADI=4
   IPERIO=1
   ITANKFPT=1
   NDIPOLE= 5 6 7
   MONITR=0
   NUMHDR=1
   NOOUT= 1 1 1 1 0 1 1 1 1
   IFIELD_ARRAYS=1              (field points input in array format in .frc file)
   USERID_PATH=\WAMITv6         (directory for *.exe, *.dll, and userid.wam)
   ipltdat=5
```

C.3 Maere model (free floating)

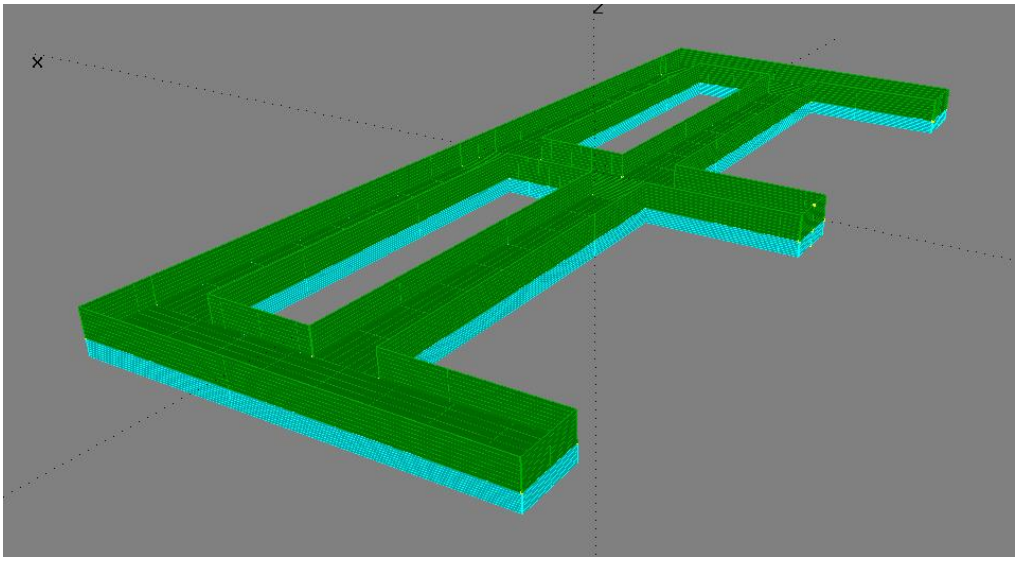

Figure C.3 Maere model MultiSurf snapshot

C2.GDF:

```
c2, s1, free floating, high-order, dipole
   1.000000  9.806650    ULEN, GRAV
   0 1                   ISX, ISY
   0  2                  NPATCH  IGDEF
```

```
   3                       NLINES
   C2.MS2
   *
   0  0  0                 Fast/acc  DivMult  Inward_normals
```

C2.POT:

```
c2, s1, free floating, high-order, dipole
   0.6                     HBOT
   1          1            IRAD, IDIFF
   20                      NPER (array PER follows)
   1 1.06 1.12 1.18 1.25 1.34 1.43 1.54 1.67 1.82 2 2.23 2.5 2.86 3.34 4 5 6.67
10 20
   1                       NBETA (array BETA follows)
   0.
   1                       NBODY
   c2.gdf
   0. 0. -0.05 0.          XBODY
   1  1  1  1  1  1        IMODE(1-6)
   0                       NEWMDS
```

C2.FRC:

```
c1, s1, free floating, high-order, dipole
    1    0    0    1    0    1  0  0 0     IOPTN(1-9)
    0.000000                               VCG
    1.830000      .0000000      .0000000
    .0000000      0.170000      .0000000
    .0000000      .0000000      0.250000       XPRDCT
    0                       (NBETAH)
    0                       (NFIELD -- no individual field points)
    10                      (NFIELD_ARRAYS -- number of arrays)
    0                       (Array is in exterior fluid domain)
    9   0.8   0.2           (NFX, X1, DELX)
    10   0.0   0.2          (NFY, Y1, DELY)
    1    0.0   0.0          (NFZ, Z1, DELZ)
    0                       (Array is in exterior fluid domain)
    7   -2.4  0.2           (NFX, X2, DELX)
    2   0.0   0.12          (NFY, Y2, DELY)
    1    0.0   0.0          (NFZ, Z2, DELZ)
    0                       (Array is in exterior fluid domain)
    3   0.0  0.15           (NFX, X3, DELX)
    8   0.2   0.2           (NFY, Y3, DELY)
    1    0.0   0.0          (NFZ, Z3, DELZ)
```

```
 0                    (Array is in exterior fluid domain)
 11   -2.4   0.2      (NFX, X1, DELX)
 13   0.2    0.1      (NFY, Y1, DELY)
 1    0.0    0.0      (NFZ, Z1, DELZ)
 0                    (Array is in exterior fluid domain)
 7   -2.4  0.2        (NFX, X2, DELX)
 3   1.6    0.1       (NFY, Y2, DELY)
 1    0.0    0.0      (NFZ, Z2, DELZ)
 0                    (Array is in exterior fluid domain)
 25   -2.4  0.2       (NFX, X3, DELX)
 12   2.0    0.2      (NFY, Y3, DELY)
 1    0.0    0.0      (NFZ, Z3, DELZ)
 1                    (Array is in interior fluid domain)
 11   -0.93  0.15     (NFX, X4, DELX)
 2   0.0    0.12      (NFY, Y4, DELY)
 1    0.0    0.0      (NFZ, Z4, DELZ)
 1                    (Array is in interior fluid domain)
 3   0.33  0.1        (NFX, X4, DELX)
 11   0.12   0.15     (NFY, Y4, DELY)
 1    0.0    0.0      (NFZ, Z4, DELZ)
 1                    (Array is in interior fluid domain)
 11   -0.93  0.15     (NFX, X4, DELX)
 3   1.62   0.12      (NFY, Y4, DELY)
 1    0.0    0.0      (NFZ, Z4, DELZ)
 1                    (Array is in interior fluid domain)
 3   -0.3  0.1            (NFX, X4, DELX)
 11   0.12   0.15              (NFY, Y4, DELY)
 1    0.0    0.0          (NFZ, Z4, DELZ)
```

C2.CFG:

```
  ILOWHI=1
  IALTPOT=2
  IRR=0
  ISOLVE=2
  KSPLIN=3
  IQUADO=3
  IQUADI=4
  IPERIO=1
  ITANKFPT=1
  NDIPOLE= (18 30)
  MONITR=0
  NUMHDR=1
```

```
NOOUT= 1 1 1 1 0 1 1 1 1
IFIELD_ARRAYS=1          (field points input in array format in .frc file)
USERID_PATH=\WAMITv6     (directory for *.exe, *.dll, and userid.wam)
ipltdat=5
```